©2016 Universidad EAFIT. All rights reserved.

Universidad EAFIT

Doctoral Publication

Compendium of Publications on:

Computational Geometry in Medical Applications

Supervisor
Prof. Oscar E. Ruiz Salguero,
Universidad EAFIT
Co-supervisor:
Prof. Julián Flórez Esnal,
Vicomtech-IK4

Doctoral Student:
Camilo A. Cortés Acosta

Jury:
Dr. Jorge L. Posada Velásquez,
Vicomtech-IK4
Prof. Carlos A. Cadavid Moreno,
Universidad EAFIT
Prof. Sebastián Durango Idárraga,
Universidad Autónoma de Manizales

Dissertation
Submitted in partial fulfillment of the requirements for the degree of Doctor of Philosophy in Engineering in the College of Engineering of the Universidad EAFIT

UNIVERSIDAD EAFIT
COLLEGE OF ENGINEERING
DOCTORAL PROGRAM IN ENGINEERING
MEDELLIN, COLOMBIA
JUNE 2016

FINAL EXAM OF DISSERTATION
DOCTORAL PROGRAM IN ENGINEERING
EAFIT UNIVERSITY

UNIVERSIDAD EAFIT®

Doctoral Student:	**Camilo Andrés Cortés Acosta**
Thesis Supervisors:	**Prof. Dr. Eng. Oscar Ruiz Salguero (U. EAFIT)** **Prof. Dr. Eng. Julián Flórez Esnal (Vicomtech)**
Topic of Examination:	**Computational Geometry in Medical Applications**
Room:	**19-703. Lecture Room. Medellín Campus**
Date:	**May 20, 2016**
Time:	**9:00 h**
Jury:	**Dr. Eng. Jorge L. Posada Velásquez** **Vicomtech, Donostia-San Sebastián, Spain**
	Prof. Dr. Math. Carlos A. Cadavid Moreno **Universidad EAFIT, Medellín, Colombia**
	Prof. Dr. Eng. Sebastián Durango Idárraga **Universidad Autónoma de Manizales, Manizales, Colombia**

The Jury considers that the Doctoral Student has approved (APPROVED/FAILED) this Final Examination, faced by the Doctoral Student in the mentioned place and date.

Juror Dr. Eng. Jorge L. Posada	Juror Prof. Dr. Math. Carlos A. Cadavid	Juror Prof. Dr. Eng. Sebastián Durango

Witnesses:

Thesis Supervisor Prof. Dr. Eng. Oscar Ruiz	Thesis Supervisor Prof. Dr. Eng. Julián Flórez

President of the Doctoral Board
Dean Alberto Rodriguez

UNIVERSIDAD EAFIT®

The College of Engineering of

EAFIT University

announces the

final examination of

Camilo A. Cortés Acosta

for the degree of

Doctor of Philosophy in Engineering

Friday, May 20, 2016
at 9:00 am
Lecture room 19 – 703
Engineering Building
Medellin Campus

COLOMBIA

Major field of Study
Computational Geometry

Dissertation
Computational Geometry in Medical Applications

Dissertation committee chairperson
Prof. Dr. Eng. Oscar Ruiz, Universidad EAFIT, Colombia

Directors of dissertation research
Prof. Dr. Eng. Oscar Ruiz, Universidad EAFIT, Colombia
Prof. Dr. Eng. Julián Flórez, Vicomtech-IK4, Spain

Examining committee
Dr. Eng. Jorge L. Posada Velásquez
Vicomtech-IK4, Donostia-San Sebastián, Spain

Prof. Dr. Math. Carlos A. Cadavid Moreno
Universidad EAFIT, Medellín, Colombia

Prof. Dr. Eng. Sebastián Durango Idárraga
Universidad Autónoma de Manizales, Manizales, Colombia

President of the Board of the
Doctoral Program in Engineering
Dean Alberto Rodriguez Garcia

This examination is open to the public

ABSTRACT

This doctoral thesis develops novel techniques in Computational Geometry and applies them to Medical Imaging, Image-Guided Surgery and Motor Neurorehabilitation.

In Medical Imaging, this Thesis contributes with: (a) optimization of parametric forms applicable to image segmentation and organic shape synthesis, and (b) simplification of topology and geometry of porous materials, which enables mechanical computations (previously intractable) while faithfully representing local pore geometry.

In Image-Guided Surgery, this Thesis addresses surgical patient registration, including: (c) a robotic research platform for the controlled acquisition of intraoperative medical images, (d) intraoperative registration of Computer Tomography and Ultrasound medical images of the patient spine, and (e) homologated and public Ultrasound Image dataset with ground-truth to test 2D-3D or 3D-3D image registration algorithms.

In Motor Neurorehabilitation this Thesis addresses the patient posture estimation in exoskeleton-based therapy. Its contributions include: (f) enhanced estimation of upper limb joint angles, significantly improving exoskeleton - based estimations, and (g) enhanced estimation of shoulder angles using low-cost marker-based optical systems along with the rehabilitation exoskeleton.

All the aforementioned contributions have been submitted to the screening and critique of the international relevant scientific communities, achieving publication, homologation and/or favorable appraisal by experts. The developed systems, data sets and algorithms are currently applied in the National Hospital for Spinal Cord Injury (Toledo, Spain) and Surgical Robotics Project ORXXI (Basque Country, Spain).

VITAE

Doctoral Student Camilo A. Cortés Acosta
Camilo Cortés (Bogotá, Colombia) obtained the B.Sc. degree in Mechatronics (2010) from Escuela de Ingeniería de Antioquia (Colombia). He joined the CAD CAM CAE Laboratory at U. EAFIT in 2011, obtaining the M.Sc in Engineering (2012), under supervision of Prof. O. Ruiz. In 2013, Camilo Cortés started the Ph.D. program under the supervision of Profs. Oscar Ruiz (U. EAFIT) and Julián Florez (Inst. Visual Communication Technologies Vicomtech-IK4, Spain). His dissertation domain is Computational Geometry Applied to Medicine, with focus in Medical Robotics, Image-Guided Surgery and Geometry Synthesis from Medical Sampling.

Doctoral Supervisor Prof. Dr. Eng. Oscar E. Ruiz Salguero
Prof. Oscar Ruiz (Tunja, Colombia) earned B.Sc. degrees in Mechanical Engineering and Computer Science (1983, 1987) at Los Andes University, Colombia, a M.Sc. degree (1991) and a Ph.D. (1995) from the Mechanical Eng. Dept. of University of Illinois at Urbana- Champaign, USA. He has been Visiting Researcher at Ford Motor Co. (USA), Fraunhofer Inst. for Computer Graphics (Germany), University of Vigo (Spain), Max Planck Inst. for Informatik (Germany) and Purdue University (USA). He coordinates the CAD CAM CAE Laboratory at U. EAFIT. His research and teaching interests are Computational Geometry applied on Design, Manufacturing, Medicine, etc.

Doctoral Co-Supervisor Prof. Dr. Eng. Julián Flórez Esnál
Prof. Julián Flórez studied Industrial Engineering at the University of Navarra (1980), and obtained his Ph.D.at the University of Manchester, Institute of Science and Technology UMIST (1985), in the Adaptive Control field. Since then, he has been involved in research projects related to Electrical and Industrial Engineering with an industrial focus. Since 2001, he is Principal Researcher and General Director in Vicomtech. He holds 10 patents and has written more than 40 research papers in the Industrial and Electric Engineering areas.

Dedication

To my beloved mother and father, Luz Mery and Rafael.

Acknowledgments

I express my sincere gratitude to my PhD Advisors, Prof. Oscar Ruiz and Prof. Julián Flórez, for their continuous support to my doctoral studies, for their trust, understanding, patience, compromise, effort, and constant motivation.

I am genuinely thankful to the Directors of Vicomtech-IK4, Dr. Jorge Posada and Prof. Julián Flórez, who provided me the opportunity to join their team and participate in their interesting projects. I also appreciate the support provided by Dr. Alessandro De Mauro, Dr. Luis Unzueta, Dr. Luis Kabongo, Dr. Álvaro Bertelsen, Dr. Iñigo Barandiarán, Dr. Carlos Toro and Dr. Eider Sanchez along this process.

I am grateful to my colleagues at the CAD CAM CAE Laboratory for their support and help. I thank Prof. Diego Acosta for his support and advice.

Many thanks to Universidad EAFIT and Vicomtech-IK4 as Institutions, for their trust and support to my master and doctoral studies, which are the first steps in my career as a researcher.

I thank the Jury members, Dr. Jorge Posada, Prof. Carlos Cadavid, and Prof. Sebastián Durango for their time and effort to assess my thesis, and for their valuable comments.

I am wholeheartedly thankful to my family and girlfriend for their love, understanding and constant support.

Summary of Contributions

This thesis develops and applies techniques from the area of computation geometry to the domain of Medicine. The specific areas of medicine that are investigated and the contributions performed in each of such areas are the following:

Table 1: Investigated domains and main contributions of this thesis.

Investigated Domain	**Contribution**
Medical Imaging	(1) An optimized algorithm for curve reconstruction. (2) A sensitivity analysis of the algorithm in (1). (3) A method for the geometry simplification of digital models of porous materials.
Image-Guided Surgery	(1) A robotic research platform that precisely handles equipment for medical image acquisition. (2) A dataset for the design and testing of algorithms for medical image analysis. (3) An algorithm for the registration of Computer Tomography and Ultrasound medical images.
Motor Neurorehabilitation	(1) A method to estimate the posture of the patient during robotic-assisted rehabilitation therapy. (2) The assessment of (1) in simple and compound movements training. (3) A hybrid system for the precise estimation of the shoulder joint angles in exoskeleton-based rehabilitation.

Publications

Table 2: List of published, accepted and submitted articles of the doctoral support team.

Item	Bibliographic Information	Type / Status
1	Oscar E. Ruiz, Camilo Cortés, Mauricio Aristizábal, Diego Acosta and Carlos Vanegas. (2013). *Parametric Curve Reconstruction from Point Clouds using Minimization Techniques*. Proceedings of the International Conference on Computer Graphics Theory and Applications GRAPP 2013, pp. 35–48. ISBN 978-989-8565-46-4, Barcelona, Spain.	Conference Article / Published
2	Camilo A. Cortés, Iñigo Barandiarán, Oscar E. Ruiz and Alessandro De Mauro. (2013). *Robotic Research Platform For Image-Guided Surgery Assistance*. Proceedings of the IASTED International Conference Biomedical Engineering BioMed-2013, pp. 427–434. ISBN 978-0-88986-942-4, Innsbruck, Austria.	Conference Article / Published
3	Sebastian Koenig, Aitor Ardanza, Camilo Cortés, Alessandro De Mauro and Belinda Lange. (2014). *Introduction to Low-Cost Motion-Tracking for Virtual Rehabilitation*. Emerging Therapies in Neurorehabilitation, pp. 287-303. ISBN 978-3-642-38555-1, Springer.	Chapter in Book / Published
4	Camilo Cortés, Aitor Ardanza, F. Molina-Rueda, A. Cuesta-Gomez, Luis Unzueta, Gorka Epelde, Oscar E. Ruiz, Alessandro De Mauro and Julián Flórez. (2014). *Upper Limb Posture Estimation in Robotic and Virtual Reality-Based Rehabilitation*. BioMed Research International, vol. 2014, 18 pages, doi:10.1155/2014/821908 (Impact Factor: 2.7).	Journal Article / Published
5	Oscar E. Ruiz, Camilo Cortés, Diego A. Acosta and Mauricio Aristizábal. (2015). *Sensitivity Analysis in Optimized Parametric Curve Fitting*. Editors Bart H.M. Gerritsen and Imre Horvath, Engineering Computations, ISSN: 0264-4401, 2015, volume 32, number 1, Issue Advancements in Modelling of Complex Product, pp. 37-61, doi: 10.1108/EC-03-2013-0086, Emerald Group Publishing (Impact Factor: 1.5).	Journal Article / Published

Continued on next page

Table 2 – *Continued from previous page*

Item	**Bibliographic Information**	**Type / Status**
6	Camilo Cortés, Luis Kabongo, Iván Macía, Oscar E. Ruiz and Julián Flórez. (2015). *Ultrasound Image Dataset for Image Analysis Algorithms Evaluation.* Innovation in Medicine and Healthcare 2015 (InMed15). Chapter in Book Series Smart Innovation, Systems and Technologies, pp. 447-457, volume 45, doi: {10.1007/978-3-319-23024-5_41}, ISBN 978-3-319-23023-8, 2015, online: August 2015. Kyoto, Japan.	Chapter in Book / Published
7	Rebeca Echeverría, Camilo Cortés, Álvaro Bertelsen, Iván Macía, Oscar E. Ruiz and Julián Flórez. (2015). *Robust CT to US 3D-3D Registration using Principal Component Analysis and Kalman Filtering.* 3rd Workshop & Challenge on Computational Methods and Clinical Applications for Spine Imaging, Held in Conjunction with MICCAI 2015, Münich, Germany, October 5, 2015. To be published as chapter in book series: Lecture in Computer Science (Springer).	Chapter In Book / Accepted
8	Camilo Cortés, Ana de los Reyes-Guzmán, Davide Scorza, Álvaro Bertelsen, Eduardo Carrasco, Ángel Gil-Agudo, Oscar Ruiz-Salguero and Julián Flórez. (2016). *Inverse Kinematics for Upper Limb Compound Movement Estimation in Exoskeleton - Assisted Rehabilitation.* BioMed Research International, vol. 2016, 14 pages, doi: 10.1155/2016/2581924 (Impact Factor: 2.1).	Journal Article / Published
9	Camilo Cortés, Luis Unzueta, Ana de los Reyes-Guzmán, Oscar Ruiz-Salguero and Julián Flórez. (2016). *Optical Enhancement of Exoskeleton-based Gleno-Humeral Angles Estimation.* Applied Bionics and Biomechanics, vol. 2016, 20 pages, doi: 10.1155/2016/5058171 (Impact Factor: 0.7).	Journal Article / Published
10	Camilo Cortés, Maria Osorno, David Uribe, Holger Steeb, Oscar Ruiz-Salguero, Iñigo Barandiarán and Julián Flórez. *Geometry Simplification of Open-Cell Porous Materials.* Submitted to the Computers & Graphics Journal.	Journal Article / Submitted

This compendium of publications has the following co-authors.

Table 3: Co-authors of this compendium of publications.

Name	**Affiliation**
Diego Acosta	Grupo de Investigación DDP, Universidad EAFIT
Aitor Ardanza	Interactive Computer Graphics, Vicomtech-IK4
Mauricio Aristizábal	Mecánica Aplicada, Universidad EAFIT
Iñigo Barandiarán	Industry and Advanced Manufacturing, Vicomtech-IK4
Álvaro Bertelsen	eHealth and Biomedical Applications, Vicomtech-IK4
Eduardo Carrasco	eHealth and Biomedical Applications, Vicomtech-IK4
A. Cuesta-Gomez	Biomechanics, Ergonomy and Motor Control Laboratory (LAMBECOM), Universidad Rey Juan Carlos
Ana de los Reyes-Guzmán	Biomechanics and Technical Aids Unit, National Hospital for Spinal Cord Injury
Alessandro De Mauro	Global Governmental Grant Office, Janssen Pharmaceutica
Rebeca Echeverría	Universidad Pública de Navarra
Gorka Epelde	eHealth and Biomedical Applications, Vicomtech-IK4
Julián Flórez	eHealth and Biomedical Applications, Vicomtech-IK4
Ángel Gil-Agudo	Biomechanics and Technical Aids Unit, National Hospital for Spinal Cord Injury
Luis Kabongo	eHealth and Biomedical Applications, Vicomtech-IK4
Sebastian Koenig	Katana Simulations
Belinda Lange	Department of Physiotherapy, Flinders University
Iván Macía	eHealth and Biomedical Applications, Vicomtech-IK4
F. Molina-Rueda	Biomechanics, Ergonomy and Motor Control Laboratory (LAMBECOM), Universidad Rey Juan Carlos
Maria Osorno	Institute of Applied Mechanics, University of Stuttgart
Oscar E. Ruiz	Laboratorio de CAD CAM CAE, Universidad EAFIT
Davide Scorza	eHealth and Biomedical Applications, Vicomtech-IK4
Holger Steeb	Institute of Applied Mechanics, University of Stuttgart
Luis Unzueta	Intelligent Transport Systems and Engineering, Vicomtech-IK4
David Uribe	Institute of Applied Mechanics, University of Stuttgart
Carlos Vanegas	Synthicity

Contents

Part I
Introduction

I-A

Goal of the Final Examination

Under the regulations of the Doctoral Program in Engineering at U. EAFIT, the purpose of the Final Examination is to assess the thesis work of the doctoral student, which should reflect the capacity of the student to: (I) conduct high-quality scientific research, (II) contribute to the state of the art, and (III) articulate in novel manners the existing knowledge to advance in the formulation and solution of theoretic and practical problems in the Engineering domain.

The Final Exam assesses these aspects:

1. The academic trajectory undertaken and opportunities profited by the doctoral student during the doctoral studies, in terms of (a) Doctoral Courses, (b) Special Trainings, (c) Attendance to Specialized Forums, Industries, Government Committees, (d) Equipment, Software, accessory materials, (e) Funding Proceedings, (f) Special Advisors, etc.

2. The thematically connected results of the research of the student and the doctoral team, and the endorsement of the international scientific community to these results, in the form of ranked publications.

The Jury approves or reproves the thesis work of the doctoral student.

I-B

Organization of this Document

The remaining of this document is organized as follows:

- Part II: Academic Trajectory. This part reports the following aspects of the doctoral process:
  (a) Doctoral Courses
  (b) Special Trainings
  (c) Attendance to Specialized Forums
  (d) Special Advisors
  (e) Projects
  (f) Training in Scientific Funds Leveraging
- Part III: Research Results. This part provides:
  (a) An overview of the domains in which the doctoral investigation has been conducted.
  (b) The list of publications generated by the doctoral support team.
  (c) The compendium of publications generated in each of the investigated domains.
- Part IV: General Conclusions.

Part II
Academic Trajectory

II-A

Academic History

II-A.1

Summary

1. In December of 2010, Camilo Cortés obtained his bachelor degree in Mechatronic Engineering from the Escuela de Ingenieros de Antioquia (EIA).
2. In January of 2011, Camilo joined the CAD/CAM/CAE Laboratory of Universidad EAFIT and began his Master studies in Engineering under the supervision of Prof. Dr. Ing. Oscar Ruiz.
3. In November of 2011, Camilo started an internship at the eHealth and Biomedical Applications Department of Vicomtech-IK4 (Spain) as part of his Master thesis.
4. In December of 2012, Camilo obtained his Master Degree in Engineering from U. EAFIT.
5. In January of 2013, Camilo started his Doctoral Studies in Engineering at U. EAFIT under the supervision of Prof. Oscar Ruiz.
6. From January of 2013 to July of 2015, Camilo performed his doctoral internship at Vicomtech-IK4 under the supervision of Prof. Dr. Ing. Julián Flórez.

In the framework of the collaborative program between EAFIT and Vicomtech-IK4, the student and his doctoral support team have achieved several publications, formalizing the doctoral work of the student. The mentioned doctoral support team is composed by the doctoral supervisors of the student and several researchers of EAFIT and Vicomtech-IK4.

II-A.2

Doctoral Courses

II-A.2.1 Preparatory Courses

According to the regulations of U. EAFIT, the courses that prepare the student to perform his doctoral thesis are taken during the master program. The preparatory courses that the student took are presented in Table II-A.2.1:

Table II-A.2.1: Preparatory Courses.

Course	**Semester**
Data Structures and Algorithms	2011-1
Computer-Aided Design	2011-1
Advanced Mathematics for Engineers	2011-1
Introduction to Finite Element Analysis	2011-1
Advanced Data Structures and Algorithms	2011-2
Computational Geometry	2011-2
Optimization Techniques	2011-2
Advanced Finite Element Analysis	2011-2

II-A.2.2 Qualifying Exams

During the first year of the doctoral program, the student prepared, took and approved the doctoral qualifying exams that are reported in Table II-A.2.2:

II-A.2.3 Preliminary Exam of Dissertation

During the third year of the doctoral studies, the doctoral student prepared, presented and approved the Preliminary Exam of Dissertation. The Preliminary Examination assessed: (a) The academic trajectory undertaken and opportunities profited by the doctoral student during the first 24-30 months of the doctoral studies, (b) The thematically connected results of the research of the student

Table II-A.2.2: Qualifying Exams.

Exam	**Date**	**Examiner**
Optimization Techniques	April 2013	Prof. Dr. Ing. Diego Acosta, U. EAFIT
Robot Kinematics	July 2013	Dr. Ing. Luis Unzueta, Vicomtech-IK4, Spain
Data Structures and Algorithms	December 2013	Prof. Dr. Ing. Juan Lalinde, U. EAFIT

and the doctoral team in the form of ranked publications, and (c) The Closure research activities and goals of the doctoral student and supporting team for the final 12 months (approx.).

On 29-09-2015 the Jury decided to permit the doctoral student to continue the academic and research activities, in order to prepare and perfect the materials, goals, publications, etc. for the Final Examination.

II-A.3

Special Trainings

As part of the doctoral formation, the student has performed the trainings presented in Table II-A.3.1:

Table II-A.3.1: Special Trainings.

Topic	**Entity-Context**	**Date**	**Supervisor**
CAD Software Database Interrogation (C++)	EAFIT - Colciencias GEMM Project.	2011-2012	Prof. Dr. Ing. Oscar Ruiz
Industrial Robot Trajectory Programming and Masterization	Keller und Knappich (KUKA) Robots Ibrica S.A., Vitoria, Spain	January 2012	Ing. Gaizka Solano
3D Printing and Carving	Vicomtech-IK4. Internal Training.	February 2012	Dr. Ing. Gregory Maclair
Medical Robotics for Surgical and Rehabilitation Applications	Vicomtech-IK4. Project HYPER (Rehabilitation Robotics)	2012-2013	Dr. Ing. Alessandro De Mauro
Medical Images (X-Rays, Computer Tomography, Ultrasound)	Vicomtech-IK4. Project ORXXI (Surgical Robotics Image-Guided Surgery).	November 2014	Dr. Ing. Luis Kabongo
Software for Medical Image Analysis	Vicomtech-IK4. Project ORXXI (Surgical Robotics Image-Guided Surgery).	April 2015 to July 2015	Dr. Ing. Álvaro Bertelsen

II-A.4

Attendance to Specialized Forums

During the doctoral formation, the student has attended to the following specialized forums:

II-A.4.1 Scientific Conferences

1. BIOMED 2013: IASTED International Conference Biomedical Engineering BioMed-2013. February 13-15, 2013, Innsbruck, Austria.
2. GRAPP 2013: International Conference on Computer Graphics Theory and Applications GRAPP 2013. February 21-24, 2013, Barcelona, Spain.

II-A.4.2 Professional Forums

1. SACAI 2012: Workshop. Systems and Architectures for Computer-Assisted Interventions. Satellite of MICCAI 2012. October 5, 2012. Nice, France.
2. MESROB 2014: Summer School on Medical Robotics. École Polytechnique Fédérale de Lausanne (EPFL). July 8-12, 2014. Lausanne, Switzerland.
3. SSNR 2014 and WeRob 2014: Summer School on Neurorehabilitation and Exoskeletons. Consejo Superior de Investigaciones Científicas (CSIC). September 14-19, 2014. Baiona, Spain.
4. HNPT 2015: Internship. Hospital Nacional de Parapléjicos de Toledo (HNPT), Experimental assessment of a method for posture estimation of patients in Robot-Assisted Rehabilitation. July 6-10, 2015. Toledo, Spain.
5. Doctoral Internship: Vicomtech-IK4. eHealth and Biomedical Applications Department. November 2011 to July 2015. Donostia-San Sebastián, Spain.

II-A.5

Special Advisors

In addition to the support provided by several professors and researchers from EAFIT and Vicomtech-IK4, the student was advised by the specialists presented in Table II-A.5.1.

Table II-A.5.1: Special Advisors.

Name	**Role**	**Entity**	**Topic**
Dr. Francisco Molina (Physiotherapist, Ph.D.)	Researcher on Neurorehabilitation of stroke patients	Biomechanics, Ergonomy and Motor Control Laboratory (LAMBECOM), Physical Therapy, Occupational Therapy, Rehabilitation and Physical Medicine Department, Rey Juan Carlos University, Madrid, Spain.	Patient Posture Estimation.
Dr. Ángel Gil (Physician, Ph.D.)	Director of the Rehabilitation Service and leader of the Biomechanics and Technical Aids Department	Hospital Nacional de Parapléjicos, Toledo, Spain.	Virtual Reality and Robot-based Rehabilitation.
Dr. Ana de los Reyes-Guzman (Ing., Ph.D.)	Researcher on Neurorehabilitation of patients with Spinal Cord Injury	Biomechanics and Technical Aids Department, Hospital Nacional de Parapléjicos, Toledo, Spain.	Motion Tracking and Patient Posture Estimation.
Prof. Diego Acosta (Ing., Ph.D)	Director of the Design and Development of Processes and Products Research Group (DDP)	Universidad EAFIT, Medellín, Colombia.	Optimized Parametric Curve Fitting.

II-A.6

Projects

During the student internship at Vicomtech-IK4, the student has participated in projects related to the areas of Motor Rehabilitation and Image-Guided Surgery:

1. HYPER: This project focuses on the development of neuro-prosthetics, neuro-robotics and virtual reality technologies to boost the rehabilitation of neuro-motor deceases (i.e. stroke, spinal-cord injury, cerebral palsy).
2. ORXXI: This project focuses on the development of CAD/CAM technologies, intra-operatory navigation systems and robotics for orthopedic surgery.

II-A.7

Training in Scientific Funds Leveraging

During the internship at Vicomtech-IK4, the student participated in the preparation of the project proposals presented in Table II-A.7.1 to obtain funding from local (Basque Government) and national (Spanish Government) and international (European Union) investigation support programs.

Table II-A.7.1: Project Proposals.

Project Name	**Project Objective**	**Call**
ORXXI	Development of CAD/CAM technologies, intra-operatory navigation and robotic systems for orthopedic surgery.	Gaitek (Basque Government)
ReHand	Development and Validation of a Low-Cost Device for the Neurorehabilitation of the hand.	Retos (Spanish Government)
Robotracker	Development of accurate intra-operatory navigation systems for spine surgery.	Gaitek (Basque Government)
MAXILARIS	Development and validation of a system for the registration of the patient in robotic-assisted maxillofacial surgery.	Retos (Spanish Government)
Robot-Assisted TRUS	Development of a Teleoperated Robotic System to acquire Ultrasound Images to guide the surgeon in prostate surgery.	Ayudas a proyectos de investigación en salud (Basque Government)
The Internet of Robots	Development of cloud technologies for robotics in order to boost the learning of autonomous robots.	ICT Call Future Internet (European Union)

The student has also participated in commercial visits and meetings with the following industrial customers (Table II-A.7.2):

Table II-A.7.2: Participation in commercial activities with industrial customers.

Company Name	**Industrial Field**	**Location**
Egile	Computer-Aided Surgery	Basque Country
Vitia	Rehabilitation Robotics	Basque Country
Virtualware	Virtual Reality for Rehabilitation	Basque Country
Rehub Health	Rehabilitation Robotics	Basque Country

Part III
Research Results

III-A

Context

This thesis develops and applies computational geometry techniques in the domain of medicine. Computational geometry applies algorithms and data structures for the solution of problems that can be stated in terms of geometry. The concepts of combinatorial and numerical computational geometry applied in this thesis are presented in Table 3.

Table 3: Application domains of the computational geometry techniques implemented in this thesis.

Computational Geometry Concept	**Area of Application**
Coordinate Frames	Patient Registration, Patient Posture Estimation.
Geometric Transformations (e.g. euclidean, affine, projective)	Patient Registration, Patient Posture Estimation.
Geometric Retrieval (e.g. nearest neighbor)	Patient Registration, Parametric Curve Fitting, Geometry Simplification.
Parametric Curves (e.g. bezier, splines)	Parametric Curve Fitting.
Geometric Data Structures (e.g. Kd-trees)	Patient Registration, Geometry Simplification.
Meshing	Patient Registration, Geometry Simplification.
Geometric Modeling	Parametric Curve Fitting, Geometry Simplification.
Mathematical Programming (e.g. Nonlinear programming)	Parametric Curve Fitting, Patient Posture Estimation.
Differential Geometry (e.g. tangent and normal vectors, curvature)	Parametric Curve Fitting, Patient Posture Estimation, Patient Registration, Geometry Simplification.
Geometric constraints	Patient Posture Estimation, Parametric Curve Fitting, Patient Registration, Geometry Simplification.

Fig. 1 shows the problems addressed in this thesis, their domain of application, and where they take place within the Clinical Practice Workflow. Next, a brief description of the Stages and Procedures presented in Fig. 1 is provided:

1. Stages:

   (a) Diagnosis: Consists in the determination of the condition (e.g. the decease) that corresponds the the patient symptoms. One of the diagnostic procedures is the acquisition and analysis of medical images.

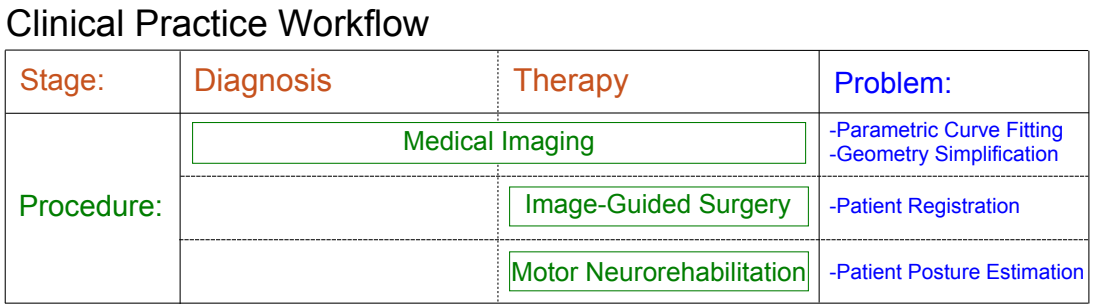

Figure 1: Problems addressed in this thesis, their domain of application and location within the Clinical Practice Workflow.

(b) Therapy: Consists in the process to remediate a health problem. The type of therapy to be provided to a patient depends on the patient condition (e.g., surgery, rehabilitation, etc.).

2. Procedures:

(a) Medical Imaging: Consists in the creation of visual digital representations of the anatomical structures of the patient. The generated medical images can be used for analysis and also to plan a surgical intervention. The medical images are not exclusively generated during the diagnostic or pre-operative stages. They can also be acquired intra-operatively in order to guide a surgical procedure.

(b) Image-guided Surgery: Consist in a surgical procedure in which pre-operatory and intra-operatory medical images are used to indirectly guide the procedure due to the lack of direct vision of the surgical target. The pre-operative images (e.g. Computer Tomography, Magnetic Resonance) serve to establish the surgical plan (e.g. the location of a tumor or the trajectory to insert a screw). The intra-operative images (e.g. ultrasound images, X-rays, etc.) are used to transfer the surgical plan to the patient coordinate system of reference.

(c) Motor Neurorehabilitation: Consists in the therapy to re-train the mobility skills of a person that suffered an injury of the central nervous system, such as stroke, spinal cord-injury and cerebral palsy. New therapies for neurorehabilitation involve the use of robotic devices and virtual reality technologies.

The description of the specific problems and contributions performed in the Medical Imaging, Image-guided Surgery and Motor Neurorehabilitation fields are presented in Parts III-C, III-D and III-E, respectively.

III-B

Publications

Table 4: List of published, accepted and submitted articles of the doctoral support team.

Item	Bibliographic Information	Type / Status
1	Oscar E. Ruiz, Camilo Cortés, Mauricio Aristizábal, Diego Acosta and Carlos Vanegas. (2013). *Parametric Curve Reconstruction from Point Clouds using Minimization Techniques*. Proceedings of the International Conference on Computer Graphics Theory and Applications GRAPP 2013, pp. 35–48. ISBN 978-989-8565-46-4, Barcelona, Spain.	Conference Article / Published
2	Camilo A. Cortés, Iñigo Barandiarán, Oscar E. Ruiz and Alessandro De Mauro. (2013). *Robotic Research Platform For Image-Guided Surgery Assistance*. Proceedings of the IASTED International Conference Biomedical Engineering BioMed-2013, pp. 427–434. ISBN 978-0-88986-942-4, Innsbruck, Austria.	Conference Article / Published
3	Sebastian Koenig, Aitor Ardanza, Camilo Cortés, Alessandro De Mauro and Belinda Lange. (2014). *Introduction to Low-Cost Motion-Tracking for Virtual Rehabilitation*. Emerging Therapies in Neurorehabilitation, pp. 287-303. ISBN 978-3-642-38555-1, Springer.	Chapter in Book / Published
4	Camilo Cortés, Aitor Ardanza, F. Molina-Rueda, A. Cuesta-Gomez, Luis Unzueta, Gorka Epelde, Oscar E. Ruiz, Alessandro De Mauro and Julián Flórez. (2014). *Upper Limb Posture Estimation in Robotic and Virtual Reality-Based Rehabilitation*. BioMed Research International, vol. 2014, 18 pages, doi:10.1155/2014/821908 (Impact Factor: 2.7).	Journal Article / Published
5	Oscar E. Ruiz, Camilo Cortés, Diego A. Acosta and Mauricio Aristizábal. (2015). *Sensitivity Analysis in Optimized Parametric Curve Fitting*. Editors Bart H.M. Gerritsen and Imre Horvath, Engineering Computations, ISSN: 0264-4401, 2015, volume 32, number 1, Issue Advancements in Modelling of Complex Product, pp. 37-61, doi: 10.1108/EC-03-2013-0086, Emerald Group Publishing (Impact Factor: 1.5).	Journal Article / Published

Continued on next page

Table 4 – *Continued from previous page*

Item	**Bibliographic Information**	**Type / Status**
6	Camilo Cortés, Luis Kabongo, Iván Macía, Oscar E. Ruiz and Julián Flórez. (2015). *Ultrasound Image Dataset for Image Analysis Algorithms Evaluation.* Innovation in Medicine and Healthcare 2015 (InMed15). Chapter in Book Series Smart Innovation, Systems and Technologies, pp. 447-457, volume 45, doi: {10.1007/978-3-319-23024-5_41}, ISBN 978-3-319-23023-8, 2015, online: August 2015. Kyoto, Japan.	Chapter in Book / Published
7	Rebeca Echeverría, Camilo Cortés, Álvaro Bertelsen, Iván Macía, Oscar E. Ruiz and Julián Flórez. (2015). *Robust CT to US 3D-3D Registration using Principal Component Analysis and Kalman Filtering.* 3rd Workshop & Challenge on Computational Methods and Clinical Applications for Spine Imaging, Held in Conjunction with MICCAI 2015, Münich, Germany, October 5, 2015. To be published as chapter in book series: Lecture in Computer Science (Springer).	Chapter In Book / Accepted
8	Camilo Cortés, Ana de los Reyes-Guzmán, Davide Scorza, Álvaro Bertelsen, Eduardo Carrasco, Ángel Gil-Agudo, Oscar Ruiz-Salguero and Julián Flórez. (2016). *Inverse Kinematics for Upper Limb Compound Movement Estimation in Exoskeleton - Assisted Rehabilitation.* BioMed Research International, vol. 2016, 14 pages, doi: 10.1155/2016/2581924 (Impact Factor: 2.1).	Journal Article / Published
9	Camilo Cortés, Luis Unzueta, Ana de los Reyes-Guzmán, Oscar Ruiz-Salguero and Julián Flórez. (2016). *Optical Enhancement of Exoskeleton-based Gleno-Humeral Angles Estimation.* Applied Bionics and Biomechanics, vol. 2016, 20 pages, doi: 10.1155/2016/5058171 (Impact Factor: 0.7).	Journal Article / Published
10	Camilo Cortés, Maria Osorno, David Uribe, Holger Steeb, Oscar Ruiz-Salguero, Iñigo Barandiarán and Julián Flórez. *Geometry Simplification of Open-Cell Porous Materials.* Submitted to the Computers & Graphics Journal.	Journal Article / Submitted

III-C

Medical Imaging

III-C.1

Curve Fitting Problem

III-C.1.1 Problem Description

The curve fitting problem is present in the segmentation of medical images. The segmentation of a medical image consists in the partitioning of regions the image into various sets according to specific criteria ([1]). For example, it can be of interest to segment the pixels that belong to a bone or tumor. Also, many segmentation tasks consist in determining the boundaries of an organ. In other words, to recover the planar curves that describe the contours of the organ from a set of 2D images. In Fig. III-C.1.1 the segmentation of the edge of a vertebra in an ultrasound image is depicted. In this case, the contour of the vertebra is represented with a smooth parametric curve.

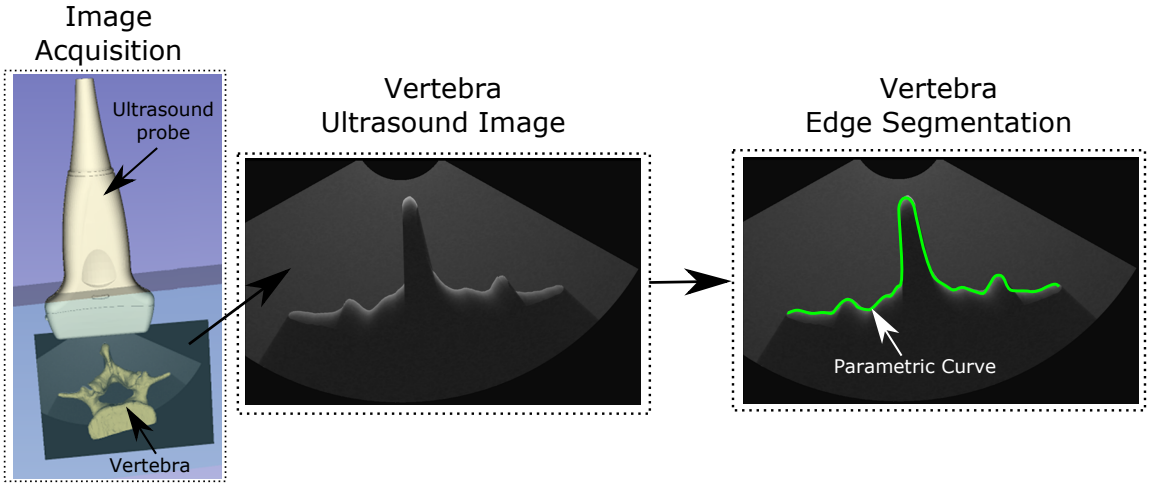

Figure III-C.1.1: Ultrasound scanning of a vertebra and segmentation of the edge the vertebra in an ultrasound image.

The usual approach to recover the planar curves is to fit a parametric curve $C(u)$ to the set $\mathbf{S}$ of noisy and unordered point samples of the surface contour in a 2D image. The shape of $C(u)$ is adjusted by placing the control points $\mathbf{P}$ of the parametric curve such that the cumulative unsigned distance function f between the points $\mathbf{S}$ and their approximating curve $C(u)$ is minimized ([2]) as

shown in Fig. III-C.1.2.

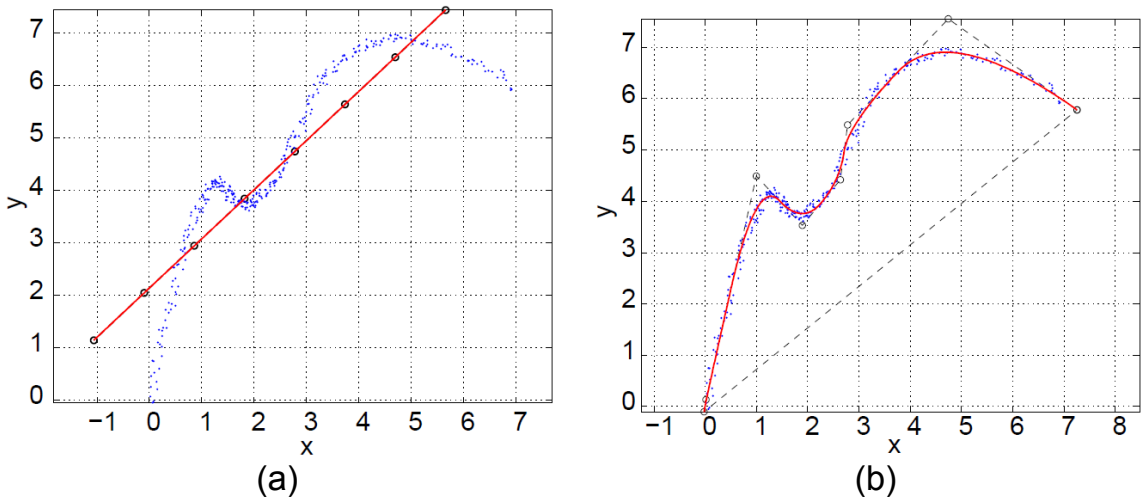

Figure III-C.1.2: Curve fitting of a noisy point cloud: (a) naive initial guess of $C(u)$ and (b) final location of control points $\mathbf{P}$ (black circles) and resulting $C(u)$.

III-C.2

Parametric Curve Reconstruction from Point Clouds using Minimization Techniques

Oscar E. Ruiz[1], Camilo Cortés[1], Mauricio Aristizábal[1], Diego A. Acosta[2] and Carlos A. Vanegas[3].

[1]Laboratorio de CAD CAM CAE, Universidad EAFIT, Carrera 49 No 7 Sur - 50, Medellín, Colombia.

[2]Grupo de Investigación DDP, Universidad EAFIT, Carrera 49 No 7 Sur - 50, Medellín, Colombia.

[3]Department of Computer Science, Purdue University, West Lafayette, IN 47907-2066, USA.

Context

This research work has been conducted in the framework of an internal project of the CAD CAM CAE Laboratory entitled *Computational Geometry and Mechanics 2013*, which focuses on the application of Computational Geometry in 3-D Solid and Surface Modeling for Computational Mechanics, Mechanism and Robot Kinematics, and Medical Image processing, among others. This work presents a novel method for the reconstruction of parametric curves from 2-D noisy points samples (e.g. Medical Images). This contribution is the result of a collaborative research between the CAD CAM CAE Laboratory and the DDP Investigation Group from EAFIT University, and the Department of Computer Science from Purdue University. The Computational Geometry and Mechanics 2013 project is funded by the EAFIT University.

Citation: *Parametric Curve Reconstruction from Point Clouds using Minimization Techniques. Oscar E. Ruiz, C. Cortes, M. Aristizabal, Diego A. Acosta, Carlos A. Vanegas. Proceedings International Conference on Computer Graphics Theory and Applications GRAPP 2013, pp. 35-48, ISBN: 978-989-8565-46-4. Feb 21-24, 2013, Barcelona, Spain. SCITEPRESS. Conference article.*

Indexing: ISI Conference Proceedings Citation Index, dblp, INSPEC, Scopus.

Abstract

Smooth (C^1-, C^2-,...) curve reconstruction from noisy point samples is central to reverse engineering, medical imaging, etc. Unresolved issues in this problem are (1) high computational expenses, (2) presence of artifacts and outlier curls, (3) erratic behavior at self-intersections and sharp corners. Some of these issues are related to non-Nyquist (i.e. sparse) samples. Our work reconstructs curves by minimizing the accumulative distance curve vs. point sample. We address the open issues above by using: (a) Principal Component Analysis (PCA) pre-processing to obtain a topologically correct approximation of the sampled curve, (b) Numerical, instead of algebraic, calculation of roots in point-to-curve distances, (c) Penalties for curve excursions by using point cloud-to-curve and curve-to-point cloud distances, and (d) Objective functions which are economic to minimize. The implemented algorithms successfully deal with self-intersecting and / or non-Nyquist samples. Ongoing research includes self-tuning of the algorithms and decimation of the point cloud and the control polygon.

Keywords: Parametric Curve Reconstruction, Noisy Point Cloud, Principal Component Analysis, Minimization.

N.B. The publisher owns the Copyright of this chapter. The interested reader may access to the manuscript at the publisher's website.

III-C.3

Sensitivity Analysis in Optimized Parametric Curve Fitting

Oscar E. Ruiz[1], Camilo Cortés[1], Diego A. Acosta[2] and Mauricio Aristizábal[1].

[1] Laboratorio de CAD CAM CAE, Universidad EAFIT, Medellín, Colombia.

[2] Grupo de Investigación DDP, Universidad EAFIT, Medellín, Colombia.

Context

This research work has been conducted in the framework of an internal project of the CAD CAM CAE Laboratory entitled *Computational Medical 3D Geometry and Robotics*, which focuses on the application of Computational Geometry in: (1) Shape reconstruction from stochastic point samples, (2) Image acquisition and registration in robot-assisted Surgery, (3) simplification of topology and geometry of porous materials for computational mechanics, (4) Property estimation for fluids in porous materials, and (5) Dimensionality reduction of surface point samples and heat transfer in thin geometries. This work presents a formal sensitivity analysis of the optimized parametric curve reconstruction method presented in Chapter III-C.2 for uniform-noise 2-D samples (e.g. Medical Images). This contribution is the result of a collaborative research between the CAD CAM CAE Laboratory and the DDP Investigation Group from EAFIT University. The *Computational Medical 3D Geometry and Robotics* project is funded by EAFIT University.

Citation: *Sensitivity analysis in optimized parametric curve fitting. Oscar E. Ruiz, Camilo Cortes, Diego A. Acosta, Mauricio Aristizabal. Engineering Computations, Issue on Advancements in Modelling of Complex Product, Editors Bart H.M. Gerritsen and Imre Horvath, pp. 37-61, volume 32, number 1, doi: 10.1108/EC-03-2013-0086, ISSN: 0264-4401, 2015. Emerald Group Publishing. Journal article.*

Indexing: ISI (IF:1.5), Scopus, INSPEC, EI Compendex.

Abstract

Purpose: Curve fitting from unordered noisy point samples is needed for surface reconstruction in many applications. In the literature, several approaches have been proposed to solve this problem. However, previous works lack formal characterization of the curve fitting problem and assessment on the effect of several parameters (i.e., scalars that remain constant in the optimization problem), such as control points number (m), curve degree (b), knot vector composition (U), norm degree (k), and point sample size (r) on the optimized curve reconstruction measured by a penalty function (f). This manuscript aims to discuss these issues.

Methodology: A numerical sensitivity analysis of the effect of m, b, k and r on f and a characterization of the fitting procedure from the mathematical viewpoint are performed. Also, the spectral (frequency) analysis of the derivative of the angle of the fitted curve $C(u)$ with respect to u as a means to detect spurious curls and peaks is explored.

Findings: It is more effective to find optimum values for m than for k or b in order to obtain good results because the topological faithfulness of the resulting curve strongly depends on m. Furthermore, when an exaggerate number of control points is used, the resulting curve presents spurious curls and peaks. The authors were able to detect the presence of such spurious features with a spectral analysis. Also, the authors found that the method for curve fitting is robust to significant decimation of the point sample.

Research limitations/implications: The authors have addressed important voids of previous works in this field. The authors determined, among the curve fitting parameters m, b and k, which of them influenced the most the results and how. Also, the authors performed a characterization of the curve fitting problem from the optimization perspective. And finally, the authors devised a method to detect spurious features in the fitting curve.

Practical implications: This paper provides a methodology to select the important tuning parameters in a formal manner.

Value: Up to the best of the knowledge, no previous work has been conducted in the formal mathematical evaluation of the sensitivity of the goodness of the curve fit with respect to different possible tuning parameters (curve degree, number of control points, norm degree, etc.).

Keywords: Parametric Curve Reconstruction, Noisy Point cloud, Sensitivity Analysis, Penalty Minimization.

N.B. The publisher owns the Copyright of this chapter. The interested reader may access to the manuscript at the publisher's website.

III-C.4

Geometry Simplification Problem

III-C.4.1 Problem Description

The geometry simplification problem consists on producing a geometric model M' that approximates an input model M by retaining only its relevant features for the target application ([3]). Within this work, we address the geometry simplification of digital models of porous materials (Fig. III-C.4.1) obtained from Computer Tomography (CT) images. In the medicine domain, the modeling of cellular solids such as bones and advanced materials (used for implants and prostheses) is relevant for applications in the fields of biomechanics, orthopedics, dentistry, and tissue engineering, among others ([4–7]).

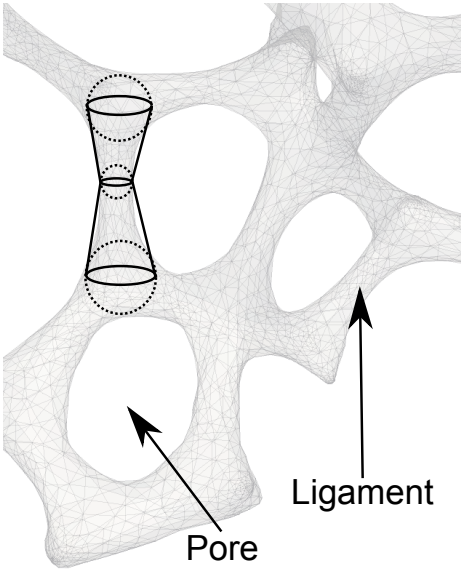

Figure III-C.4.1: Simplification of the mesh representation of a foam material by using beams with varying cross-section for finite element analysis.

III-C.5

Geometry Simplification of Open-Cell Porous Materials

Camilo Cortés[1,2], María Osorno[3], David Uribe[3], Holger Steeb[3], Oscar Ruiz-Salguero[1], Iñigo Barandiarán[2] and Julián Flórez[2].

[1]Laboratorio de CAD CAM CAE, Universidad EAFIT, Medellín, Colombia.

[2]eHealth and Biomedical Applications, Vicomtech-IK4, Donostia-San Sebastián, Spain.

[3]Institute of Applied Mechanics, University of Stuttgart, Stuttgart, Germany.

Context

This research work has been conducted in the framework of the project *Computational Medical 3D Geometry and Robotics*. This work presents a novel method for the simplification of the geometry of open-cell foam materials. This contribution is the result of a collaborative research between the CAD CAM CAE Laboratory of EAFIT University, Vicomtech-IK4 and the Institute of Applied Mechanics from the University of Stuttgart. The *Computational Medical 3D Geometry and Robotics* project is funded by EAFIT University.

Status: Submitted to the Computers & Graphics Journal.

Indexing: ISI (IF: 0.9), Scopus, INSPEC

Abstract

Estimation of mechanical properties of porous materials is relevant in industrial and medical applications. However, the massive (e.g. Computer Tomograph -CT-) data size of accurate porous material geometries makes the numerical estimation of properties impractical. Existing methods for porous material modeling simulate a given lattice topology and massively replicate it. The material statistical specifications dictate the lattice geometry. These methods do not seek to preserve local

material structure. This article presents a simplification method that is faithful to local material geometry. Our method takes a material CT as input and renders as output a graph - based truss model of the material. Our approach is based on the extraction and simplification of the Medial Axis of the CT model, building the basic topology of a truss (truncated cone bars with spherical nodes). The local geometrical characteristics are identified via optimized fittings. Finite Element Analysis (FEA) simulations are conducted to compare Truss vs. Full B-Rep representations of the porous material. The Truss models prove to be significantly more efficient for FEA, departing from the Full B-Rep FEA by a maximum of 16% in the estimation of equivalent Young, Shear or Poisson moduli. Ongoing efforts concentrate on alternative CT Medial Axis synthesis and geometric algorithms for standardized material testing.

Keywords: Porous Materials, Open-Cell Foams, Geometry Simplification.

N.B. The publisher owns the Copyright of this chapter. The interested reader may access to the manuscript at the publisher's website.

III-D

Image-Guided Surgery

III-D.1

Patient Registration Problem

III-D.1.1 Problem Description

Consider a domain $\Omega \subset \mathbb{R}^3$ of interest within the human body. A pre-operatory scan of Ω is conducted, with its own sampling parameters (e.g. coordinate system, patterns, intervals, set size, etc.). An intra-operatory scan is also conducted on Ω, with similar parameters. Given a subset of interest of Ω, corresponding to an organ, bone, etc., of interest, the goal is to find a rigid transformation $\mathbf{T}$ that maps the subset of the pre-operatory scan onto the corresponding subset of the intra-operatory scan with minimal spatial error (Fig. III-D.1.1).

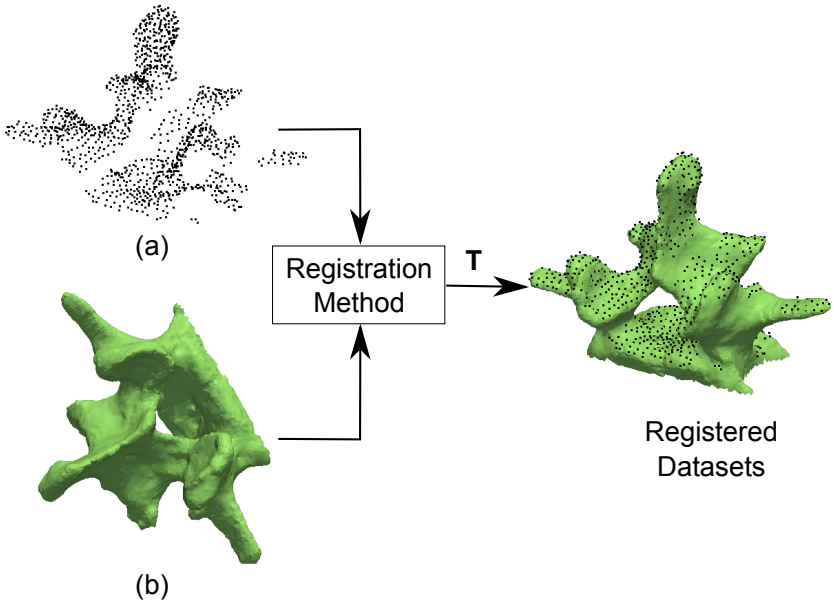

Figure III-D.1.1: Rigid registration calculates the rigid transformation $\mathbf{T}$ that aligns the pre-operatory dataset (b) with the intra-operatory dataset (a).

III-D.2

Robotic Research Platform for Image-Guided Surgery Assistance

Camilo Cortés[1], Iñigo Barandiarán[1], Oscar E. Ruiz[2] and Alessandro De Mauro[1].

[1] eHealth and Biomedical Applications, Vicomtech-IK4, Donostia-San Sebastián, Spain.

[2] Laboratorio de CAD CAM CAE, Universidad EAFIT, Medellín, Colombia.

Context

This research work has been conducted in the framework of an internal project of Vicomtech-IK4 in the area of Image-Guided Surgery. This work presents a novel robotic research platform that handles medical image acquisition equipment for medical image registration tasks. This contribution is the result of a collaborative research between Vicomtech-IK4 and the CAD CAM CAE Laboratory of EAFIT University.

Citation: *Robotic Research Platform for Image-Guided Surgery Assistance. C. Cortes, I. Barandiaran, O.E. Ruiz, A. De Mauro. Proceedings of the IASTED International Conference Biomedical Engineering BioMed-2013, pp. 427–434, doi: 10.2316/P.2013.791-067, ISBN: 978-0-88986-942-4. Feb 13-15, 2013. Innsbruck, Austria. ACTA Press. Conference article.*

Indexing: Scopus, INSPEC, EI Compendex.

Abstract

In the context of surgery, it is very common to face challenging scenarios during the preoperative plan implementation. The surgical technique complexity, the human anatomical variability and the occurrence of unexpected situations generate issues for the intervention goals achievement. To support the surgeon, robotic systems are being integrated to the operating room. However, current commercial solutions are specialized for a particular technique or medical application, being difficult

to integrate with other systems. Thus, versatile and modular systems are needed to conduct several procedures and to help solving the problems that surgeons face. This article aims to describe the implementation of a robotic research platform prototype that allows novel applications in the field of image-guided surgery. In particular, this research is focused on the topics of medical image acquisition during surgery, patient registration and surgical/medical equipment operation. In this paper, we address the implementation of the general purpose teleoperation and path following modes of the platform, which constitute the base of future developments. Also, we discuss relevant aspects of the system, as well as future directions and application fields to investigate.

Keywords: Robotic Surgery, Master-Slave Systems, Teleoperation, Image-Guided Surgery.

N.B. The publisher owns the Copyright of this chapter. The interested reader may access to the manuscript at the publisher's website.

III-D.3

Ultrasound Image Dataset for Image Analysis Algorithms Evaluation

Camilo Cortés[1,2,3] Luis Kabongo[1,3] Iván Macía[1,3] Oscar E. Ruiz[2] and Julián Flórez [1]

[1] eHealth and Biomedical Applications, Vicomtech-IK4, Donostia-San Sebastián, Spain

[2] Laboratorio de CAD CAM CAE, Universidad EAFIT, Medellín, Colombia.

[3] Biodonostia Health Research Center, Donostia-San Sebastián, Spain

Context

The Basque project *ORXXI* focuses on the development of CAD/CAM technologies, intra-operatory navigation systems and robotics for orthopedic surgery. This work presents a novel Ultrasound image dataset for the testing and design of registration algorithms and other image analysis methods that was generated by using the robotic platform introduced in Chapter III-D.2. This contribution is the result of a collaborative research between Vicomtech-IK4 and the CAD CAM CAE Laboratory of EAFIT University. The *ORXXI* project is funded by the GAITEK program from the Basque Government.

Citation: *Ultrasound Image Dataset for Image Analysis Algorithms Evaluation. Camilo Cortes, Luis Kabongo, Ivan Macia, Oscar E. Ruiz, and Julian Florez. Conference Innovation in Medicine and Healthcare INMED-2015, September 11-12. Chapter in Book Series Smart Innovation, Systems and Technologies, pp. 447-457, volume 45, doi: {10.1007/978-3-319-23024-5_41}, ISBN 978-3-319-23023-8, 2015, online: August 2015. Kyoto, Japan. Chapter in Book.*

Indexing: Scopus, Springerlink.

Abstract

The use of ultrasound (US) imaging as an alternative for real-time computer assisted interventions is increasing. Growing usage of US occurs despite of US lower imaging quality compared to other techniques and its difficulty to be used with image analysis algorithms. On the other hand, it is still difficult to find sufficient data to develop and assess solutions for navigation, registration and reconstruction at medical research level. At present, manually acquired available datasets present significant usability obstacles due to their lack of control of acquisition conditions, which hinders the study and correction of algorithm design parameters. To address these limitations, we present a database of robotically acquired sequences of US images from medical phantoms, ensuring the trajectory, pose and force control of the probe. The acquired dataset is publicly available, and it is specially useful for designing and testing registration and volume reconstruction algorithms.

Keywords: Ultrasound, Dataset, Registration, Reconstruction, Data Fusion, Tracking, Verification, Validation, Evaluation, Medical Images.

N.B. The publisher owns the Copyright of this chapter. The interested reader may access to the manuscript at the publisher's website.

III-D.4

Robust CT to US 3D-3D Registration by using Principal Component Analysis and Kalman Filtering

Rebeca Echeverría [1,2], Camilo Cortés[1,3], Álvaro Bertelsen[1], Iván Macía [1], Oscar E. Ruiz[3] and Julián Flórez[1]

[1] eHealth and Biomedical Applications, Vicomtech-IK4, Donostia-San Sebastián, Spain.

[2] Universidad Pública de Navarra, Pamplona, Spain.

[3] Laboratorio de CAD CAM CAE, Universidad EAFIT, Medellín, Colombia.

Context

This work is part of the *ORXXI* project. Here we present a novel registration algorithm for 3-D Ultrasound and CT images of the spine. This contribution is the result of a collaborative research between Vicomtech-IK4, the CAD CAM CAE Laboratory of EAFIT University and the Public University of Navarra. The *ORXXI* project is funded by the GAITEK program from the Basque Government.

Status: Accepted. To be published as a Chapter in Book of the series: Lecture Notes in Computer Science (LNCS), Springer.

Indexing: ISI Conference Proceedings Citation Index, Scopus, EI Compendex, INSPEC, dblp.

Abstract

Algorithms based on the Unscented Kalman Filter (UKF) have been proposed as an alternative for registration of point clouds obtained from vertebral ultrasound (US) and CT scans, effectively handling the US limited depth and low signal-to-noise ratio. Previously proposed methods are ac-

curate, but their convergence rate is considerably reduced with initial misalignments of the datasets greater than 30 degrees or 30 mm. We propose a novel method which increases robustness by adding a coarse alignment of the datasets' principal components and batch-based point inclusions for the UKF. Experiments with simulated scans with full coverage of a single vertebra show the method's capability and accuracy to correct misalignments as large as 180 degrees and 90 mm. Furthermore, the method registers datasets with varying degrees of missing data and datasets with outlier points coming from adjacent vertebrae.

Keywords: Registration, Computerized Tomography, Ultrasound, Principal Component Analysis, Kalman Filter.

N.B. The publisher owns the Copyright of this chapter. The interested reader may access to the manuscript at the publisher's website.

III-E

Motor Neurorehabilitation

III-E.1

Problem of the Estimation of the Patient Posture in Neurorehabilitation

III-E.1.1 Problem Description

In the realm of motor neurorehabilitation, the patient posture estimation consist in determining the angles of the joints of the patient limb that is under treatment. In conventional rehabilitation therapy, the joint angles of the patient limb are measured with a goniometer ([8]) (Fig. III-E.1.1). However, goniometry presents the following limitations:

(a) The angle measurements are heavily influenced by the operator visual perspective.

(b) The joint angles cannot be measured continuously.

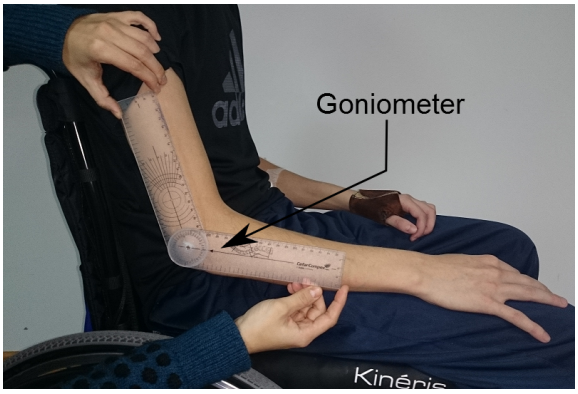

Figure III-E.1.1: Measurement of the flexion angle of the elbow joint with a goniometer.

In modern rehabilitation platforms, Virtual Reality (VR) and Robotic technologies are being integrated to boost the rehabilitation results (Fig. III-E.1.2). In such platforms, the proper estimation of the patient limb posture is a fundamental prerequisite for:

(a) Animation of realistic avatars representing the patient in VR scenarios.

(b) Verification of the compliance of the patient movements with the prescribed exercises of the therapy.

(c) Acquisition of kinematic data for long-term assessment of the patient improvement.

Hence, alternatives to goniometry are required in modern rehabilitation platforms.

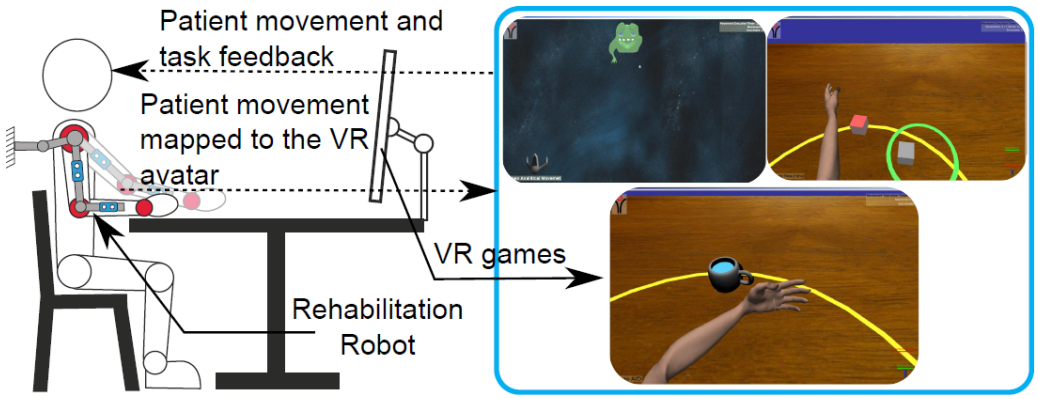

Figure III-E.1.2: Rehabilitation Platform involving Virtual Reality and Robotic Technologies.

III-E.2

Upper Limb Posture Estimation in Robotic and Virtual Reality-based Rehabilitation

Camilo Cortés[1,2], Aitor Ardanza[1], F. Molina-Rueda[3], A. Cuesta-Gomez[3], Luis Unzueta[1], Gorka Epelde[1], Oscar E. Ruiz[2], A. De Mauro[1] and Julián Flórez[1].

[1]eHealth and Biomedical Applications, Vicomtech-IK4, Mikeletegi Pasealekua 57, Donostia-San Sebastián, Spain

[2]Laboratorio de CAD CAM CAE, Universidad EAFIT, Carrera 49 No 7 Sur - 50, Medellín, Colombia.

[3]Biomechanics, Ergonomy and Motor Control Laboratory (LAMBECOM), Universidad Rey Juan Carlos, Madrid, Spain.

Context (open access material)

The *HYPER* project focuses on the development of neuro-prosthetics, neuro-robotics and virtual reality technologies to boost the rehabilitation of neuro-motor deceases, such as stroke, cerebral palsy, and spinal cord injury. This work presents a novel computational method for the estimation of the posture of the patient limbs in robot-assisted rehabilitation. This contribution is the result of a collaborative research between Vicomtech-IK4, the CAD CAM CAE Laboratory of EAFIT University and LAMBECOM from Rey Juan Carlos University. The *HYPER* project is funded by the CONSOLIDER-INGENIO 2010 program from the Spanish Ministry for Science and Innovation.

Citation: *Upper Limb Posture Estimation in Robotic and Virtual Reality-Based Rehabilitation. Camilo Cortes, Aitor Ardanza, F. Molina-Rueda, A. Cuesta-Gomez, Luis Unzueta, Gorka Epelde, Oscar E. Ruiz, A. De Mauro, Julian Florez. BioMed Research International, pages 1-18, Volume 2014, , doi: 10.1155/2014/821908, ISSN: 2314-6141, 2014. Hindawi Publishing Corporation. Journal article.*

Indexing: ISI (IF:2.7), Scopus, MEDLINE, Pubmed.

Abstract

New motor rehabilitation therapies include virtual reality (VR) and robotic technologies. In limb rehabilitation, limb posture is required to (1) provide a limb realistic representation in VR games and (2) assess the patient improvement. When exoskeleton devices are used in the therapy, the measurements of their joint angles cannot be directly used to represent the posture of the patient limb, since the human and exoskeleton kinematic models differ. In response to this shortcoming, we propose a method to estimate the posture of the human limb attached to the exoskeleton. We use the exoskeleton joint angles measurements and the constraints of the exoskeleton on the limb to estimate the human limb joints angles. This paper presents (a) the mathematical formulation and solution to the problem, (b) the implementation of the proposed solution on a commercial exoskeleton system for the upper limb rehabilitation, (c) its integration into a rehabilitation VR game platform, and (d) the quantitative assessment of the method during elbow and wrist analytic training. Results show that this method properly estimates the limb posture to (i) animate avatars that represent the patient in VR games and (ii) obtain kinematic data for the patient assessment during elbow and wrist analytic rehabilitation.

Keywords: Limb Posture Estimation, Virtual Reality, Upper Limb Rehabilitation, Robot-Assisted Therapy, Stroke.

Glossary

Clavicle	: One of the bones of the shoulder girdle. It is located at the root of the neck
DLS	: Damped Least Squares
DOF	: Degrees of Freedom
EFE	: Elbow flexion/extension
FPS	: Forearm pronation/supination
GH	: Gleno-Humeral
Humerus	: Upper arm bone
IK	: Inverse Kinematics
IMMS	: Inertial and Magnetic Measurement Systems
OTS	: Optical Tracking System
RMSE	: Root Mean Square Error
ROM	: Range of Motion
Scapula	: One of the bones of the shoulder girdle. It connects the humerus with the clavicle
SEFEFPS	: Simultaneous EFE and FPS
VR	: Virtual Reality
V-REP	: Virtual Robot Experimentation Platform
WFE	: Wrist flexion/extension
v	: Total number of constraints of the IK problem ($v \in \mathbb{N}$)
e	: IK error vector ($e \in \mathbb{R}^v$)
k	: Total DOF of the human kinematic model ($k \in \mathbb{N}$)
n	: Total DOF of the exoskeleton kinematic model ($n \in \mathbb{N}$)
Z	: Jacobian matrix of the IK problem ($Z \in \mathbb{R}^{v \times k}$)
I	: $v \times v$ Identity matrix
W_q	: Diagonal matrix of joints weights ($W_q \in \mathbb{R}^{+^{k \times k}}$)
W_e	: Diagonal matrix of constraints weights ($W_e \in \mathbb{R}^{+^{v \times v}}$)
q_{H_t}	: Vector of joint angles of the human kinematic model in instant t ($q_{H_t} \in \mathbb{R}^k$)
q_{R_t}	: Vector of joint angles of the exoskeleton kinematic model in instant t ($q_{R_t} \in \mathbb{R}^n$)
α	: Damping factor of DLS method ($\alpha \in \mathbb{R}^+$)

III-E.2.1 Introduction

Robotic and VR technologies are important components of the modern neuro-rehabilitation systems for pathologies such as stroke or spinal cord injury [9–11]. In this field, our general research has two main goals:

(a) To improve the assessment of the rehabilitation progress through precise estimation of the patient kinematics. This is the focus of this article.

(b) To optimize the rehabilitation processes by using the kinematic (and other) patient models. This optimization includes hybrid technologies (e.g. robotics, virtual reality, functional electrical

stimulation [12], etc.). Even though this domain is very important for rehabilitation, we see it as a natural consequence of (a) and we concentrate on (a) at this time.

In the mentioned scenario, the proper estimation of the patient limb posture is a fundamental prerequisite for:

1. Design and control of the advanced robotic exoskeletons which provide assistance to the patient during motor rehabilitation [13, 14].
2. Animation of realistic avatars representing the patient in virtual reality (VR) scenarios (e.g. games, bionics).
3. Acquisition of kinematic data of the patient during the training exercises to assess improvement along the therapy.

This article presents a method for estimation of limb posture from the exoskeleton posture. Notice that such an estimation is not trivial, since the limb is not rigid, is not standard and has kinematic topology different from the exoskeleton topology.

Our method delivers limb postures estimates to strengthen and to enable downstream applications in robotic rehabilitation (among others, using VR [12]).

III-E.2.1.1 Robot-based motor rehabilitation Therapy

The inclusion of robotic devices in motor rehabilitation therapies has been increasing over the last decade. The robot-assisted therapies complement conventional rehabilitation by providing intensive, repetitive, task-specific and interactive treatment. All these factors contribute to a more effective rehabilitation [15–17].

Robot-assisted therapy has shown to improve active movement, strengthening and coordination in stroke patients [18]. The majority of clinical studies have reported that robot-assisted therapy can ease impairments and lower disabilities of the affected patient [19]. Moreover, evidence suggests that task-oriented exercises using robotic devices produce significant improvements in recovering lost abilities [20].

Combining these exercises with VR games makes the therapy more attractive to the patient, increasing motivation and treatment effects [12, 21]. It is important that these games are designed to be consistent with the principles of physical therapy and adjustable to the level of impairment [22].

A central element in designing a therapy is the feedback that patients receive. To achieve relatively permanent changes in the capability for producing skilled action, it is crucial to provide the patient with proper feedback in order to produce a positive impact on the neural mechanism promoting motor learning [23].

Feedback includes all the sensory information as the result of a movement and it is divided into two classes: (1) intrinsic or inherent feedback, which is information captured by human sensory systems as a result of the normal production of the movement, and (2) extrinsic or augmented feedback, which is information that supplements intrinsic feedback [23, 24]. Robot-assisted therapy with VR games including animated realistic avatars may improve the quality and specificity of extrinsic feedback that the patient receives.

From the perspective of the therapist, robotic devices can be used to obtain quantitative metrics for the assessment of the improvement of the patient. The kinematic information of the affected

limb during the exercises is required to compute several evaluation metrics, such as joint amplitudes, speeds, movement smoothness and directional control.

III-E.2.1.2 Case Study Armeo Exoskeleton

Our proposed therapy uses the Armeo® Spring exoskeleton for the upper limb intervention (Figure III-E.2.1). We find the following limitations of this system:

1. Currently, the gaming platform provides an elementary assessment of the patient performance with metrics such as Hand Path Ratio [25] and joint range of motion, which are only available in certain games of the Armeo proprietary platform. We propose a continuous quantification of the patient performance along the treatment therapies, involving metrics that are highly correlated with the functional recovery of the patient.

2. Currently, the games only provide the patient with feedback of his hand position. We propose to provide a 3-dimensional representation of the arm, which would help the patient to immerse in the VR environment.

The kinematic data provided by the exoskeleton samples the angular position of its joints. This information cannot be used directly to represent the human arm, since the patient limb and the exoskeleton kinematic models differ significantly.

This article presents a method to estimate the posture of the limb by using the kinematic data provided by the exoskeleton. We propose to solve the limb's Inverse Kinematics (IK) problem extended with the kinematic constraints of the exoskeleton fixations on the limb. This extended problem is solved in real-time with standard robotic libraries. In this manner, we aim to overcome the limitations of the Armeo system regarding to the feedback and assessment of the patient.

Figure III-E.2.1: Armeo® Spring Orthosis.

This paper is organized as follows: Section III-E.2.2 presents a brief literature review. Section III-E.2.3 addresses the formal statement of the problem and the proposed method to solve it.

Section III-E.2.4 discusses the implementation of our approach and its use in VR games. Section III-E.2.5 presents the evaluation methodology of our approach in the realm of motor rehabilitation. Section III-E.2.6 informs and discusses the results of the experiments conducted using our solution strategy. Section III-E.2.7 concludes the article and identifies future developments.

III-E.2.2 Literature Review

Several estimation methods and human models have been proposed in the literature to solve the problem of limb posture estimation. Next, we present a brief review of developments in these areas.

III-E.2.2.1 Limb Posture Estimation

III-E.2.2.1.1 Free Movement Scenario

Most of the existing work in limb posture estimation focuses on free movement scenarios. We define a free movement scenario as a situation in which the patient limb does not wear an exoskeleton or interact with any other robotic interface. Under the mentioned conditions, literature that addresses upper limb posture estimation considers tasks in which the human subject has to reach a desired object. Therefore, these approaches are designed to estimate the posture of the upper limb based on a given target position and orientation of the hand.

Statistical [26, 27], IK [28–30] and direct optimization [31–36] methods are the most used approaches to estimate the limb posture [37].

Statistical or data-based approaches model the human kinematics with regressive models from empirical data [38]. Factors such as the size of the database of captured motions [39] and the characteristics of the population involved in the experiments impact the accuracy and usefulness of these models.

Kinematic approaches model the human limbs with links, joints of different degrees of freedom and end-effectors [35]. The IK problem is then solved with either closed-form or numerical methods. The quality of the kinematic model, and the convergence speed and robustness of the approach used to solve the IK problem directly affect the accuracy of the estimations.

Optimization approaches require a non-trivial function to minimize, which actually leads to the desired configuration (typically, a minimal energy one [39]). When optimization is used to solve an IK problem, additional constraints can be easily included in the formulation [34–36].

Approaches combining optimization-based and statistical models have been also proposed to overcome the individual limitations of optimization and statistical methods [39, 40]. Naturally, the composed method requires a high-quality dataset of motions and the formulation of proper objective and constraints functions.

III-E.2.2.1.2 Robot-assisted Scenario

There is a shortage of literature addressing posture estimation of the human limb while interacting with an exoskeleton. Although exoskeletons are designed with the ultimate goal of minimizing their kinematic differences with human limbs and interact seamlessly with them, the following factors influence the human motion patterns, and therefore the posture of the limb:

1. The mechanic design of the exoskeleton (inertia, back-drivability, friction, joint motion limits, etc.).

2. The type of assistance that the exoskeleton provides (passive, active, assist-when-needed).

3. The performance of the exoskeleton motion controller. Here, using a naive one-to-one mapping between the joint angles of the human limb and exoskeleton leads to poor positioning results [41].

References [14, 29] propose the computation of the arm's IK by using a disambiguation criteria for its redundancy which chooses a swivel angle such that the palm points to the head region. This methodology is suitable for real-time implementation and it is used in the control strategy of the active 7-DOF exoskeleton developed by the authors' research team [42]. The authors report that the mean error in the estimation of the swivel angle is less than 5 degrees. The magnitude of the errors in the estimation of the wrist, elbow and GH-joint angles is not reported.

References [14, 29] do not consider the motions of the clavicle and scapula (which affect the position of the GH-joint center) in the estimation of the posture of the arm, as they assume the position of the GH-joint center to be known. Therefore, this approach should not be used in cases in which the position of the GH-joint center cannot be determined from data provided by the exoskeleton (e.g. Armeo Spring) or by any additional motion capture system.

Other common methods to estimate the posture of human limbs cannot be used for, or are impractical in robot-assisted scenarios. For example, Inertial and Magnetic Measurement Systems (IMMSs) presented in [43, 44] are unusable because the magnetic disturbances produced by the metallic components of the exoskeleton corrupt the magnetic sensor measurements.

If optical tracking systems are used, arrays of markers need to be attached to the patient in order to measure the limb joint angles. Occlusions of such markers are frequently produced by the mechanic structure of the exoskeleton when performing the rehabilitation exercises. To overcome the occlusions of the markers, a redundant setup is necessary [37]. This limitation makes the use of optical tracking systems cumbersome for frequent use in the rehabilitation therapy.

III-E.2.2.2 Human Model

A central element in human posture estimation is the human kinematic model itself. Simple models based on hierarchies of links and lower kinematic pairs can be found in [35,45–48]. These approaches result convenient for real-time tasks and for implementation. However, more elaborated models should be used to describe complex kinematic relationships [49], such as the shoulder rhythm [50]. On the other hand, musculoskeletal models reported in [51–53] offer better accuracy for dynamics computations, since they include forces from muscles and ligaments.

The selection of the human kinematics model rests not only on the kinematic statement of the problem, but also on the compromise between accuracy and speed required in a particular application.

III-E.2.2.3 Conclusions of Literature Review

Although the methods designed to estimate the posture of the upper limb (in absence of a robotic interface) reviewed in section III-E.2.2.1.1 could be used in robot-assisted rehabilitation, we have not found any actual implementation of them in this context. Usage of these methods without any change in their design parameters in robot-assisted applications may lead to erroneous posture estimations, given the influence of the exoskeleton on human motion patterns. Therefore, the validity of these methods in the robot-assisted scenario remains to be proven. An additional limitation

of these methods is that only few of them have been validated quantitatively by determining the errors in their estimations.

On the other hand, the few posture estimation approaches that address limb interaction with an exoskeleton (section III-E.2.2.1.2) have been designed to specifically solve the arm posture estimation problem, limiting their usability in posture estimation of other human limbs.

In response to the mentioned issues, in this article we present:

1. A method that can be applied, in a general manner, to solve the limb posture estimation problem using kinematic data provided by the exoskeleton attached to the limb.
2. The implementation of our proposed method for the upper limb posture estimation using the Armeo Spring exoskeleton.
3. The quantitative validation of our proposed method by determining the estimation errors during the training of meaningful upper limb rehabilitation exercises.

III-E.2.3 Materials and Methods

III-E.2.3.1 Problem description

In this section, we state the problem of estimating the joint angles of the patient limb during robot-assisted rehabilitation therapy from the kinematic information provided by the robot. The elements that are considered inputs to the problem are the following: (1) the geometry and topology (e.g., the Denavit-Hartenberg parameters [54]) of the exoskeleton and the human limb, (2) a known configuration of the angles of the joints of the exoskeleton, (3) the kinematic constraints imposed by the fixations of the exoskeleton over the patient limb (which result from wearing the exoskeleton) and (4) the constraints that govern the posture of the patient limb while interacting with the exoskeleton, which are related to mechanical and control factors of the exoskeleton that influence the patient movement. The goal of the proposed algorithm is to find the approximate joint angles of the patient limb, such that the mentioned constraints are met.

This problem can be formally stated as follows:

Given:

1. The kinematic model of the exoskeleton $R(L_R, J_R)$, where L_R and J_R are sets of links and joints, respectively.
   (a) $L_R = \{l_{R_0}, \ldots, l_{R_{f+1}}\}$.
   (b) $J_R = \{j_{R_0}, \ldots, j_{R_f}\}$.
      i. $N(j_{R_i})$ denotes the degrees of freedom (DOF) of j_{R_i}.
      ii. $v_{R_i} = \{\theta_1, \ldots, \theta_{N(j_{R_i})}\}$ is a vector that contains the angles of each DOF of j_{R_i} $(i \in [0, f])$.
   (c) R is an open kinematic chain. Therefore, l_{R_i} and $l_{R_{i+1}}$ are connected by joint j_{R_i}, where $i \in [0, f]$.
   (d) The vector $q_R \in \mathbb{R}^n$, $n = \sum_{i=0}^{f} N(j_{R_i})$, contains the set of independent coordinates that defines a configuration of R uniquely.

i. $q_R = \{v_{R_0}, \ldots, v_{R_i}, \ldots, v_{R_f}\}$.
ii. q_{R_t} represents the state of q_R in instant t and its value is known.

2. A human patient with a kinematic model of his limb $H(L_H, J_H)$, where L_H and J_H are sets of links and joints, respectively.

   (a) $L_H = \{l_{H_0}, \ldots, l_{H_{g+1}}\}$.
   (b) $J_H = \{j_{H_0}, \ldots, j_{H_g}\}$.
      i. $N(j_{H_i})$ denotes the DOF of j_{H_i}.
      ii. $v_{H_i} = \{\theta_1, \ldots, \theta_{N(j_{H_i})}\}$ is a vector that contains the angles of each DOF of j_{H_i} $(i \in [0, g])$.
   (c) H is an open kinematic chain. Therefore, (l_{H_i}) and $(l_{H_{i+1}})$ are connected by joint (j_{H_i}), where $i \in [0, g]$.
   (d) The vector $q_H \in \mathbb{R}^k$, $k = \sum_{i=0}^{g} N(j_{H_i})$, contains the set of independent coordinates that defines a configuration of H uniquely.
      i. $q_H = \{v_{H_0}, \ldots, v_{H_i}, \ldots, v_{H_g}\}$.
      ii. The i-th element of q_H, θ_i, is subject to $h_i(\theta_i) = \theta_{min_i} \leq \theta_i \leq \theta_{max_i}$ $(i \in [0, k-1])$.
      iii. q_{H_t} represents the state of q_H in instant t and its real value is unknown.

3. A set of passive mechanisms $M = \{m_0, \ldots, m_p\}$ that connect R and H.

   (a) m_i $(i \in [0, p])$ connects l_{R_a} $(a \in [0, f+1])$ and l_{H_b} $(b \in [0, g+1])$.
   (b) m_i imposes a movement constraint of $N(m_i)$-DOF to l_{H_b} with respect to l_{R_a}.
   (c) The set $C(M) = \{c_0, \ldots, c_p\}$ contains vector-valued functions $c_i(q_{H_t}, q_{R_t}) \in \mathbb{R}^{N(m_i)}$ $(i \in [0, p])$ that model the kinematic constraint imposed by m_i.
   (d) Each $c_i(q_{H_t}, q_{R_t})$ is an equality constraint of the form $c_i(q_{H_t}, q_{R_t}) = 0$.

4. A set of vector-valued constraint functions $D = \{d_0, \ldots, d_s\}$ that intend to represent the performance measures that govern the posture of the limb in a specific situation.

   (a) Each $d_i(q_{H_t})$ $(i \in [0, s])$ is an equality constraint of the form $d_i(q_{H_t}) = 0$.
   (b) The dimension of the d_i vector is denoted by $dim(d_i)$.

Goal:

1. Find the vector $\tilde{q}_{Ht} \in \mathbb{R}^k$, which approximates q_{H_t} such that:

   (a) $c_i(q_{H_t}, q_{R_t}) = 0 \ \forall i \in [0, p]$
   (b) $h_j(\theta_j) = \theta_{min_j} \leq \theta_j \leq \theta_{max_j} \ \forall j \in [0, k-1]$.
   (c) $d_u(q_{H_t}) = 0 \ \forall u \in [0, s]$

To solve this problem, a method based on IK of the limb has been developed. The following sections describe the methodology implemented.

III-E.2.3.2 Kinematic Modeling of the Exoskeleton

The Armeo® Spring (Figure III-E.2.1) is a passive exoskeleton (orthosis) that supports the weight of the arm of the patient. The level of support provided by the system springs can be adjusted, regulating the effort of the patient arm to overcome gravity. The exoskeleton has a total of seven angle sensors to measure the position of its rotational joints and one pressure sensor to measure the gripping force at the hand [55].

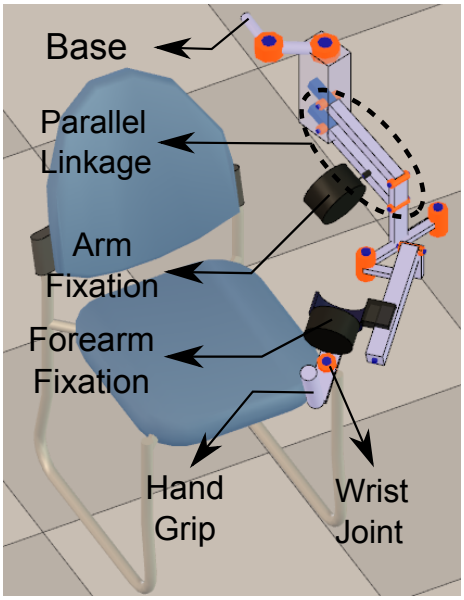

Figure III-E.2.2: Exoskeleton kinematic model.

We built a kinematic model of the Armeo® Spring (Figure III-E.2.2), which contains both prismatic and revolute joints. The prismatic joints of the exoskeleton allow to adjust it to the different sizes of the patients, and they remain fixed during the training.

Our implementation models the links and joints of the Armeo exoskeleton and creates a hierarchical structure of them.

Although the Armeo exoskeleton presents a parallelogram mechanism in its kinematic chain, the exoskeleton can be modeled with a serial chain extended with a dependency equation among the joints used to represent the parallel mechanism.

III-E.2.3.3 Kinematic Modeling of the Human Upper Body

Figure III-E.2.3 shows the kinematic model of the human upper body that we created for this application. The joints of the model are represented with green color. The upper limb is highlighted using links in light green color.

Our upper body model (33-DOF) includes joints of the spine, shoulder complex, elbow and wrist. It is based on the ones presented in [35–37, 46, 47, 56], which have been widely used in the area of human posture estimation. The main advantages of those models are their easy implementation and their suitability for solving the posture estimation problem in real-time, which is one of the main

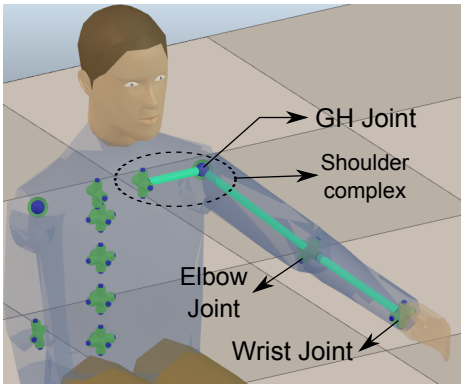

Figure III-E.2.3: Human upper body kinematic model.

requirements of our application. A weakness of those kinematic models is that the Gleno-Humeral (GH) joint is modeled with a kinematic chain of three concurrent revolute joints, orthogonal to each other. In this way, the rotation of the GH joint is parameterized with Euler angles and suffers from gymbal lock [57]. In order to avoid this limitation, the GH joint is represented in our model with a spherical joint, such that other rotation parameterizations (e.g., quaternion or exponential map) can be used.

Although there are more complex and accurate kinematic models of the upper body, the results obtained in [47], in a scenario where the subject does not interact with an exoskeleton in an application that is not related to motor rehabilitation, show that posture estimations for the upper limb can be obtained with a reasonable accuracy by using their original model.

The neutral or rest posture of the arm is defined with the arm fully extended along the body as in [58]. The range of motion of the joints of the arm obtained in [42] (derived from a motion study during the execution of activities of daily living) are used as reference to establish the joint limits of our model, which correspond to the constraint 2(d)ii in the list presented in section III-E.2.3.1.

III-E.2.3.4 Modeling the kinematic constraints of interaction of the upper limb and the exoskeleton

The Armeo provides fixations for the human limb. These fixations introduce constraints on the position and orientation of the coordinate systems attached to the arm, forearm and hand.

There are several factors that affect the satisfaction of the constraints during the execution of the exercises. This set includes: (1) deformation of the coupling mechanisms and (2) uncertainty or errors in the modeling of the human upper limb. Therefore, these constraints are exactly met only under ideal conditions and in practice they do not capture all the details of the real interaction. However, as we prove, they suffice to obtain a reasonable accuracy in the estimation of the limb posture.

III-E.2.3.4.1 Arm constraint

The arm fixation imposes a position (3-DOF) constraint on the human arm. The point on the arm that follows the position of the fixation is determined by a initialization process between the R and

H kinematic chains (see section III-E.2.3.6).

In our model, the fixations are modeled as rigid bodies. However, the exoskeleton fixations are made of flexible materials, such that their geometry is deformed when large forces are applied on them.

The arm fixation suffers significant deformation when the arm is moved towards a horizontal configuration (e.g., when performing a complete stretching of the arm along the sagittal or frontal plane). In those cases, the coordinate system at the exoskeleton arm fixation center undergoes a translation, resulting from the deformation of the fixation mechanism, that is not reproduced by our model.

To deal with this kind of situations, the weights of constraints representing fixations that suffer less deformation than other ones are adjusted such that they receive more importance when solving the IK problem. In this way, the limb posture is estimated meeting the constraints that model with more fidelity the observed behavior. In this case, the weight of the arm constraint is lower than the ones belonging to the forearm and arm restrictions.

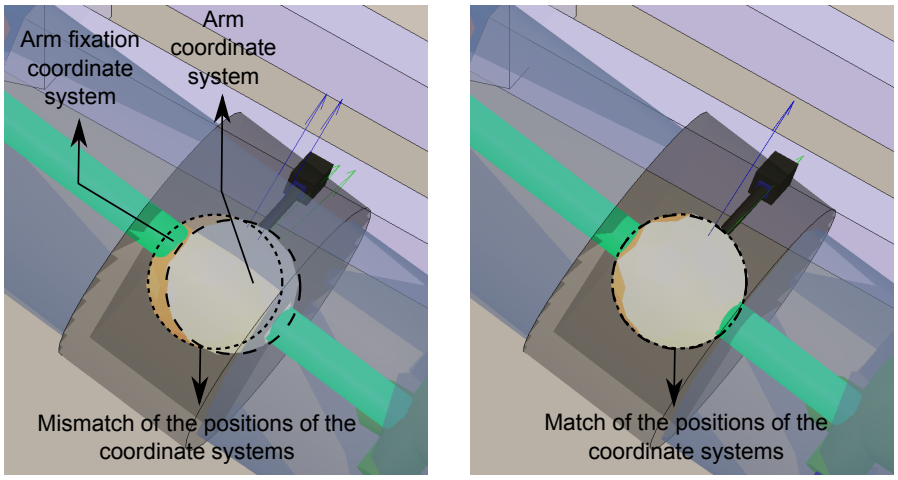

(a) Small error while meeting the arm fixation constraint

(b) Negligible error while meeting the arm fixation constraint

Figure III-E.2.4: Constraint modeling the interaction of the Armeo's arm fixation.

Figure III-E.2.4 shows the human arm (blue transparent cylinder) with the fixation of the exoskeleton for the arm (black transparent ring) around it. The constraint imposed by this fixation to the arm is represented by the matching of (a) human arm (white disk) vs. (b) fixation (yellow disk) coordinate systems. Figures III-E.2.4(a) and III-E.2.4(b) correspond to unsatisfied and satisfied constraints, respectively.

III-E.2.3.4.2 Forearm constraint

The forearm fixation imposes a 3-DOF position constraint on the human forearm. The point on the human forearm that moves together with the fixation is determined in the initializing stage. Additionally, the fixation is able to rotate around its longitudinal axis, according to the forearm

pronation/supination movement (1-DOF orientation constraint). The rotation angle is measured with an encoder. The forearm constraint forces the human wrist flexion/extension axis to be approximately aligned with the exoskeleton's wrist joint axis.

III-E.2.3.4.3 Hand constraint

The hand constraint forces the human hand to follow the position and orientation (6-DOF) of the Armeo hand grip. The patient exercises while grabbing the handle of the exoskeleton. The mechanic design of the Armeo avoids the slippage of the hand with respect to the axis of the handle during the execution of the exercises. As with the previous fixations, the point on the hand where the coordinate system of the hand is located is calculated in the initialization stage.

III-E.2.3.4.4 Shoulder constraint

The shoulder constraint does not belong to the set of movement restrictions imposed by the coupling mechanisms of the Armeo. Instead, it is related to the restrictions intended to produce a natural posture of the upper limb considering also the influence of the exoskeleton on the patient movements. This constraint helps to disambiguate among the multiple configurations of the human kinematic chain that comply with the other categories of constraints.

Currently, it is implemented to attract the GH joint to a position (3-DOF position constraint) below the first joint of the Armeo (j_{R_0} joint represented with symbol A in Figure III-E.2.6), which does not suffer any translation during the training of the patient. By keeping the GH joint near j_{R_0} comfortable postures for the spine and arm can be achieved.

Figure III-E.2.5 shows that the shoulder constraint prevents the excessive motion of the joints of the spine, which is a compensatory movement that should be also avoided during the rehabilitation therapy. The shoulder constraint is central to proper posture estimation during shoulder abduction.

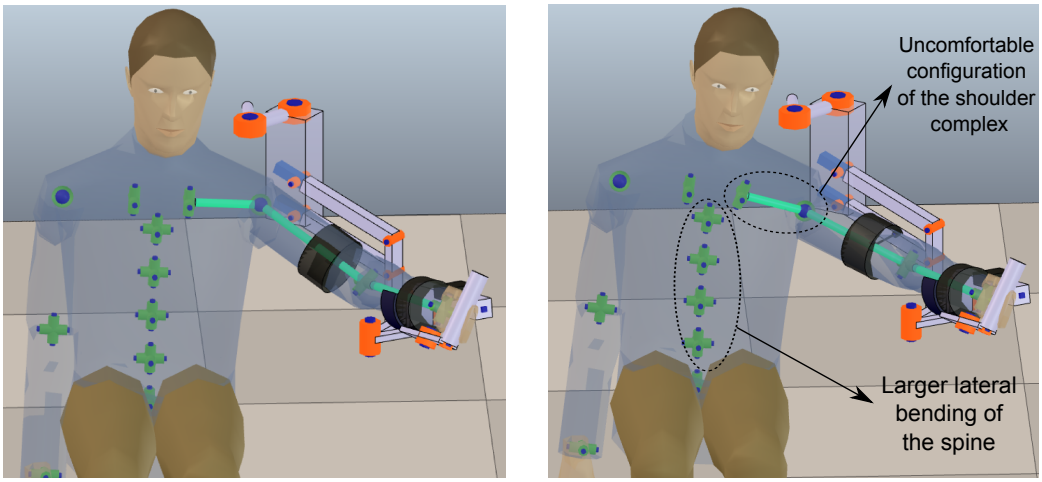

(a) Estimation using the shoulder constraint

(b) Estimation without using the shoulder constraint

Figure III-E.2.5: Effect of the shoulder constraint in the upper limb posture estimation.

III-E.2.3.5 Inverse Kinematics

Given a desired pose (position and orientation) vector $T_r \in \mathbb{R}^6$ for the end-effector of an open kinematic chain r, the IK problem is to find the vector of angles of the robot's joints $q_r \in \mathbb{R}^N$ (where N corresponds to the DOFs of r), such that the difference $e = T_r - X_r$ between T_r and the actual pose of the end-effector of r, $X_r \in \mathbb{R}^6$, approaches zero.

There are several approaches to solve this problem, including analytic [59] and numerical methods [60, 61]. The iterative strategy used to solve the IK problem is based on the Jacobian matrix of the manipulator $Z(q_r)$, which linearly relates the velocity of the end-effector and the joints by:

$$\dot{X}_r = Z(q_r)\dot{q_r} \tag{III-E.2.1}$$

By replacing ΔX_r for e in Eq.III-E.2.2, which is obtained by discretizing Eq.III-E.2.1, the necessary Δq_r to approximate T_r is obtained.

$$\Delta q_r = Z(q_r)^{-1}\Delta X_r \tag{III-E.2.2}$$

Notice that $Z(q_r)$ may not be square (consider for example a kinematic chain with more than 6-DOF) or invertible. In those cases, the pseudo-inverse and Damped Least Squares (DLS) methods (among others) can be used to obtain Δq_r, such that $\|e\|$ is minimized. The pseudo-inverse method is computationally faster than the DLS, but tends to be unstable when the robot approaches to a singular configuration. The DLS method offers more robustness (specially when T_r is out of reach) at the cost of a slower convergence [60].

III-E.2.3.5.1 Relation among End-effectors and Targets

The aforementioned strategy to solve the IK problem, can also be used in situations in which the manipulator has more than one end-effector. In this case, the error vector e is given by $e = \{T_{r_1} - X_{r_1}, \ldots, T_{r_i} - X_{r_i}, \ldots, T_{r_{Nee}} - X_{r_{Nee}}\}$ where Nee is the number of end-effectors of the robot. Notice that vector $e_i = T_{r_i} - X_{r_i}$ is not necessarily a point $\in \mathbb{R}^6$. For example, if only the position (and no the orientation) of the i-th end-effector is specified, $e_i \in \mathbb{R}^3$.

In our application, the formulation of the IK problem with multiple end-effectors and targets can be used to represent the constraints discussed in section III-E.2.3.4. In this way, each constraint can be represented by a target and end-effector pair. The coordinate frames of the end-effectors $X_{H_i}(q_{H_t})$ $(i \in [1, \ldots, Nee])$ are attached to the human limb, so their position and orientation depend on the current configuration of the limb, q_{H_t}. The coordinate frames of the targets of the limb $T_{H_i}(q_{R_t})$ $(i \in [1, \ldots, Nee])$ are attached to the exoskeleton, such that they are transformed according to its current configuration q_{R_t}. Then, the IK problem is solved for the limb, finding q_{H_t} such that $e_i = \|T_{H_i}(q_{R_t}) - X_{H_i}(q_{H_t})\| \approx 0$ $(i \in [1, \ldots, Nee])$. Notice that if e_i represents a kinematic constraint, $e_i \in \mathbb{R}^{N(m_i)}$ where $i \in [0, p]$. Otherwise, e_i represents a restriction related to the natural posture of the limb, and therefore $e_i \in \mathbb{R}^{dim(d_i)}$ where $i \in [0, s]$, and $Nee = p + s + 2$.

Notice that, due to modeling inaccuracies of the kinematic chains or the constraints, it is possible that for a configuration q_{R_t} some constraints cannot be satisfied within the desired tolerance. That situation can be interpreted as if some targets $T_{H_i}(q_{R_t})$ are not reachable. It is important that the method used to solve the IK problem handles this situation robustly, avoiding oscillations. For this reason the DLS method was used.

III-E.2.3.5.2 Joints and Constraint Weights

References [46, 47] state that giving more importance to some of the model joints over others, by assigning weights to the joints, allows to estimate more accurately the posture of the human limb.

Let us assume that w_{J_i} is the weight of joint J_{H_i} and that joints J_c and J_d can contribute to the movement of end-effector i to diminish e_i. Then, if $w_{J_c} > w_{J_d}$, the displacement that J_c performs is larger than the one done by J_d. This means that J_c is preferred to be moved over J_d to reach a desired target.

In our model, the weights of the joints of the upper body were adjusted such that the joints on the spine of the model perform small displacements in comparison with the movement performed by the shoulder, elbow and wrist joints.

On the other hand, applying weights to the error vector e gives more importance to reach a specific target over others. In our approach, this translates into giving some constraints more importance than others. Let us define with w_{c_i} $(i \in [0, p])$ the weight of the c_i constrain and with w_{d_u} $(u \in [0, s])$ the weight of d_u constraint.

In our model, high weights were adjusted for the kinematic constraints imposed by the exoskeleton fixations ($w_{c_i} \approx 1.0$). Otherwise, low weights ($w_{d_i} \approx 0.2$) were assigned to the other type of constraints.

There are different formulations of the DLS method that incorporate weights for the joints and error vector (e.g., reference [62]). In V-REP, the following DLS formulation is used to solve IK problems: The angles of the joints of the human model are given by $q_{H_t} = \sqrt{W_q} q_{H_{t_w}}$, where $q_{H_{t_w}} = Z_w^* e_w$ and $Z_w^* = Z_w^t (Z_w Z_w^t + \alpha I)^{-1}$. The weighted Jacobian matrix is given by $Z_w = Z\sqrt{W_q}$ where $W_q = diag\{w_0, \ldots, w_{k-1}\}$. Here, if w_a and w_b are related to J_{H_i} (e.g., a joint with DOFs > 1), $w_a = w_b = w_{J_i}$. The weighted error vector is given by $e_w = W_e e$, where $W_e = diag\{w_0, \ldots, w_{v-1}\}$ and $v = \sum_{i=0}^{p} N(m_i) + \sum_{j=0}^{s} dim(d_j)$. If w_a and w_b are related to the same c_i constraint, $w_a = w_b = w_{c_i}$. This also applies for weights related to constraints d_u. However, independent weights can be assigned for the position and orientation components of a constraint.

III-E.2.3.6 Initialization of the kinematic chains

To accurately estimate the limb posture, it is required to properly couple the human and exoskeleton kinematic models. To do so, we require to correctly position the end-effectors of the human kinematic model with respect to the arm, forearm and hand coordinate systems. These end-effectors must be positioned such that they are able to move together with the coordinate systems of the fixations of the exoskeleton model (targets). Notice that the position of the end-effectors with respect to the links of the human model changes according to the actual patient and exoskeleton dimensions.

Figure III-E.2.6 depicts an state in which the human and exoskeleton models are decoupled. The correct position and orientation of the coordinate systems of the end-effectors of the human model have not been calculated, and therefore, they do not match the position and orientation of the exoskeleton's fixations coordinate systems.

The initialization of the kinematic chains requires a reference pose of the exoskeleton in which (a) the human joints angles can be determined accurately and (b) the exoskeleton's fixations undergo negligible deformation, reducing the uncertainty about the position of the human model end-effectors.

The pose of the exoskeleton that meets the mentioned requirements is the one in which the flexion/extension of the shoulder and elbow take place in the sagittal plane (Figure III-E.2.6). In

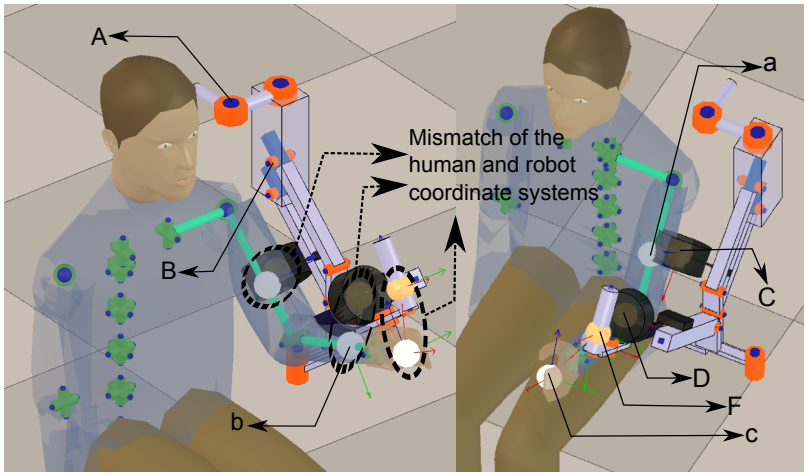

Figure III-E.2.6: State of the kinematic chains before the initialization process (notation in Table III-E.2.1).

Table III-E.2.1: Glossary related to the Figure III-E.2.6.

Symbol	Description
A	j_{R_0}
B	j_{R_2}
C	Arm fixation coordinate system
D	Forearm fixation coordinate system
F	Armeo hand grip coordinate system
a	Human arm end-effector coordinate system
b	Human forearm end-effector coordinate system
c	Human hand end-effector coordinate system

this pose, the position of the human GH joint with respect to the exoskeleton base can be easily determined because the joints of the spine and shoulder complex are in their rest position.

The coupling process involves the following steps:

1. Position the exoskeleton model such that the joint j_{R_0} lies above the human GH joint. Adjust the height of the exoskeleton model such that j_{R_2} is at the level of the human GH joint. These instructions are prescribed by the manufacturer of exoskeleton to use it with the actual patient.

2. Compute the arm flexion and abduction angles such that the arm passes through the origin of the arm fixation coordinate system. Adjust the origin of the arm end-effector coordinate system to match the origin of the arm fixation.

3. With the position of the elbow joint defined, compute the elbow flexion and the GH internal rotation angles such that the forearm passes through the origin of the exoskeleton forearm

fixation. Adjust the origin of the forearm end-effector coordinate system to match the origin of the forearm fixation.

4. Compute the wrist extension angle such that the human hand is able to grasp the exoskeleton's hand grip. Adjust the hand end-effector to match the position of the Armeo's end-effector at the hand grip.

5. Calculate the forearm pronation/supination angle such that the wrist's extension/flexion axis matches the orientation of the Armeo's hand grip longitudinal axis with respect to the human forearm pronation/supination axis.

6. Adjust the human forearm and hand end-effector coordinate systems to match the orientation of the forearm and Armeo's end-effector coordinate systems respectively.

The result of the initialization process is depicted in Figure III-E.2.7.

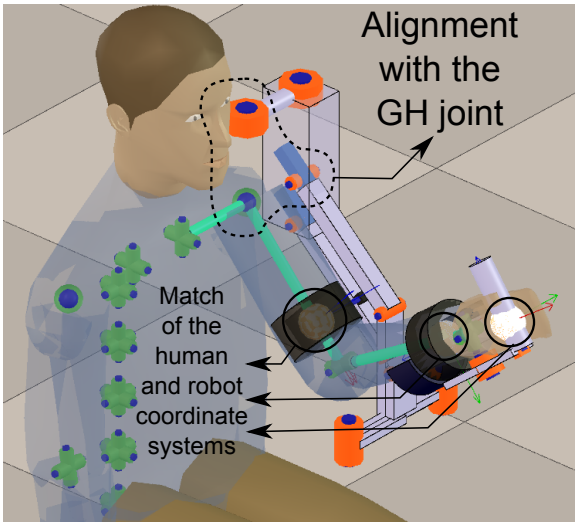

Figure III-E.2.7: Result of the initialization procedure.

III-E.2.4 Implementation

To implement the proposed method the Virtual Robot Experimentation Platform (V-REP) was used [63], which is an open source robotics simulator. V-REP provides tools to easily and efficiently create kinematic models of rigid multi-body systems and to solve IK problems. Using the simulator, a scene was created, which contains both the human upper body and Armeo kinematic models (Figures III-E.2.2 and III-E.2.3). The weights of the human kinematic model were adjusted (section III-E.2.3.5.2) and the simulator's IK module was configured to include the kinematic constraints (section III-E.2.3.4).

The source code of the simulator was compiled, modified and integrated into our rehabilitation platform. Custom classes and functions were programmed to allow easy data exchange among the Armeo, the rehabilitation game platform and the IK module of the simulator.

The limb posture estimation process consists of the following steps:

1. Obtain the angles of the Armeo's joints by using hardware and software interfaces provided by Hocoma [55].
2. Use the obtained angles to update the joints angles of the Armeo's kinematic model in the simulator.
3. Retrieve the angles of the joints of the human model computed by the simulator's IK module.

Computing the inverse kinematics of our upper limb kinematic model, once the Armeo model is updated in the simulator with the real joint measurements of the exoskeleton, takes less than 4ms on a 2.13 GHz dual-core CPU. Therefore, the implemented method is suitable for real-time posture estimation without using high-performance hardware.

After the joint estimates are produced, we use them to update the patient avatar in VR games. We also store them in a database for a posterior patient assessment.

Figure III-E.2.8 presents an user test of the limb posture estimation algorithm feeding the Armeo kinematic model in the simulator (in real-time) with the Armeo Spring joint positions measured by its encoders. This figure presents the posture of the test subject and Armeo Spring in parallel with estimations of the user posture in the simulator. The test subject performed:

(a) Reaching exercises, in which the subject recreated the postures of his arm to reach and grab objects that are close to his body (Fig.III-E.2.8(a)). These exercises are frequently practiced during the arm rehabilitation.

(b) Extreme region exercises, in which the subject positioned his hand in the boundaries of his arm workspace (Fig.III-E.2.8(b)). These exercises result challenging for the subject and are less likely to occur during the therapies due to its difficulty.

III-E.2.4.1 VR Games

Currently, we have implemented two types of games for the robot-assisted upper limb rehabilitation therapy. The first type of games focuses on the rehabilitation of reaching movements. The second type of games addresses the rehabilitation of analytic movements of the GH, elbow and wrist joints.

III-E.2.4.1.1 Reaching rehabilitation

Reaching rehabilitation is performed by training the movements that are required to reach and grasp objects with the hand. These exercises involve several joints of the upper limb, and therefore, they are considered complex.

To train these exercises, we have programmed a game in which the patient controls the movement of a virtual human arm by moving his own arm (Fig. III-E.2.9(a)). The target of the patient is to reach a specific object (e.g. cube) in the scene, grab it, and bring it to a releasing area (e.g. green circle).

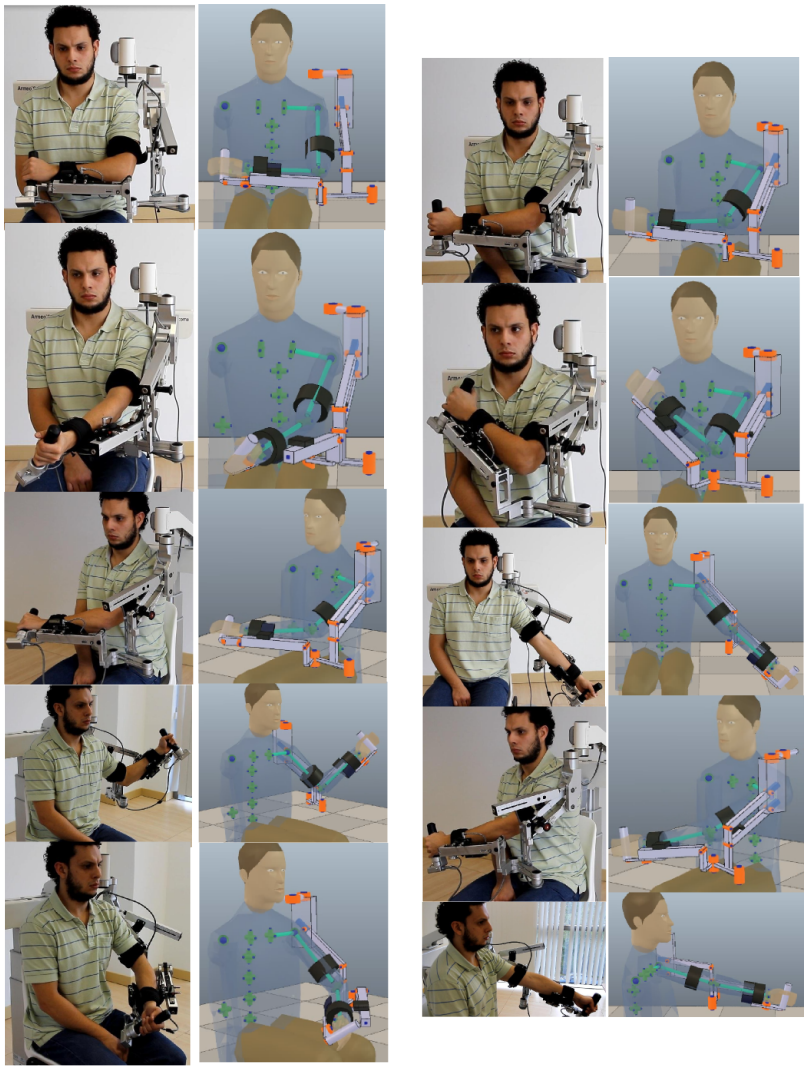

Figure III-E.2.8: Test subject in parallel with estimations of his posture in the simulator. Subfigure (a) shows reaching exercises and Subfigure (b) shows extreme region exercises.

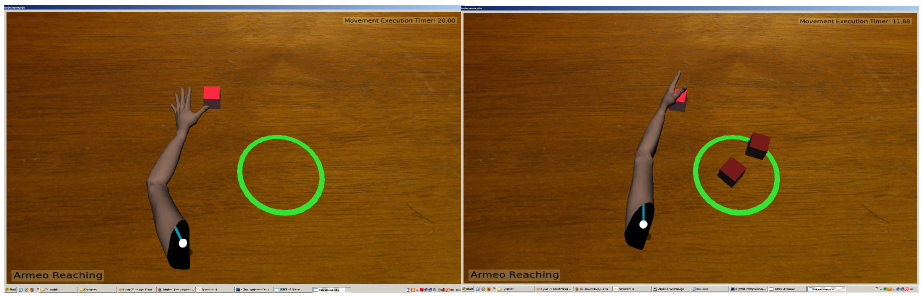

(a) Reaching game

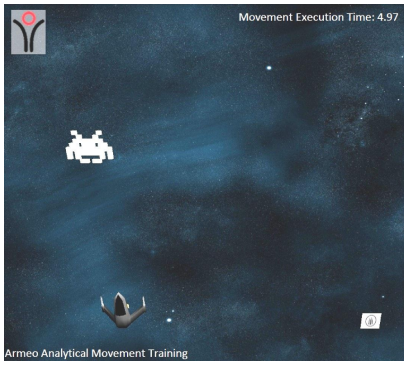

(b) Analytic game

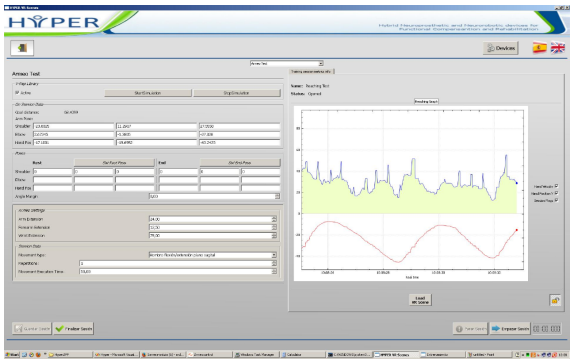

(c) Medical Interface

Figure III-E.2.9: Games and Medical Interface.

III-E.2.4.1.2 Analytic movements rehabilitation

According to motor learning theories, the training of analytic movements constitute the first step into learning complex motor tasks. In such a step, simple movements involving few DOFs of the limb are practiced [64–66].

For this scenario, we have programmed a game (Fig. III-E.2.9(b)) in which the patient controls the position of a spaceship, along the horizontal axis of the screen, by performing 1-DOF movements with the wrist, elbow or GH joint. The target of the game is that the patient positions the spaceship under an alien that moves along a vertical path from the top to the bottom of the screen. When the position of the spaceship is correct, it fires a gun and destroys the alien.

For both games, the limitations of the mobility of the patient are identified in a calibration phase, guarantying that the target of the games is properly located. Other game parameters (number of executions, max execution time per task, target size, etc.) are adjusted through the medical interface (Fig.III-E.2.9(c)). The medical interface allows the physician to select the games for the training, configure its parameters and review metrics related to the performance of the patient during a game.

The VR games were programed with the OpenSceneGraph API [67], which allows to animate deformable virtual objects and create scenes with dynamic simulations using the Bullet Physics package. The graphic rendering of the VR Game runs at 30 frames per second using a ATI Radeon HD 4600 GPU, which is a mid-range graphic card.

During the therapy, the patient sees the VR scene. The kinematic models are used for IK computations and they are not displayed.

III-E.2.5 Evaluation

In order to determine the accuracy of our developed method, the joint angles of 4 voluntary healthy male test subjects (average age 34 years) were measured by using an optical tracking system and compared with the angles obtained from our posture estimation algorithm during the execution of typical (in this case, analytic movements) robot-assisted rehabilitation exercises. As discussed in section III-E.2.4.1.2, the rehabilitation of analytic movements is a necessary step before addressing the rehabilitation of complex motor tasks.

The specific exercises performed by the test subjects were:

1. Wrist flexion/extension (WFE)
2. Elbow flexion/extension (EFE)
3. Forearm pronation/supination (FPS)
4. Simultaneous elbow flexion/extension and forearm pronation/supination (SEFEFPS)

The evaluation of our method has been conducted without performing any previous setting or automatic adjustment of the weights or other parameters of the approach in order to reduce the estimation errors. However, algorithm training might be used in the future to improve the method's performance.

III-E.2.5.1 Measurement of the upper limb joint angles

A detailed explanation of the method that was used to measure the human joint angles would merit an additional manuscript. Nevertheless, a basic description of this method is provided next.

In order to measure the limb joint angles of the test subject, we use a Polaris Spectra® optical tracking system (OTS) [68]. In order to track the limb movements, it is necessary to install on test subject limb a set of rigid bodies with passive markers. By detecting these passive markers (reflective spheres), the OTS is able to compute the position and orientation of each rigid body.

One rigid body (reference rigid body) is used as the coordinate system of reference for the measurements of the OTS. The position and orientation of the other rigid bodies (mobile rigid bodies) are computed with respect to the reference rigid body.

The reference and mobile rigid bodies are installed on different arm segments (i.e., upper arm, forearm and hand) according to the joint angle to be measured. Table III-E.2.2 shows the installation of the reference and mobile rigid bodies for each of the joint angles that we measured. Fig.III-E.2.10 shows the configuration of the rigid bodies to measure the elbow flexion/extension angle.

Table III-E.2.2: Installation of the reference and mobile rigid bodies in the evaluation.

Angle to measure:	**Reference rigid body installed on:**	**Mobile rigid body installed on:**
WFE	Forearm	Hand
EFE	Upper arm	Forearm
FPS	Upper arm	Forearm

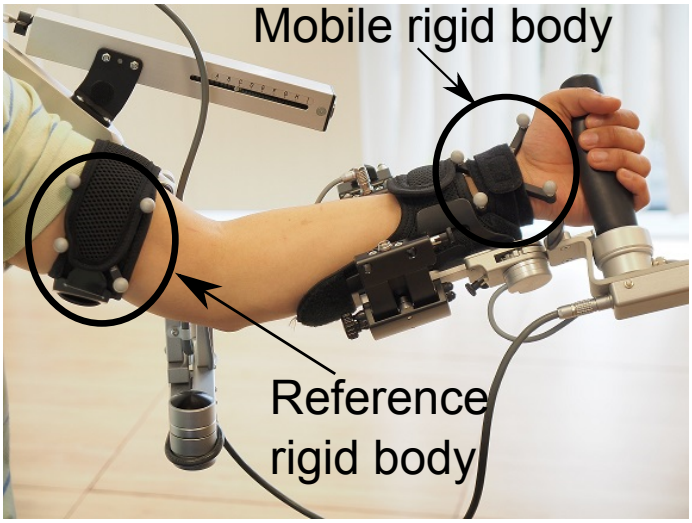

Figure III-E.2.10: Setup for the quantitative assessment of the estimation errors in elbow flexion/extension exercise.

In order to measure the human joint angles, we have adapted the method presented in [69],

which is originally proposed to be used with IMMSs, to implement it by using an OTS. In [69] it is proposed to measure the joint angles by following the next steps:

1. Compute a reference coordinate system for the joint of interest. A subset of the axes of the resulting coordinate system match with the axes of rotation of the joint. The position and orientation of the joint coordinate system is defined with respect to the reference rigid body.
2. Compute the orientation of the mobile rigid body with respect to the joint coordinate system.
3. Compute the joint angles that result from rotations of the mobile rigid body by using Euler-angles decomposition. The rotations of the mobile rigid body are caused by the exercising of the subject joint.

To build an orthogonal right-handed coordinate system of reference for the joint, we identify each axis of rotation of the joint, as proposed in [69].

To identify each rotation axis of the joint, we use the instant helical axis method described in [70]. A rotational axis of the joint is computed from the kinematic data of the mobile rigid body while the subject performs 1-DOF movements of the joint.

In contrast to the proposal presented in [69] to compute the wrist joint coordinate system, we build this coordinate system by identifying only the flexion/extension axis, given that the ulnar/radial deviation cannot be trained with the Armeo Spring.

Accuracy of the limb joint angles measurement method

In motor rehabilitation, *goniometry* is the standard method to measure the angle at the patient joints. This is a manual method, and therefore, its efficacy depends on the examiner experience [71]. One of the limitations of this method is that it provides a resolution (minimal detectable change) in measuring limb joint angles of about 8 degrees [72]. In other words, this method should not be used to measure angles smaller than 8 degrees, because in those cases measurements present large uncertainty.

Alternative approaches to measure the patient limb joint angles are IMMS-based methods. One of the methods that provide better accuracy than goniometry is presented in [43]. This method provides a measurement accuracy characterized by a RMSE of less than 3.6 degrees. The authors of the mentioned work conclude that this accuracy is proper for measuring elbow and shoulder angles of clinical relevance in ambulatory settings.

In tests with an artificial 1-DOF joint, the method to measure the limb joint angles that we have adapted from [69], allowed us to estimate the joint angle with a RMSE smaller than 1 degree. According to a comparison with the accuracy provided by the reviewed methods, we conclude that the method proposed by [69] to measure the limb posture is valid to determine the accuracy of our proposed limb posture estimation method.

III-E.2.5.2 Protocol

Table III-E.2.3 summarizes the main features of the evaluation that we have conducted.

For each trial of the evaluation exercises we performed the following steps:

1. Compute the joint coordinate system corresponding to the evaluation exercise (section III-E.2.5.1).
2. Instruct the subject to perform the corresponding evaluation exercise until the number of desired joint angle measurements are taken.

Table III-E.2.3: Summary of main features of the evaluation tests.

Number of test subjects	**Number of exercises performed by each test subject**	**Number of trials per exercise**	**Joint angles measurements per trial**
4	4 (WFE, EFE, FPS and SEFEFPS)	4	2960 at 66.6 Hz

3. Compute the RMSE in the estimation of each joint angle by comparing the measured angle with the estimation provided by our algorithm.

4. Compute the ROM of the subject movements from the measured angles.

During the execution of the evaluation exercises the amplitude, speed and the number of cycles of the movements in each trial were left to the discretion of each test subject. In the evaluation, the VR games were not executed, given that they are not necessary to assess the accuracy of the posture estimation algorithm. Furthermore, in this way the influence of the VR games on the subject movement amplitude, speed and repetitions is avoided, which derives in a richer variety of movement features in the evaluation exercises.

However, it is worth mentioning that the joint limits of the exoskeleton, the need to avoid occlusions of the passive markers on the rigid bodies attached to the test subject, and the limited detection volume of the OTS do constraint the subject's movements.

III-E.2.6 Results and Discussion

In this section, we present the results of the experiments described in section III-E.2.5. Tables III-E.2.4, III-E.2.6, III-E.2.7 and III-E.2.8 (angles expressed in degrees) present the average RMSE obtained in the estimation of the angle of interest by using our proposed algorithm. Each table presents the average ROM of the movement performed by each test subject. The average RMSE and ROM metrics mentioned previously are obtained from the 4 trials that each subject performed for each exercise. The last row in the tables presents the average values of each of the computed metrics for all subjects.

N.B.: in this section we compare our results against freely moving subject cases reported in literature. We resort to such free movement cases since we found no reports concerning estimations errors of the wrist or elbow angles in limbs constrained with exoskeletons.

III-E.2.6.1 Wrist Flexion/Extension

Table III-E.2.4 presents angle estimation statistics for Wrist Flexion and Extension. The ROM exercised by the subjects presents small variability and seems not to correlate with RSME. However, we did observe that subjects 1 and 2 performed slow movements while subjects 3 and 4 moved fast. Such a difference reflects on the RMSE values.

To elaborate on this point, we present in Fig.III-E.2.11 the history of the measured vs. estimated angle, for subjects 1 and 3. The sampling span is 250 (approx. 3.75 seconds). The motion features

Table III-E.2.4: Estimation errors in wrist flexion/extension exercise (units in degrees).

Subject	**Average WFE RMSE**	**Average WFE ROM**
1	1.137	53.389
2	1.432	54.824
3	3.282	63.869
4	3.555	53.977
Average	2.351	56.265

of the movements shown in Fig.III-E.2.11 are summarized in Table III-E.2.5. In such table, the time delay aspect refers to the time delay that the estimations provided by our algorithm present with respect to the measured angles. The time delay is larger when the subject moves fast. This causes the increment in the RMSE estimation values.

These results suggest that the response speed of our algorithm, given a change in the Armeo joint angles caused by the movement of the human subject, allows to provide better estimates when the subject moves slowly (as in rehabilitation therapy). In our algorithm, the response speed largely depends on the damping constant used in the DLS method to solve the limb's IK. By using a smaller damping constant in the DLS method, the response speed can be improved, sacrificing some stability.

Table III-E.2.5: Motion features for subjects 1 and 3 in WFE exercise.

Aspect	**Subject 1**	**Subject 3**
Average Angular Speed (deg/s)	26	82
Time Delay (ms)	15	60

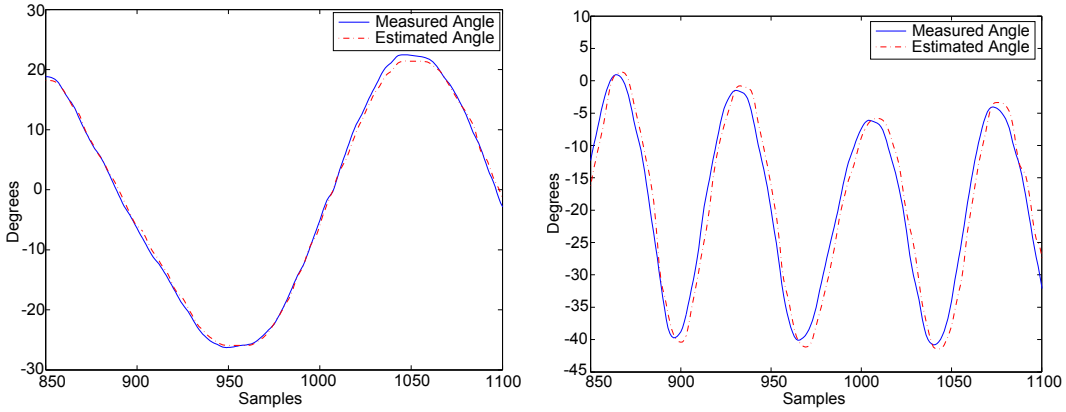

(a) Motion of subject 1

(b) Motion of subject 3

Figure III-E.2.11: Motion patterns of subjects 1 and 3 during a trial of wrist flexion/extension.

Nevertheless, the average RMSE obtained for all subjects shows a better performance of our method with respect to reference [47], an optimization-based approach which presents errors around

3.5 degrees. Compared to reference [44], which presents a IMMS-based method to estimate the wrist angles with a RMSE of less than 3 degrees, our results are slightly better.

III-E.2.6.2 Elbow Flexion/Extension

In flexion and extension of elbow (Fig. III-E.2.12, Table III-E.2.6), involuntary movement along the pronation/supination axis is not avoided. Therefore, small excursions in this DOF were observed.

For all subjects, our method over-estimates the amplitude of rotational movements about the flexion/extension axis, when compared against the measured values (see Fig.III-E.2.12(a) for subject 2).

Table III-E.2.6: Estimation errors in elbow flexion/extension exercise (units in degrees).

Subject	**Av. EFE RMSE**	**Av. EFE ROM**	**Av. FPS RMSE**	**Av. FPS ROM**
1	1.636	36.948	0.980	4.148
2	1.553	33.897	1.408	4.921
3	2.815	49.333	2.187	5.216
4	4.381	36.442	1.128	7.160
Average	2.596	39.150	1.426	5.361

Our method performs better than the one in reference [47], in which the reported mean error in estimating the flexion/extension angle is approximately 14 degrees. Compared to the approach in reference [43], which uses a IMMS-based method, and presents a RMSE of 3.6 degrees in estimating elbow and shoulder angles, our method also presents better performance.

We include in Table III-E.2.6 the estimation statistics for pronation/supination angle in order to illustrate the performance of our method with small angular displacements. Fig.III-E.2.12(b) displays the estimation and measurement of pronation/supination angle for a trial of subject 2. In this figure, we observe that there is a under-estimation of the angle. However, it must be taken in account that estimation errors for small ROMs are in the same order of the measurement method accuracy (RMSE : 1 degree).

III-E.2.6.3 Forearm Pronation/Supination

Table III-E.2.7 and Fig.III-E.2.13 show the statistics of our method for forearm pronation/supination angle estimation. We remark that motion in the elbow flexion/extension axis may occur during the forearm pronation/supination exercise. Therefore, we also report (in Table III-E.2.7 and Fig.III-E.2.13) the estimation results for the small angular movements around the flexion/extension axis.

The average RMSE in the estimation of the pronation/supination DOF of our method presents an accuracy similar to the one of reference [43] (RMSE 3.6 degrees).

Figure III-E.2.13 shows the elbow angles estimation results for a trial of the FPS exercise of subject 1. Fig.III-E.2.13(a) shows that estimations in the flexion/extension DOF, in which small movements were performed, do not present the oscillations of the measured angle (RMSE 1.175 degrees). On the other hand, Fig.III-E.2.13(b) shows that estimations of the pronation/supination angle are very close to the measured values.

For the pronation/supination angle, the worse estimations were obtained for subject 4, who performed short but very fast movements, affecting the estimation accuracy as described in section III-E.2.6.1.

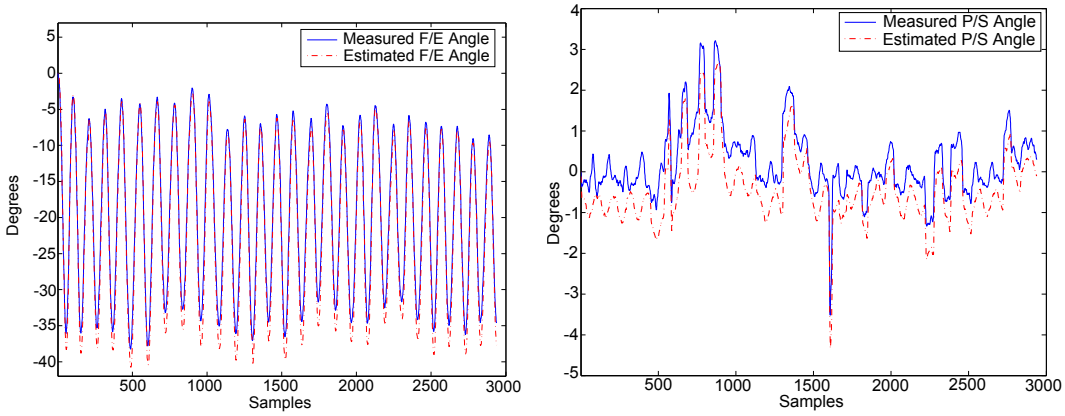

(a) Estimation results of the flexion/extension angle (b) Estimation results of the pronation/supination angle

Figure III-E.2.12: Estimation results of the elbow angles during flexion/extension for trial of subject 2.

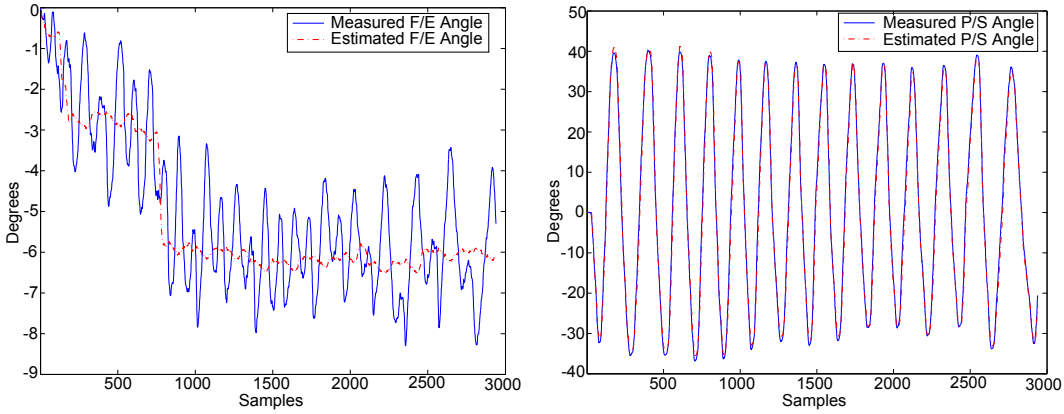

(a) Estimation results of the flexion/extension angle (b) Estimation results of the pronation/supination angle

Figure III-E.2.13: Estimation results of the elbow angles during pronation/supination for a trial of subject 1.

Table III-E.2.7: Estimation errors in forearm pronation/supination exercise (units in degrees).

Subject	Av. EFE RMSE	Av. EFE ROM	Av. FPS RMSE	Av. FPS ROM
1	1.221	5.799	1.965	70.453
2	1.799	7.395	2.639	48.500
3	1.627	9.691	4.147	90.527
4	1.132	2.459	4.568	37.717
Average	1.445	6.336	3.330	61.799

According to results presented here and in section III-E.2.6.2, it seems that for small movements the estimation approach is slightly more sensitive to movements in the pronation/supination DOF than on the flexion/extension DOF.

III-E.2.6.4 Simultaneous Elbow Flexion/Extension and Forearm Pronation/Supination

Table III-E.2.8: Estimation errors in simultaneous elbow flexion/extension and forearm pronation/supination exercise (units in degrees).

Subject	Av. EFE RMSE	Av. EFE ROM	Av. FPS RMSE	Av. FPS ROM
1	2.224	35.762	2.707	59.878
2	2.773	40.837	3.037	58.441
3	5.212	47.850	4.429	55.228
4	2.679	36.654	2.158	59.673
Average	3.222	40.276	3.083	58.305

The objective of this exercise is to evaluate how simultaneous movements of both DOFs of the elbow affect the angle estimations for this joint. The results are presented in Table III-E.2.8. In this table, it is shown that, for both elbow DOFs, the average of the RMSE for all the subjects is similar to the one presented in [43] (RMSE 3.6 degrees).

This result also suggests that during the performance of a functional rehabilitation exercise, such as reaching, in which simultaneous flexion/extension and pronation/supination movement is necessary, the accuracy of the estimations would remain in an adequate range.

Figure III-E.2.14 presents the estimation results of a trial of this exercise of subject 4. In this figure, it can be observed that estimations follow closely the measured angles.

III-E.2.7 Conclusions and Future Work

This article presents a method that can be applied to estimate the posture of the human limbs during the interaction with exoskeletons by solving the limb IK problem extended with the kinematic constraints of the exoskeleton fixations on the limb. The few approaches in the literature that deal with limb posture estimation in a robot-assisted scenario are specifically designed to estimate the arm posture. In contrast, the method that we propose provides a general formulation, which is not specific to any human limb or exoskeleton. Our method is based on inverse kinematics and it can be implemented using standard robotics libraries.

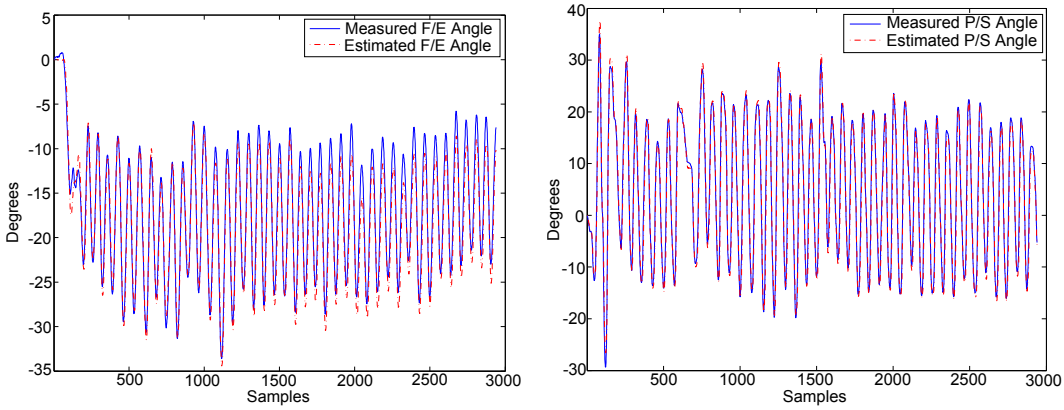

(a) Estimation results of the flexion/extension angle (b) Estimation results of the pronation/supination angle

Figure III-E.2.14: Estimation results of the elbow angles during simultaneous flexion/extension and pronation/supination for a trial of subject 4.

In this paper, we have also shown the implementation of the method to provide upper limb posture estimations, in real-time, using the Armeo® Spring. We have also presented the use of the resulting limb postures estimations in the animation of avatars in VR rehabilitation games.

We have evaluated the accuracy of the estimations of our method during the performance of analytic rehabilitation exercises of the wrist and elbow. The obtained results show that our approach presents an accuracy that is better than the one provided by goniometry, which is the traditional method to measure the patient angles in motor rehabilitation. Compared to the accuracy provided by IMMSs-based methods, which are considered enough accurate to measure clinical relevant limb joint angles in non robot-assisted scenarios, we have obtained very similar results.

Based on the mentioned results, we conclude that our approach can be used to (a) provide a estimation of the pose of the human upper limb with enough accuracy to be used for avatar animation in VR games and (b) to obtain the kinematic data for the patient assessment during analytic training of the elbow and wrist.

Future work includes (a) the exploration of other approaches to model the flexible fixations of the exoskeleton, (b) the definition of a set of weights for the human model joints that represent the movement features of a set of human subjects and (c) a quantitative assessment of the performance of our method in a functional rehabilitation scenario.

III-E.3

Inverse Kinematics for Upper Limb Compound Movement Estimation in Exoskeleton - Assisted Rehabilitation

Camilo Cortés[1,2], Ana de los Reyes-Guzmán[3], Davide Scorza[1], Álvaro Bertelsen[1], Eduardo Carrasco[1], Ángel Gil-Agudo[3], Oscar Ruiz-Salguero[2] and Julián Flórez[1].

[1]eHealth and Biomedical Applications, Vicomtech-IK4, Mikeletegi Pasealekua 57, Donostia-San Sebastián, Spain

[2]Laboratorio de CAD CAM CAE, Universidad EAFIT, Carrera 49 No 7 Sur - 50, Medellín, Colombia.

[3]Biomechanics and Technical Aids Unit, National Hospital for Spinal Cord Injury, SESCAM, La Peraleda, s/n, Toledo, Spain

Context (open access material)

This work is part of the *HYPER* project. Here, we continue with the study on the posture estimation method presented in Chapter III-E.2 by assessing its performance during the training of compound movements. This contribution is the result of a collaborative research between Vicomtech-IK4, the CAD CAM CAE Laboratory from EAFIT University and the Biomechanics and Technical Aids Unit from the National Hospital for Spinal Cord Injury. The *HYPER* project is funded by the CONSOLIDER-INGENIO 2010 program from the Spanish Ministry for Science and Innovation.

Citation: *Inverse Kinematics for Upper Limb Compound Movement Estimation in Exoskeleton-Assisted Rehabilitation. Camilo Cortes, Ana de los Reyes-Guzman, Davide Scorza, Alvaro Bertelsen, Eduardo Carrasco, Angel Gil-Agudo, Oscar Ruiz-Salguero, Julian Florez. BioMed Research International, pages 1-14, Volume 2016, doi: 10.1155/2016/2581924, ISSN: 2314-6141, 2016. Hindawi Publishing Corporation. Journal article.*

Indexing: ISI (IF: 2.1), Scopus, MEDLINE, Pubmed

Abstract

Robot-Assisted Rehabilitation (RAR) is an important scenario of treatment of patients affected by nervous system injuries (e.g., Stroke, Spinal-Cord Injury). The accurate estimation of the joint angles of the patient limbs in RAR is critical to assess the patient improvement. The economical prevalent method to estimate the patient posture in exoskeleton-based RAR is to approximate the limb joint angles with the ones of the exoskeleton. This approximation is rough, since their kinematic structures differ. Motion Capture Systems (MOCAPs) can improve the estimations, at the expenses of considerable overload of the therapy setup. Alternatively, the Extended Inverse Kinematics Posture Estimation (EIKPE) computational method models the limb and exoskeleton as differing parallel kinematic chains. EIKPE has been tested with single DOF movements of the Wrist and Elbow joints. This article presents the assessment of EIKPE with Elbow - Shoulder compound movements (i.e. object prehension). Ground truth for estimation assessment is obtained from an Optical MOCAP (not intended for the treatment stage). The assessment shows EIKPE rendering good numerical approximation of the actual posture during the compound movement execution, especially for the Shoulder joint angles. This work opens the horizon for clinical studies with patient groups, exoskeleton models and movements types.

Keywords: Limb Posture Estimation, Exoskeleton, Rehabilitation Robotics, Estimation Error, Kinematics.

Glossary

ADL	: Activity of Daily Living
CS	: Coordinate System
DOF	: Degree of Freedom
EFE	: Elbow Flexion-Extension
EIKPE	: Extended Inverse Kinematics Posture Estimation
GH	: Gleno-Humeral
IK	: Inverse Kinematics
MOCAP	: Motion Capture System
RAR	: Robot-Assisted Rehabilitation
ROM	: Range of Motion
RMS	: Root Mean Square
RMSE	: Root Mean Square Error
SAA	: Shoulder Abduction-Adduction
SFE	: Shoulder Flexion-Extension
SIER	: Shoulder Internal-External Rotation
VR	: Virtual Reality
w.r.t.	: with respect to

III-E.3.1 Introduction

Robot-Assisted Rehabilitation (RAR) supplements conventional therapy in the treatment of nervous system injuries (e.g., Stroke, Spinal Cord Injury, etc.), as robots enable repetitive, task-specific, intensive and interactive treatment ([15–17]). In RAR, the accurate estimation of the patient limb posture (i.e. determination of joint angles) is a fundamental prerequisite for:

1. The verification of the compliance of the patient movements with the prescribed exercises. Patient movements must follow the medically prescribed ones, without using the healthy joints to compensate for treated joints ([73, 74]).

2. The long-term assessment of the patient evolution. Objective evaluation methods based on the analysis of the patient kinematic data have been recently developed ([75–77]) to overcome the limitations (subjectivity, low sensitivity [78]) of traditional scales (e.g. Barthel Index [79], Functional Independence Measure [80]) to assess the functionality of a patient.

Traditional motion capture systems (MOCAPs), such as optical, electromagnetic and inertial ones, have been used in many rehabilitation scenarios to accurately estimate the human posture ([81–83]). However, the use of the currently existing MOCAPs in exoskeleton-based RAR is impractical because the exoskeleton body causes optical occlusions and magnetic disturbances in the MOCAP components. Furthermore, in RAR therapies involving functional electrical stimulation (e.g. [84]) and / or electromiography the markers or sensors of the MOCAP interfere with the setup. Even if MOCAP devises can be arranged to coexist with the exoskeleton, the operation is complex and incompatible with the time and resources available for a typical patient appointment. Therefore, they can be used in specific assessment sessions but not for daily patient attention.

In exoskeleton-based therapy, the prevalent approach to estimate the limb joint angles is to approximate them directly with the exoskeleton joint angles (e.g. [77, 85–87]). However, the accuracy of this strategy is limited by the differences between the kinematic structure of the patient limb and exoskeleton ([75]). In the case of the upper limb (focus of this research), a direct accurate measurement of the shoulder angles is particularly difficult, since it demands an exoskeleton with a complex kinematic model that considers the simultaneous motion of the sternoclavicular and acromioclavicular joints.

Computational methods in [29, 34, 88] for exoskeleton-based therapy estimate the arm swivel angle, which parametrizes the arm pose ([89]), by solving the arm Inverse Kinematics (IK). In the mentioned methods, the arm redundancy is solved by estimating a swivel angle that allows the subject to retract the palm to the head efficiently. Results in [29, 34] are improved in [88] by considering the effect of the wrist orientation on the swivel angle estimation. These references do not report how the error in the swivel angle estimation is traced to individual errors in the wrist, elbow, and Gleno-Humeral (GH) joint angles.

The method in [88] requires: (a) the position of the GH joint center, (b) the pose of the wrist, (c) the initial position of the elbow and (d) a point in the head neighborhood that minimizes the swivel angle estimation error. The unavailability of the required inputs in clinical scenarios makes cumbersome to apply the method in [88] ([89, 90]).

Acknowledging different kinematic structures in limb and exoskeleton, Ref. [90] introduces the EIKPE (Extended Inverse Kinematics Posture Estimation) method. EIKPE considers the parallel kinematic chains Limb and Exoskeleton as related through the cuff constraints that fix them together. EIKPE then solves the IK problem of the parallel chain, therefore finding the limb

joint angles. The real - time EIKPE accuracy (circa 3 degrees RMS) is reported for (1) Wrist flexion - extension, (2) Elbow flexion - extension, and (3) Forearm pronation - supination. Limitations of Ref. [90] are (a) restriction to 1 DOF movements due to constraints in the ground truth reading equipment, (b) Elbow and Wrist angle estimations.

III-E.3.1.1 Contributions of this article

The present manuscript complements Ref. [90] (see Table III-E.3.1) by addressing the training of compound movements (simultaneous movement of multiple joints). In particular, it is shown how EIKPE enhances the accuracy in the estimation of the GH joint angles with respect to (w.r.t.) the exoskeleton-based approach. Specifically, this article:

(1) Illustrates the capacity of EIKPE in addressing compound movements (i.e. object prehension), extending the results of Ref. [90], which had individual joint movements. This added complexity requires the usage of (a) more evolved marker and camera sets, (b) a more complex biomechanical and kinematic model, (c) an optimized posture estimation for full arms.

(2) Computes the error in the GH and elbow joint angles of EIKPE w.r.t. the measurements of a marker-based optical MOCAP.

(3) Computes the error in the GH and elbow joint angles of the rehabilitation exoskeleton encoders w.r.t the measurements of the MOCAP.

(4) Applies various statistical measures (RMSE, ROM Error, Box Plots, Significance Test) to assess the differences between items (3) and (4), showing the feasibility of using EIKPE to enhance posture estimates from exoskeletons.

Table III-E.3.1 shows further details on the differences and contributions of the present manuscript when contrasted against related publications.

III-E.3.2 Materials and Methods

This section briefly introduces EIKPE and describes how the Ground-Truth values are used to assess the accuracy of the angle estimations provided by EIKPE and exoskeleton joints.

III-E.3.2.1 EIKPE Method

Since the purpose of the present manuscript is the experimental assessment of the theoretical construct in [90], only the key aspects of EIKPE are discussed here.

To estimate the angles of the limb joints of the patient (denoted by vector $v^H(t)$) during RAR, the human limb and exoskeleton are modeled as a parallel kinematic chain connected by the fixations of the exoskeleton (Fig. III-E.3.1 (a)).

The elements that are considered inputs to the problem are (Fig. III-E.3.1 (b)):

1. Patient: The human limb kinematic model is denoted by $H(L^H, J^H)$ (e.g., the Denavit-Hartenberg parameters [91]), where L^H and J^H are sets of links and joints, respectively. The human kinematic model used in EIKPE includes joints of the spine, Scapulo-Clavicular system and arm. The upper limb is modeled with 9-DOF: 2-DOF of the Scapulo-Clavicular system, 3-DOF of the GH joint (spherical joint), 2-DOF of the elbow and 2-DOF of the wrist.

Table III-E.3.1: Contributions of this article w.r.t. closely related works.

Work	**Method**	**Method Inputs**	**Method Evaluation**	**Metrics**
[90]	EIKPE applied to single 1-DOF joint movements	(a) Exoskeleton and Human link lengths (b) Exoskeleton joint angles	(1) Studied angles: Elbow and wrist joint angles (2) Reference angles: Obtained from marker-based MOCAP (3) Movements: Single 1-DOF elbow and wrist joint movements (wearing the exoskeleton)	RMSE of elbow and wrist angles
[88]	Estimation of the arm swivel angle such that the hand is efficiently retracted towards the head region	(a) Shoulder position (b) Initial Elbow position (c) Wrist pose (d) Point on the head region that minimizes the estimation errors	(1) Studied angles: Arm swivel angle (2) Reference angles: Obtained from redundant marker-based MOCAP (3) Movements: Compound movements of (a) object reaching and (b) rotation of a doorknob (not wearing the exoskeleton)	Mean error of the arm swivel angle
This article	EIKPE applied to compound movements (multi - DOF and multi - joint)	Same as [90]	(1) Studied angles: GH and elbow joint angles (2) Reference angles: Obtained from redundant marker-based MOCAP (3) Movements: Compound movement of object prehension (wearing the exoskeleton)	(i) RMSE and ROM Error of the GH and elbow angle estimations provided by the Exoskeleton and EIKPE (ii) Statistical significance test of the results in item (i)

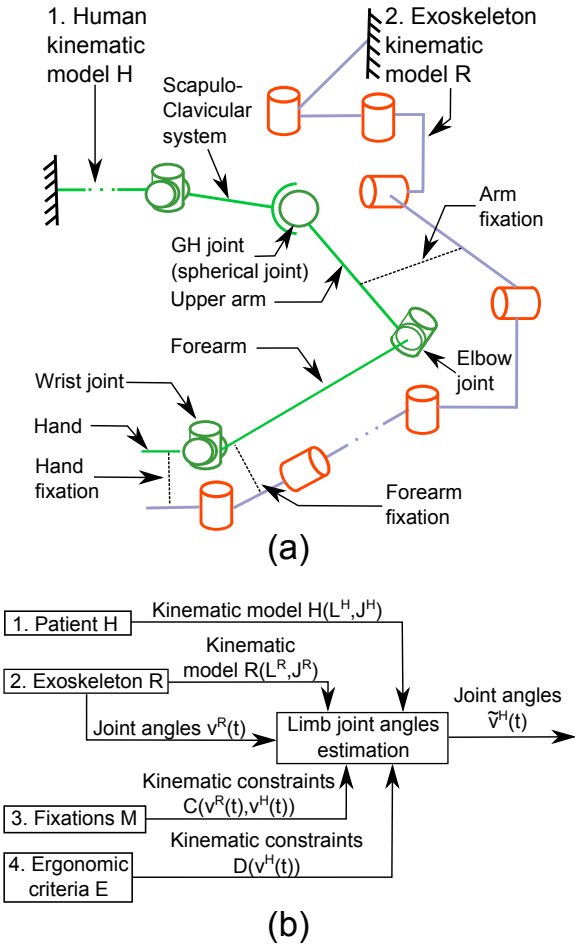

Figure III-E.3.1: (a) Schematic diagram of the human and exoskeleton kinematic models and their interaction. (b) Inputs and outputs of the limb posture estimation algorithm.

2. Exoskeleton: The exoskeleton kinematic model is denoted by $R(L^R, J^R)$. The exoskeleton joint angles are denoted by vector v^R. The values of v^R at any instant t of the therapy ($v^R(t)$) are known. In the rehabilitation platform where EIKPE is implemented the exoskeleton corresponds to the Armeo Spring ® (Hocoma, AG) ([55]), which has 7-DOF.

3. Set of fixations M: The fixations M are passive mechanisms that connect the exoskeleton and the patient. $C(v^H(t), v^R(t))$ is the set of vector-valued functions that model the kinematic constraints imposed by the fixations M to the patient limb.

4. Set of ergonomic criteria E: E consists of a set of principles that dominate the posture of the patient limb while interacting with the exoskeleton (e.g. the preference of the human to put the limb in a rest posture v^H_{rest}). $D(v^H(t))$ is the set of vector-valued functions that model the kinematic constraints imposed on the patient limb by the set of ergonomic criteria E.

The goal of the implemented algorithm is to find the approximate angles of the joints of the patient limb $\tilde{v}^H(t)$, such that the sets of constraints C and D are met.

In order to obtain the estimations $\tilde{v}^H(t)$, the IK of $H(L^H, J^H)$ is solved considering the sets of constraints C and D. The IK solution is obtained in real-time using the V-REP® simulator (Coppelia Robotics, GmbH) ([63]). The joint angles of the Exoskeleton and EIKPE are sampled with frequency $f_s = 60$ Hz.

III-E.3.2.2 Ground-Truth Motion Capture and Analysis

III-E.3.2.2.1 Biomechanical Model

The biomechanical model (Fig. III-E.3.2) of the upper limb described in [92] was used as the reference kinematic model for the assessment of the accuracy of EIKPE. This model was developed in the software Visual3D™ (C-Motion, Inc) ([93]) and presents 6-DOF: 3-DOF of the GH-joint (spherical joint), 2-DOF of the elbow joint and 1-DOF of the wrist joint. The biomechanical model can be scaled to match the anthropomorphic measures of each of the test subjects.

The biomechanical model includes virtual markers (gray spheres) that allow to reconstruct the motion of the limb by using motion data from MOCAPs. In order to do so, the 3D positions of the real markers (which were installed on the patient and tracked by a MOCAP) are treated as the desired positions of the virtual markers. Then, the limb joint angles are computed by solving the IK of the limb such that the position of the virtual markers match the position of the real markers. The detailed geometry depicted in Fig. III-E.3.2 is only used for visualization purposes and a simplified version is used in the IK computation. The joint angles obtained by using this methodology are the ground-truth $v^H(t)$ angles.

III-E.3.2.2.2 Marker Placement Protocol

A total of 21 markers are installed on each test subject to precisely track the movement of the upper limb. The markers are distributed on the subject arm and trunk as described in Table III-E.3.2 and Fig. III-E.3.3.

III-E.3.2.2.3 Motion Capture System

The CODAMOTION ® (Charnwood Dynamics Ltd) [94] is an optical-marker based MOCAP. This MOCAP uses active markers that emit infrared light, which is detected by 3 sensor units (Fig.

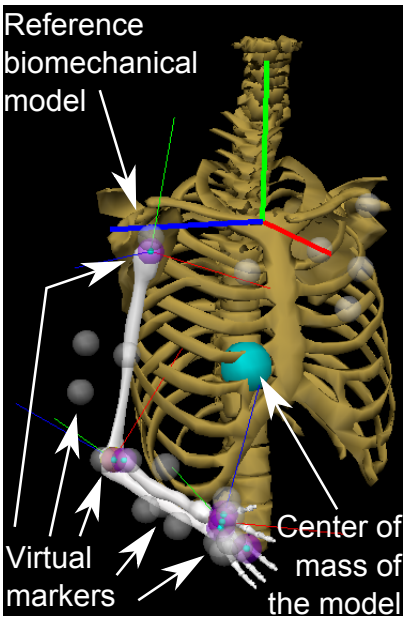

Figure III-E.3.2: Reference biomechanical model and virtual markers for motion reconstruction ([92]).

Table III-E.3.2: Marker setup for upper limb motion tracking.

Markers on bony landmarks	**Markers on body segments**
Individual markers are located on: 1. Left and right acromion 2. Right iliac crest 3. Lateral and medial epicondyles of the right elbow 4. Radial and ulnar styloid processes of the right wrist 5. Third metacarpal head of the right hand	Marker clusters (groups of 3 markers) are located on: 1. Trunk 2. Upper arm 3. Forearm 4. Hand dorsal Only the hand cluster is not rigid.

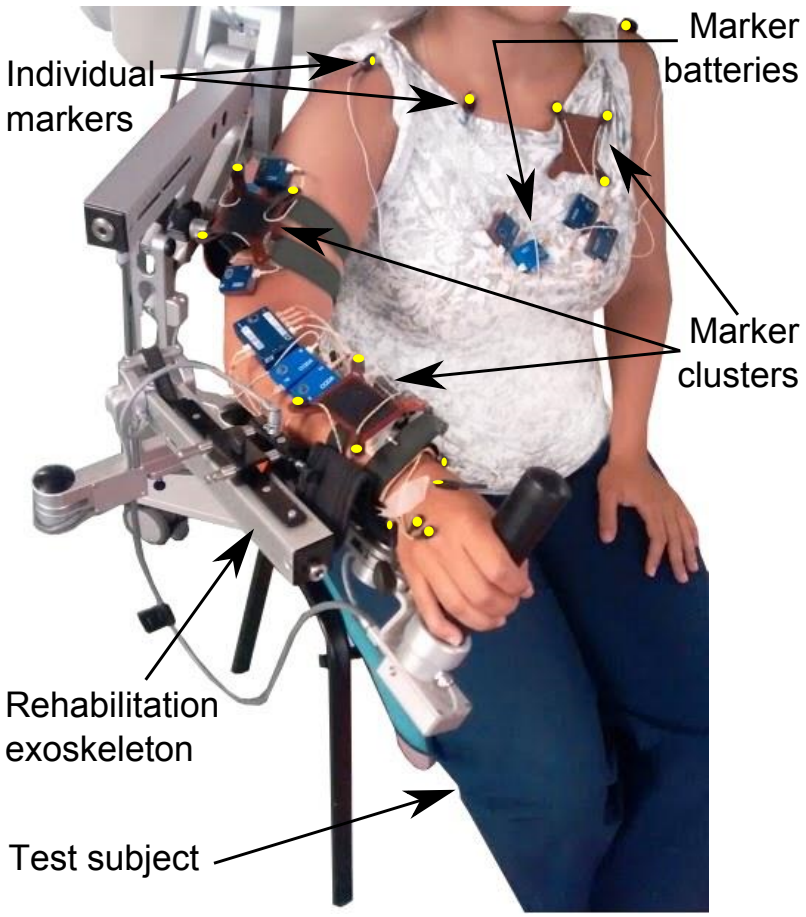

Figure III-E.3.3: Setup of the markers (highlighted in yellow) of the MOCAP system.

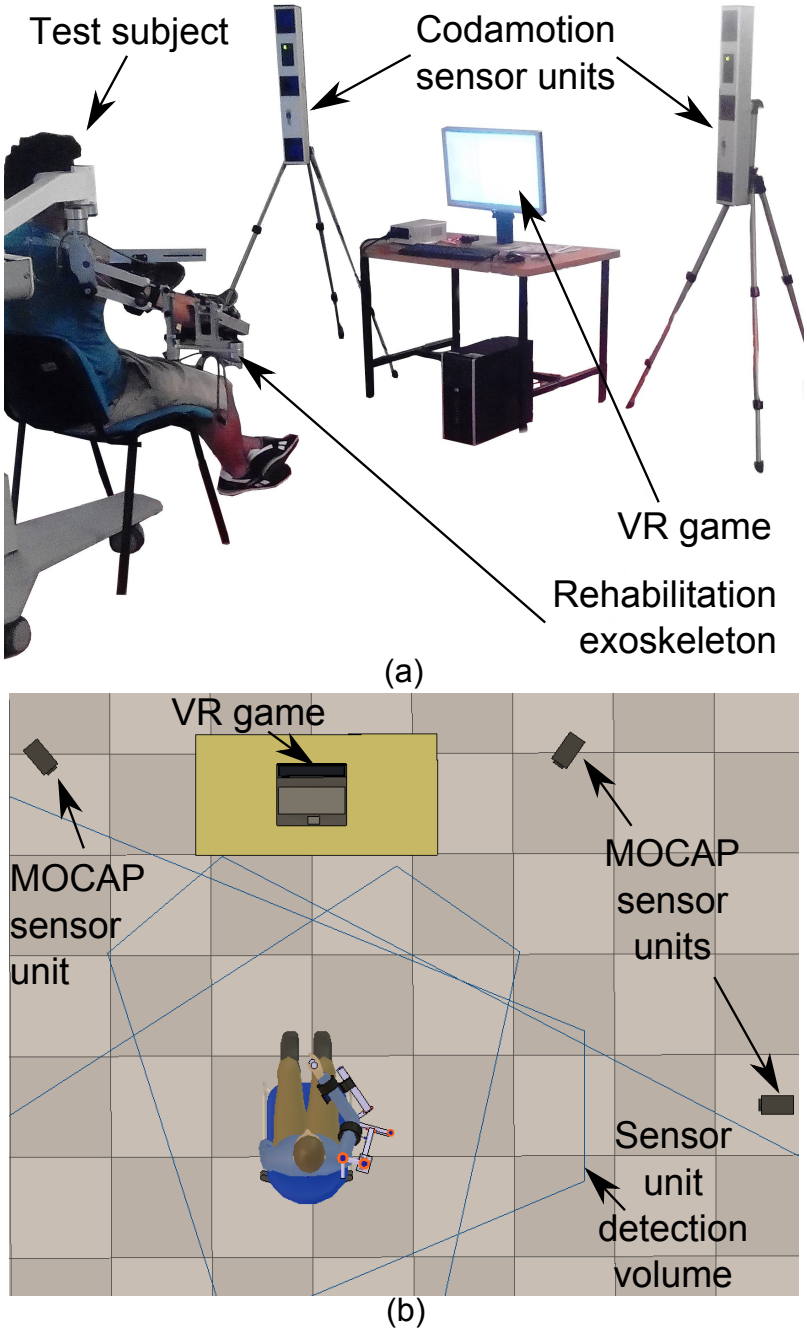

Figure III-E.3.4: Setup for motion capturing in RAR: (a) MOCAP sensor units and (b) their distribution around the test subject.

III-E.3.4 (a)). For the accuracy assessment experiments, the MOCAP sensor units are distributed as depicted in Fig. III-E.3.4 (b). With the described marker setup, the marker position sampling frequency is f_c =200 Hz.

III-E.3.2.2.4 Experimental protocol

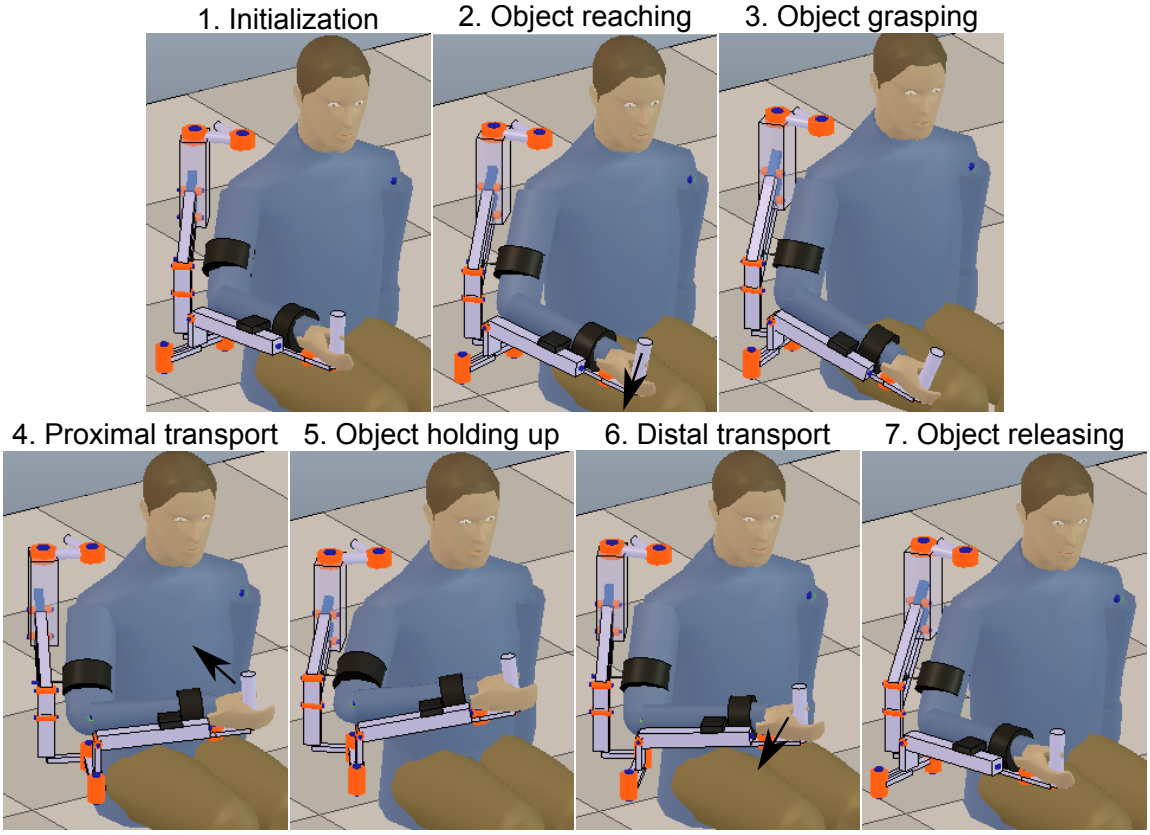

Figure III-E.3.5: Stages of the prehension ADL. Black arrows indicate the approximate direction of movement of the hand of the test subject.

The functional task that was chosen to conduct the accuracy assessment is the Activity of Daily Living (ADL) of prehension, which has its stages shown in Fig. III-E.3.5. Notice that the prehension task shares movement stages with other ADLs, such as drinking and eating, which are among the most relevant tasks to rehabilitate ([95]).

The prehension movements are performed with the forearm pronation - supination and the wrist flexion-extension DOFs blocked in the Exoskeleton in order to avoid marker occlusions during the ADL movement (such joint blockage does not affect the angle estimation capabilities of the MOCAP or EIKPE). The joint angles of the blocked DOFs are not studied in this work.

In the setup stage of this protocol, the lengths of the arm and forearm of each test subject are manually measured and entered into the EIKPE software (as it would be done in a clinical

application). The Exoskeleton arm and forearm link lengths are adjusted for every subject according to the device manufacturer instructions. The Exoskeleton link lengths are also entered into the EIKPE software. Next, the optical markers are installed on the subject and the MOCAP calibration procedure is conducted.

After the subjects wear the Exoskeleton, they perform some practice trials with the Virtual Reality (VR) game. In the VR game, the hand positions at the grasping and object holding up stages are calibrated for each subject. For each test subject, 4 repetitions of the prehension movement are recorded. Each prehension movement execution is limited to 20 seconds. A total of 4 healthy subjects participate in the movement recordings.

III-E.3.2.2.5 Signal Processing and Analysis

The accuracy assessment presented in this article involves the comparison of the upper limb joint angle estimates that come from the following sources:

(a) The joint angles obtained from the MOCAP.

(b) The joint angles obtained from EIKPE.

(c) The joint angles obtained from the Exoskeleton encoders.

Table III-E.3.3 summarizes the measured angles of the joints of the upper limb, the methods and reference coordinate systems (CS) used to compute such joint angles.

Table III-E.3.3: Method to compute the limb joint angles of interest with the various measuring systems.

<table>
<tr><th rowspan="2">Limb joint</th><th rowspan="2">Angle</th><th colspan="3">Method to compute the limb joint angles</th></tr>
<tr><th>MOCAP</th><th>EIKPE</th><th>Exoskeleton</th></tr>
<tr><td rowspan="3">GH</td><td>SFE</td><td rowspan="3">Euler angle decomposition of the rotations of the upper arm marker CS w.r.t. the thorax marker CS (Fig. III-E.3.3)</td><td rowspan="3">Euler angle decomposition of the rotations of the upper arm CS w.r.t. the Exoskeleton reference CS (Fig. III-E.3.6)</td><td>Angle of joint 2 (Fig. III-E.3.6)</td></tr>
<tr><td>SAA</td><td>Sum of the angles of joints 0 and 1 (Fig. III-E.3.6)</td></tr>
<tr><td>SIER</td><td>Angle of joint 6 (Fig. III-E.3.6)</td></tr>
<tr><td>Elbow</td><td>EFE</td><td>Euler angle decomposition of the rotations of the forearm marker CS w.r.t. the upper arm marker CS (Fig. III-E.3.3)</td><td>Euler angle decomposition of the rotations of the forearm CS w.r.t. the upper arm CS (Fig. III-E.3.6)</td><td>Angle of joint 4 (Fig. III-E.3.6)</td></tr>
</table>

In order to compare the various joint angle measurements along the execution of the prehension movement, the obtained joint angle signals are filtered and synchronized as follows:

(a) Resampling and filtering. The joint angle profiles obtained from the MOCAP are resampled to match the sampling frequency of the Exoskeleton and EIKPE. Then, a low-pass Butterworth filter with a 5Hz cuttoff frequency is applied to all the obtained signals. Figs. III-E.3.7 (a-c) show the angle estimations of the Elbow flexion of one of the trials of a subject after resampling and filtering.

(b) Signal trimming. The joint angle profiles obtained from EIKPE and Exoskelton are manually trimmed such that they approximately contain the same movement segment recorded with the MOCAP. Fig. III-E.3.7 (d) shows the trimmed Exoskeleton and EIKPE estimations of the movement trial mentioned in the previous step.

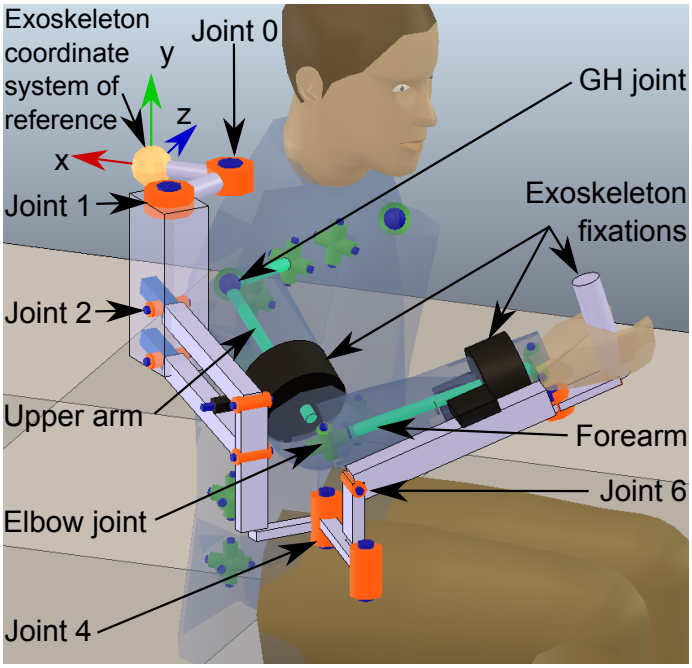

Figure III-E.3.6: Human and Exoskeleton kinematic models and their joints of interest for the experiments.

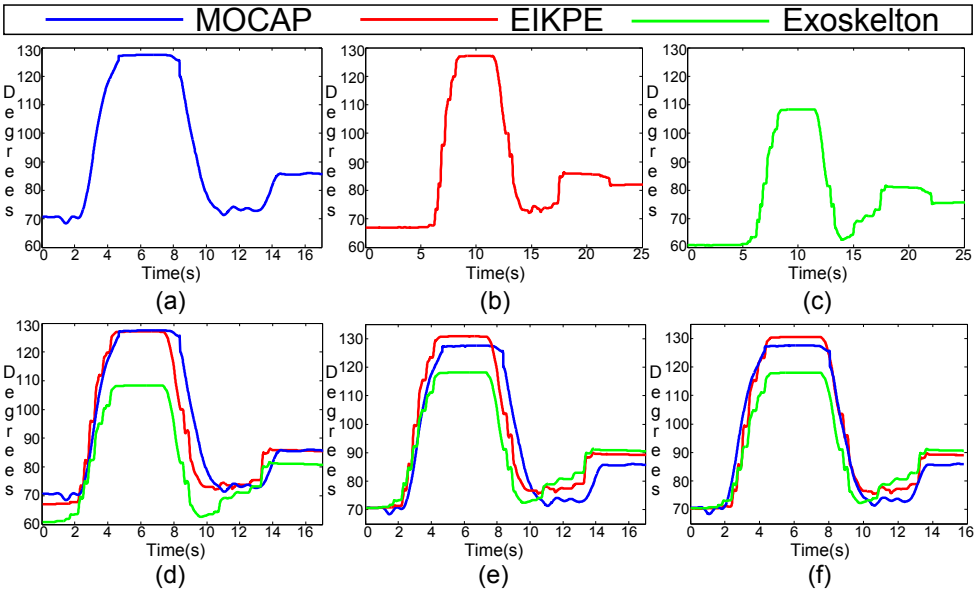

Figure III-E.3.7: Signal synchronization process of elbow flexion angle estimations from a movement trial.

(c) Signal reference adjustment. The coordinate systems of reference of the MOCAP, EIKPE and Exoskeleton are not registered to each other, which impedes to transform the angle estimations to a common coordinate system to compare them. In order to compare the angle estimations, they are related to each other by using the steady limb joint angles at the initialization posture (subjects were asked to remain static in this posture for a few seconds). To do so, the joint angles measured by the MOCAP at the initial stage of the movement are set as the initial values for the angle estimations of the Exoskeleton and EIKPE. In this way, the estimations of the joint movements performed w.r.t. the initialization posture can be compared. Fig. III-E.3.7 (e) shows an example of the result of this step.

(d) Temporal axis offset adjustment. A fine tuning in the aliment of the signals in the temporal axis is performed by applying a time offset to the EIKPE and Exoskeleton estimations such that their correlation with the MOCAP measurements is maximized. Fig. III-E.3.7 (f) shows an example of the result of this step.

After synchronization of the joint angle signals, the following error metrics are computed:

1. Error in the estimation of the ROM. The amplitude of the Exoskeleton and EIKPE joint angles are compared with the ones of the MOCAP.

2. RMS Error (RMSE) of the joint angle profiles. The RMS of the pairwise differences between the joint angle profiles of the Exoskeleton and EIKPE w.r.t. the ones of the MOCAP are computed.

The obtained ROM error and RMSE metrics of the Exoskeleton and EIKPE are compared with a paired difference test to check if there is an statistically significant difference between their means (confidence interval 95%).

III-E.3.3 Results and Discussion

The results of the experiments are summarized in Table III-E.3.4. This table presents the average RMSE and ROM errors ($\pm$ their standard deviation) of the joint angles measured by the Exoskeleton and EIKPE for all the trials of the test subjects when compared to the joint angles provided by the MOCAP (ground-truth). Around 12200 samples were compared to compute each of the RMSE values presented in Table III-E.3.4. A Wilcoxon signed-rank test ([96]) was performed to check if there is a statistically significant difference between the mean accuracy of the methods in estimating the various joint angles and ROMs (by using the SPSS statistical analysis software (IBM Corp.) [97]). Values in bold in Table III-E.3.4 indicate statistically significant differences between the accuracy provided by the Exoskeleton and EIKPE.

III-E.3.3.1 Angle estimations of the GH joint

For the GH joint, EIKPE presents small errors in estimating the SFE and SAA angles and ROMs w.r.t. the measurements of the MOCAP system. In comparison with the results obtained for the SFE and SAA, a larger error is presented by EIKPE in the SIER angle and ROM estimation. In order to explain the differences in the accuracy of the mentioned angles, consider that in EIKPE the SFE and SAA angles can be computed from the movement constraints imposed by the Exoskeleton

Table III-E.3.4: Error metrics (mean ± std. dev.) of the angle estimations provided by the Exoskeleton and EIKPE. Values in bold indicate statistically significant differences in the accuracy of the approaches ($p - value \leq 0.05$).

Metric	Exoskeleton	EIKPE	Improvement[a]
RMSE of SFE angle	**8.367 ± 4.652**	**3.947 ± 0.888**	53%
ROM Error of SFE angle	**17.984 ± 11.621**	**5.723 ± 2.756**	68%
RMSE of SAA angle	**8.195 ± 4.577**	**3.304 ± 1.909**	60%
ROM Error of SAA angle	**16.900 ± 10.324**	**5.567 ± 4.701**	67%
RMSE of SIER angle	**16.195 ± 6.550**	**6.500 ± 3.116**	60%
ROM Error of SIER angle	**17.400 ± 12.608**	**6.921 ± 5.559**	60%
RMSE of EFE angle	6.616 ± 1.370	5.782 ± 2.716	13%
ROM Error of EFE angle	8.756 ± 5.468	5.693 ± 3.698	35%

[a] Error reduction w.r.t. the Exoskeleton by using EIKPE.

on the upper arm. However, the estimation of the SIER angle involves information of the pose of the forearm (which also depends on the elbow movement), and therefore is subject to additional estimation and modeling errors.

In Fig. III-E.3.8, it can be observed that EIKPE joint movement profiles follow closely the magnitude and direction of the ones estimated with the MOCAP. The movement trial depicted in Fig. III-E.3.8 is a good example of the large errors in the estimation of the joint angles that are produced by the misalignment of the axes of the Exoskeleton joints w.r.t. the ones of human joints. Such misalignment causes under or over estimation of an angle and also failures in the estimation of the direction of the motion.

Regarding the Exoskeleton accuracy in the estimation of the angles of the GH joint (Table III-E.3.4), the worst results are for the SIER angle. In Fig. III-E.3.5, it can be observed how the axis of rotation of the joint 6 of the Exoskeleton (Fig. III-E.3.6) is significantly misaligned with the longitudinal axis of the upper arm in most of the ADL movement stages. Only in the object hold up stage the alignment is better and the angle is estimated more accurately. Regarding the Exoskeleton accuracy in the estimation of SFE and SAA angles, it was noticed that it is strongly reduced when the subject mobilizes the scapulo-clavicular system.

III-E.3.3.2 Angle estimations of the elbow joint

In the case of the EFE angle accuracy, EIKPE presents a fair accuracy in estimating the angle magnitude and ROM w.r.t. the measurements of the MOCAP. A source of error in the estimation of the EFE angle is in the modeling of the elbow joint. Traditionally, the EFE DOF has been modeled with a revolute joint with its rotation axis normal to both the upper arm and forearm links ([98]), which is the one used in the EIKPE model. However, the angle between the EFE axis of rotation and the upper arm and forearm longitudinal axes differs between subjects ([99]) and even varies with the angle of flexion of the elbow ([100]). In the case of the MOCAP, the mentioned axis of rotation is estimated by using markers installed on bony landmarks of the elbow at the calibration stage of the system.

In the case of the Exoskeleton, notice that the axis of rotation of the joint 4 of the Exoskeleton is always aligned with the vertical axis of the world (Fig. III-E.3.6). For the case of the movement that the subjects performed, in which the forearm lies on the horizontal plane and reaches the height of the chest, the angle of joint 4 fairly resembles the EFE angle of the subjects. However, it should

be remarked that such accuracy will not be maintained when the EFE movement is performed in other plane, as it occurred in the movement trial in Fig. III-E.3.8 (Object holding up stage).

III-E.3.3.3 Comparison of the accuracy of the Exoskeleton and EIKPE

Regarding the accuracy in the estimation of the GH joint, it can be observed in Table III-E.3.4 that EIKPE provides significantly better estimations for all the angles of the GH joint than the Exoskeleton. With respect to the RMSE, the EIKPE errors are 50 to 60% less than the ones of the Exoskeleton. Fig. III-E.3.9 (a) shows that the RMSE variance of EIKPE is significantly lower than the one of the Exoskeleton for the GH joint angles. Regarding the ROM, the EIKPE errors are 60 to 68% less than the ones of the Exoskeleton (Fig. III-E.3.9 (b)). Statistically significant differences between the means of the RMSE and ROM errors provided by the Exoskeleton and EIKPE were found for all the GH joint angles.

With respect to the angles of the elbow joint, it can be observed in Table III-E.3.4 that EIKPE provides slightly better estimations of the EFE angle and ROM than the Exoskeleton. However, as shown in Fig. III-E.3.9 (a), the variance of the EIKPE RMSE for the EFE angle is larger than the one of the Exoskeleton. The difference between the Exoskeleton and EIKPE accuracy is more pronounced in the ROM where the EIKPE error is 35% less than the one of the Exoskeleton (Fig. III-E.3.9 (b)). Nevertheless, the difference between the means of the RMSE and ROM errors provided by the Exoskeleton and EIKPE is small and does not reach statistical significance. Table III-E.3.5 shows the global RMSE and ROM errors for all the studied joint angles provided by the Exoskeleton and EIKPE.

Table III-E.3.5: Global estimation accuracy of the studied joint angles and ROMs.

Error Metric	**Exoskeleton**	**EIKPE**	**Improvement**[a]
Global Angle RMSE (deg)	10.526	5.055	52%
Global ROM Error (deg)	15.260	5.976	60%

[a] Error reduction w.r.t. the Exoskeleton by using EIKPE.

A visual guide of how the joint angle errors are mapped to the reconstructed pose of the upper limb is shown in Fig. III-E.3.10. This figure presents a comparison of the reconstructed upper limb poses at the object holding up stage of the movement trial depicted in Fig. III-E.3.8 with the joint angle estimations provided by the MOCAP, EIKPE and Exoskeleton.

III-E.3.3.4 Comparison with related works

The conducted literature review did not produce any other citations than [29, 34, 88, 90] in the area of posture estimation of the upper limb in exoskeleton-based rehabilitation by using computational methods. We consider that the method in article [88] would be the strongest competitor to EIKPE (Table III-E.3.1). Notice that the arm swivel angle representation may suffice for the targeted application in [88]. However, for the application addressed in this work (patient follow-up and evaluation), the joint angles of the limb are required. A direct comparison of EIKPE with the method in [88] is not possible because in this reference only the arm swivel angle is reported.

EIKPE accuracy is close to the ones of MOCAPs that deal with the upper limb posture estimation in ambulatory settings (no robotic devices interacting with the subjects are involved). For instance, the method in [83] presents an average RMSE of 5.5 deg. in the estimation of the angles

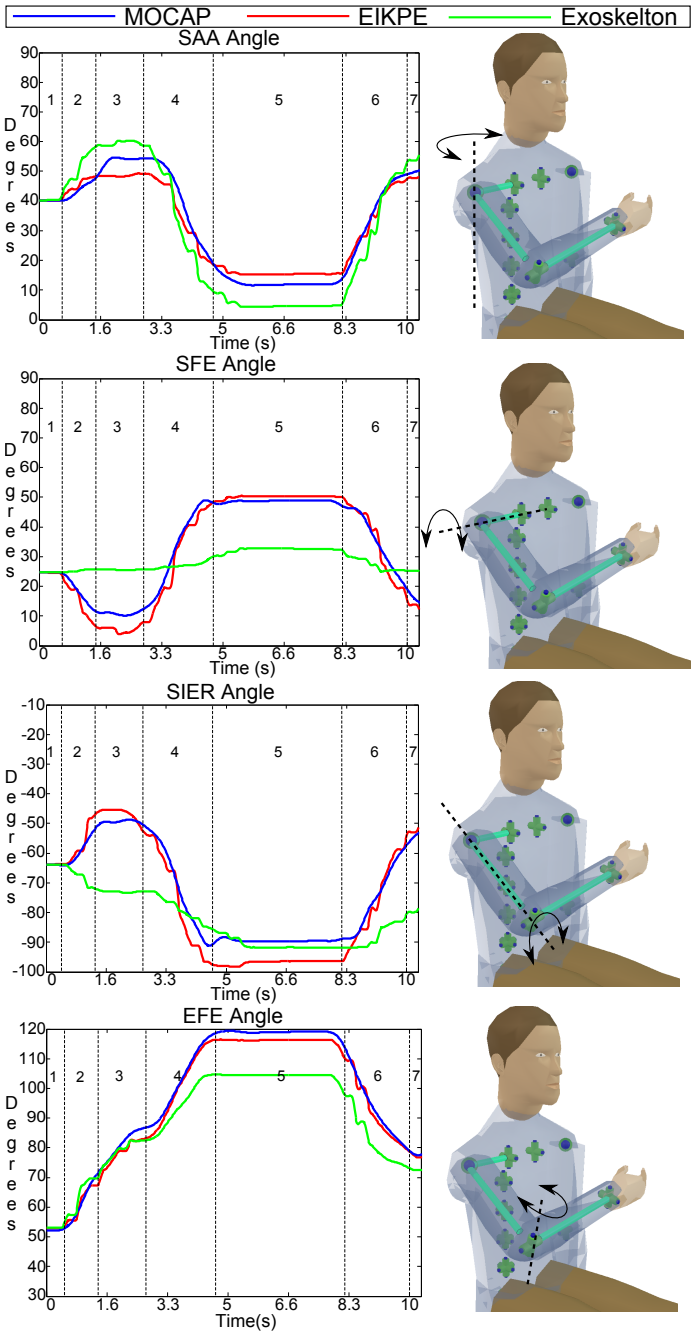

Figure III-E.3.8: Measurement and estimations of the angles of the shoulder and elbow joints of one of the trials of a test subject. Dashed lines bound the various stages of the prehension movement (Fig. III-E.3.5).

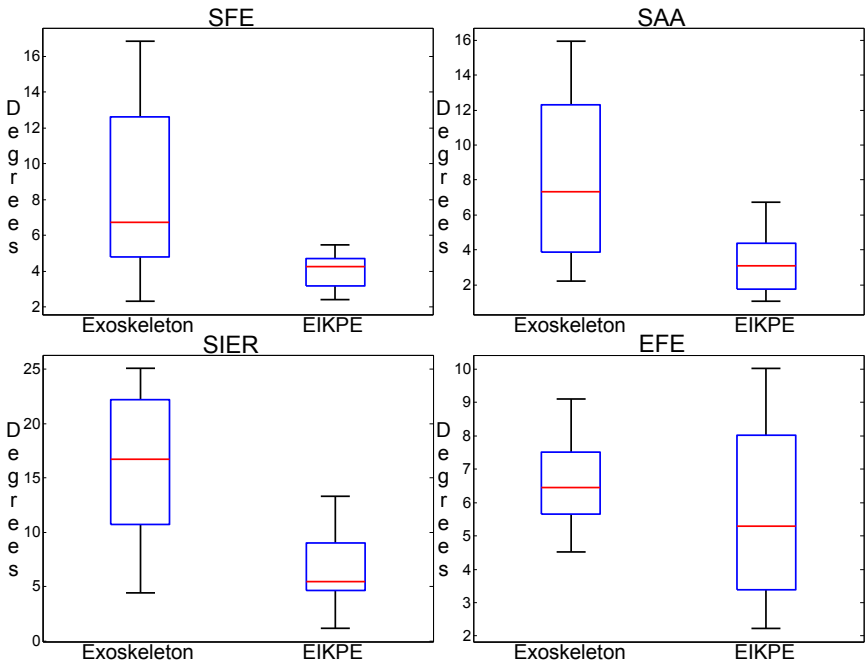

(a) Box plots of angle RMSE

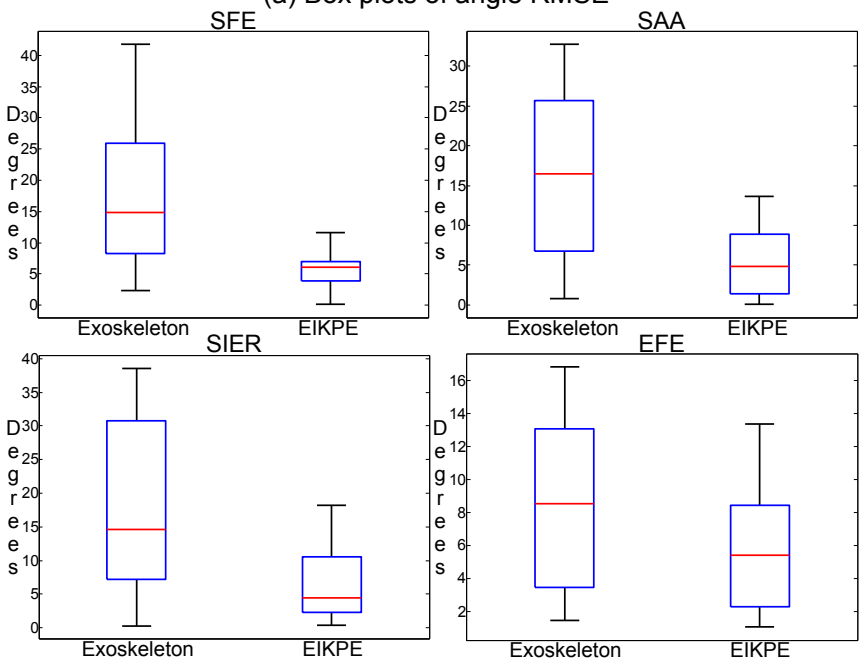

(b) Box plots of ROM Errors

Figure III-E.3.9: Box Plots of (a) RMSE of angle estimations and (b) ROM Errors provided by the Exoskeleton and EIKPE for the assessed joint angles.

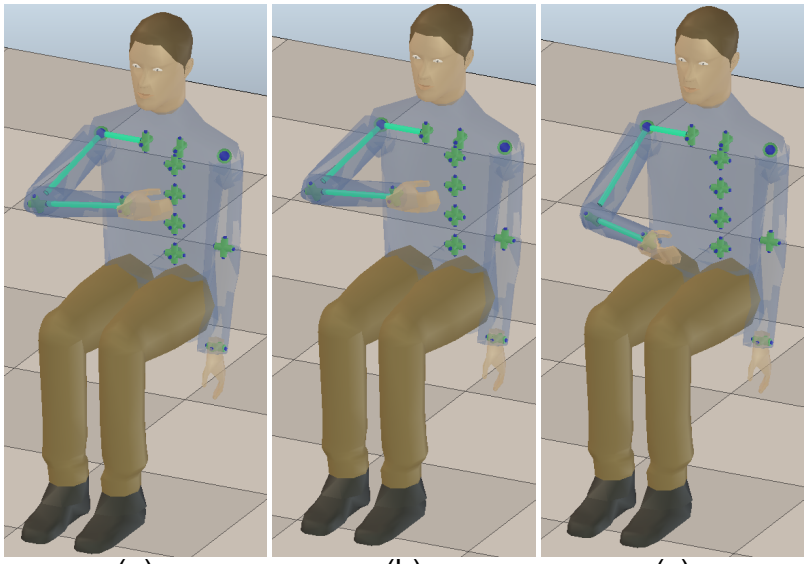

Figure III-E.3.10: Reconstructed poses of the upper limb at the object holding up stage of the trial depicted in Fig. III-E.3.8 with the joint angle measurements of the: (a) MOCAP, (b) EIKPE and (c) Exoskeleton.

of the shoulder and elbow joints by using inertial sensors during the ADL movement of reaching for a doorknob.

III-E.3.4 Conclusion

This article studied the feasibility of using the EIKPE method for the estimation of the patient limb posture in the robotic-assisted rehabilitation (RAR) of the compound movement of object prehension. In order to do so, the comparison of the estimations of the GH and elbow joint angles provided by (a) EIKPE, (b) the joint encoders of a state-of-the-art commercial exoskeleton (typical practice in RAR) and (c) an optical motion capture system (ground-truth) was conducted.

The performed test intended to replicate the conditions of use of EIKPE by an end-user. In this way, the estimation of parameters that affect the method accuracy, such as the ones related to the kinematic model of the human subject (arm, forearm and hand lengths) and to the exoskeleton kinematic model (adjustable link lengths) was not optimized in any way.

The obtained results suggest that EIKPE is accurate for the application. The studied joint angles were estimated with a RMSE of 5.055 degrees with respect to the measurements of the optical motion capture system. EIKPE accuracy approaches the one of inertial MOCAPs, avoiding the difficulty of using MOCAPs in RAR.

EIKPE improved markedly the accuracy of the estimations of the GH joint angles provided by the Exoskeleton. Statistically significant differences were found in the accuracy of the Exoskeleton and EIKPE for all the angles of the GH joint. EIKPE provided RMSE and ROM errors 52% and 60%, respectively, smaller than the ones of the Exoskeleton for all the studied angles. This

suggests that EIKPE may be used to enhance the accuracy in the estimation of the patient posture in exoskeleton-based rehabilitation platforms.

Future Research Opportunities

The methodology introduced in this manuscript implies the following future activities for interested researchers: (a) Tests with a statistical significant sample of patients (e.g. Stroke, Spinal-Cord Injury), (b) tests on other exoskeleton-based platforms, (c) tests with other compound movements. All of these activities are a natural follow-up given the enhanced posture estimation via the fixture constraints applied here.

III-E.4

Optical Enhancement of Exoskeleton-based Gleno-Humeral Angles Estimation

Camilo Cortés[1,2], Luis Unzueta[1], Ana de los Reyes-Guzmán[3], Oscar Ruiz-Salguero[2] and Julián Flórez[1].

[1]eHealth and Biomedical Applications, Vicomtech-IK4, Mikeletegi Pasealekua 57, Donostia-San Sebastián, Spain

[2]Laboratorio de CAD CAM CAE, Universidad EAFIT, Carrera 49 No 7 Sur - 50, Medellín, Colombia.

[3]Biomechanics and Technical Aids Unit, National Hospital for Spinal Cord Injury, SESCAM, La Peraleda, s/n, Toledo, Spain

Context (open access material)

This work is part of the *HYPER* project. Here we introduce a novel hybrid system for the precise estimation of the shoulder joint angles in exoskeleton-based rehabilitation. This contribution is the result of a collaborative research between Vicomtech-IK4, the CAD CAM CAE Laboratory of EAFIT University and the Biomechanics and Technical Aids Unit from the National Hospital for Spinal Cord Injury. The *HYPER* project is funded by the CONSOLIDER-INGENIO 2010 program from the Spanish Ministry for Science and Innovation.

Citation: *Optical Enhancement of Exoskeleton-Based Estimation of Glenohumeral Angles. Camilo Cortes, Luis Unzueta, Ana de los Reyes-Guzman, Oscar E. Ruiz, Julian Florez. Applied Bionics and Biomechanics, pages 1-20, Volume 2016, doi: 10.1155/2016/5058171, ISSN: 1754-2103, 2016. Hindawi Publishing Corporation. Journal article.*

Indexing: ISI (IF: 0.7), Scopus, INSPEC, Pubmed, EI Compendex

Abstract

In Robot-Assisted Rehabilitation (RAR) the accurate estimation of the joint angles of the patient limbs is critical to assess the therapy effectiveness. In RAR, the use of classic motion capture

systems (MOCAPs) (e.g., optical and electromagnetic) to estimate the Gleno-Humeral (GH) joint angles is hindered by the exoskeleton body, which causes occlusions and magnetic disturbances. Besides, the exoskeleton posture does not faithfully reflect the limb posture, as their kinematic models differ. To address the mentioned limitations in posture estimation, we propose to install the cameras of an optical marker-based MOCAP on the rehabilitation exoskeleton. Then, by combining the estimated marker poses and the exoskeleton Forward Kinematics, the GH joint angles are estimated. Such hybrid system avoids the problems related to marker occlusions, reduced camera detection volume and imprecise joint angle estimation due to the kinematic mismatch of the patient and exoskeleton models. This paper presents the formulation, simulation and accuracy quantification of the proposed method with simulated human movements. Also, a sensitivity analysis of the method accuracy to marker position estimation errors, produced by system calibration errors and marker drifts, is conducted. The results show that, even with significant errors in the marker position estimation, the method accuracy is adequate for RAR.

Keywords: GH Joint Angle Estimation, Upper Limb Rehabilitation, Rehabilitation Robotics.

Glossary

Acromion	: Region of the scapula bone above the GH joint.
Clavicle	: Bone of the shoulder girdle located at the root of the neck.
CS(s)	: Coordinate System(s).
COMB	: Combination of movements of the GH joint (SAbAd, SFE and SIR).
DOF(s)	: Degree(s) of Freedom.
GH	: Gleno-Humeral.
Humerus	: Upper arm bone.
MOCAP(s)	: Motion Capture System(s).
mts	: meters.
RAR	: Robot-Assisted Rehabilitation.
RMS	: Root Mean Square.
Scapula	: Bone that connects the humerus with the clavicle.
SAbAd	: Shoulder Horizontal Abduction-Adduction.
SFE	: Shoulder Flexion-Extension.
SIR	: Shoulder Internal Rotation.
VR	: Virtual Reality.
V-REP	: Virtual Robot Experimentation Platform.
w.r.t.	: With respect to.
E	: Exoskeleton Kinematic Model.
H	: Human Upper Body Kinematic Model.
M	$= \{m_0, m_1\}$. Set of planar markers mounted on the patient.
p^E_G	: Position of the GH joint w.r.t. the E CS.
p^E_{elw}	: Position of the Elbow joint w.r.t. the E CS.
R	$= \{r_0, r_1\}$. Set of vision sensors that compose the optical MOCAP.
$v^H_G(t)$	: 3-tuple of joint angles of the GH joint at instant t.
$v^E(t)$	: Tuple of joint angles of the exoskeleton kinematic model at instant t.
$T^E_{m_i}$	: Transformation matrix of marker m_i w.r.t. the E base CS.
$T^{r_i}_{m_i}$	: Transformation matrix of marker m_i w.r.t. the r_i CS.
$T^{m_0}_G$	: Transformation matrix of the GH joint w.r.t. the m_0 marker.
$T^{m_1}_{elw}$	: Transformation matrix of the elbow joint w.r.t. the m_1 marker.
Notation x^y_z	: x can be a position, transformation, etc. of object z w.r.t. object y CS.

III-E.4.1 Introduction

The application of Robotics and Virtual Reality (VR) to motor Neurorehabilitation (Fig. III-E.4.1) has been beneficial for patients, as they receive an intensive, repetitive, task-specific and interactive treatment ([15–17, 101]).

The assessment of: (a) the compliance of the patient movements with the prescribed exercises and (b) the patient long-term improvement is critical to plan and evaluate the effectiveness of RAR therapies. In order to obtain the patient motion data to conduct the mentioned assessments, it is necessary to estimate the patient posture (i.e. the joint angles of the limbs). The methods to estimate the patient posture need to be practical and easy to set up for the physician, such that the mentioned assessments can be indeed an integral part of the therapy.

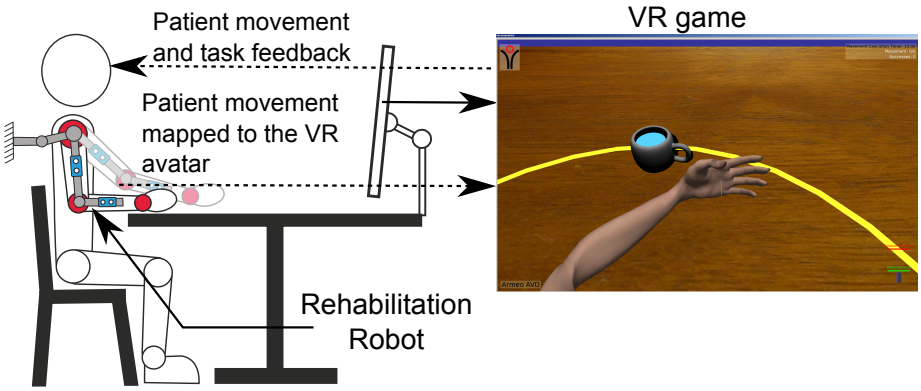

Figure III-E.4.1: Robotic and VR-based Rehabilitation.

Current methods to estimate the patient posture are cumbersome to use or not enough accurate in exoskeleton-based therapies. In order to overcome such limitations, we propose a method in which low-cost RGB-D cameras (which render color and depth images) are directly installed on the exoskeleton and colored planar markers are attached to the patient limb to estimate the angles of the patient GH joint, overcoming the individual limitations of each of these systems.

III-E.4.2 Literature Review

Optical, electromagnetic and inertial MOCAPs have been used in many rehabilitation scenarios for accurate posture estimation ([81]). However, the use of the mentioned MOCAPs in exoskeleton-based rehabilitation is limited by the factors that are discussed next:

1. Optical marker-based systems (e.g. Optotrack, CODA, Vicon) are considered the most accurate systems for human motion capture ([81]). Ref. [102] reports Optotrack errors of 0.1 - 0.15 mm. However, in the specific case of exoskeleton-based therapy, these systems require redundant sensors and markers to cope with occlusions caused by the exoskeleton body. Therefore, their specific usage for therapy is limited. Besides, the cost of these systems is high (50K - 300K USD [103]) compared to non-optical MOCAPs.

2. Electromagnetic systems do not suffer from optical occlusions. However, they are easily perturbed by surrounding metallic objects (e.g. exoskeleton body) and electric / magnetic fields ([81]). An additional drawback of these systems is their limited detection volume when compared to optical systems.

3. Inertial and Magnetic Measurement Systems are robust, handy, and economical for full-body human motion detection (upper limb tracking in [104,105]). With the use of advanced filtering techniques, the drift errors of inertial sensors is reduced and are able to achieve a dynamic accuracy of 3 deg. RMS ([81]). However, these systems require performing calibration motions / postures, which may not be suitable for patients with neuromotor impairments.

In exoskeleton-based rehabilitation, the prevailing approach to estimate the human limb joint angles (e.g. [77,85–87]), is to approximate them with the angles of the exoskeleton joints. However,

misalignment between the axes of the exoskeleton and human joints may produce large estimation errors ([75, 106]). In particular, the accurate estimation of the GH joint angles is hard to achieve by using this approach, since it requires an exoskeleton with a complex kinematic structure that considers the concurrent motion of the sternoclavicular and acromioclavicular joints.

Recognizing the differences in the kinematic structures of the limb and exoskeleton, Ref. [90] presents a computational method that considers the Limb and Exoskeleton as parallel kinematic chains related by the cuff constraints that fix them together. Then, the IK problem of the parallel chain is solved to find the limb joint angles. A limitation of this method is that its performance was demonstrated only for analytic (1-DOF movements) of the elbow and wrist joints. The accuracy in the estimation of the GH joint angles remains to be determined.

Ref. [88] presents a computational method based on the estimation of the arm swivel angle (which parametrizes the arm posture) for exoskeleton-based therapy. The arm IK is solved with a redundancy resolution criterion that chooses a swivel angle that allows the subject to retract the palm to the head efficiently. The approach in [88] extends their previous work in [29, 34] by considering the influence of the wrist orientation on the swivel angle estimation. Although the error of the swivel angle estimation (mean error $\approx$ 4 deg.) is reported for compound movements in [88], the individual errors in the wrist, elbow, and GH joint angles are not indicated.

Ref. [107] extends the method in [88] to estimate the wrist angles and assesses its performance for compound movements (mean RMSE $\approx$ 10 deg. in the swivel angle estimation). Ref. [107] reports the individual errors of the arm joint angles only for the movement task in which the swivel angle was best estimated (mean RMSE $\approx$ 5 deg. in the swivel angle estimation). No errors of the arm joint angles are discussed for the other cases. A limitation of the work in Ref. [107] is that the MOCAP used to obtain the reference angles to assess their method performance is a custom-made inertial system with no reported measurement accuracy.

III-E.4.2.1 Conclusions of the Literature Review

We remind the reader that the general context of this article is the estimation of the GH joint angles.

1. As per our Literature Review, no MOCAPs have been developed for the specific scenario of exoskeleton-based rehabilitation. Even if current MOCAPs and the exoskeleton could be arranged to be used simultaneously (e.g. [90, 106]), the setup protocol and operation is intricate and conflicting with the typical time and resources available for patient treatment.

2. Exoskeleton-based posture estimations present limitations in their accuracy due to the kinematic mismatch of the limb and exoskeleton ([90, 106]).

3. The accuracy of the estimations of the GH joint angles provided by the computational methods in [88, 90] is unknown. Ref. [107] extends the work in [88] by estimating the wrist angles. This work reports the accuracy in the estimation of GH angles for the best-case scenario and the precision of its ground - truth MOCAP is not indicated.

III-E.4.2.2 Contributions of this Article

In response to the discussed limitations in the estimation of the patient joint angles in exoskeleton-based therapy (sections III-E.4.2 and III-E.4.2.1), this article proposes, implements and assesses,

in silico, a methodology to estimate, in real-time, the GH joint angles in RAR by using a hybrid approach composed by a low - cost marker-based vision system and the rehabilitation robot, overcoming the individual limitations of its constitutive subsystems:

(a) Occlusions are minimized, which are a major limitation of optical systems.

(b) Accuracy of joint angle estimation is improved, which is a major limitation of exoskeleton-based systems.

We consider the following scenarios of application of the proposed method in the RAR domain:

(A) Precise estimation of the GH joint angles during rehabilitation or evaluation sessions of analytic movements of the GH joint.

(B) Acquisition of movement data of the GH joint that allow the validation and improvement of other posture estimation methods without using expensive redundant optical MOCAPs.

III-E.4.3 Methods

III-E.4.3.1 Problem Definition

This section presents the problem of estimating the GH joint angles of the patient limb during the RAR of the GH joint by using the proposed hybrid motion capture system (a detailed version of the problem definition is presented in Appendix III-E.4.A). This problem can be stated as follows:

Given:

1. Patient: (a) The kinematic model (e.g., the Denavit-Hartenberg parameters [54]) of the human upper limb (H) (Fig. III-E.4.2(a)).
2. Exoskeleton: (a) The kinematic model of the exoskeleton (E) and (b) the exoskeleton joint angles at any instant of the therapy ($v^E(t)$) (Fig. III-E.4.2(b)).
3. Marker-based optical motion capture system (R): (a) The color and depth information captured by the RGB-D cameras installed on the exoskeleton links and (b) the geometry and color of the markers attached to the patient upper limb (Fig. III-E.4.2(c)).

Goal:

To estimate with minimum error the angles of the GH joint of the patient ($v_G^H(t)$) during the GH joint rehabilitation exercises.

III-E.4.3.2 Kinematic Models

This section discusses the main features of the kinematic models of the human limb and exoskeleton that were used for the posture estimation method.

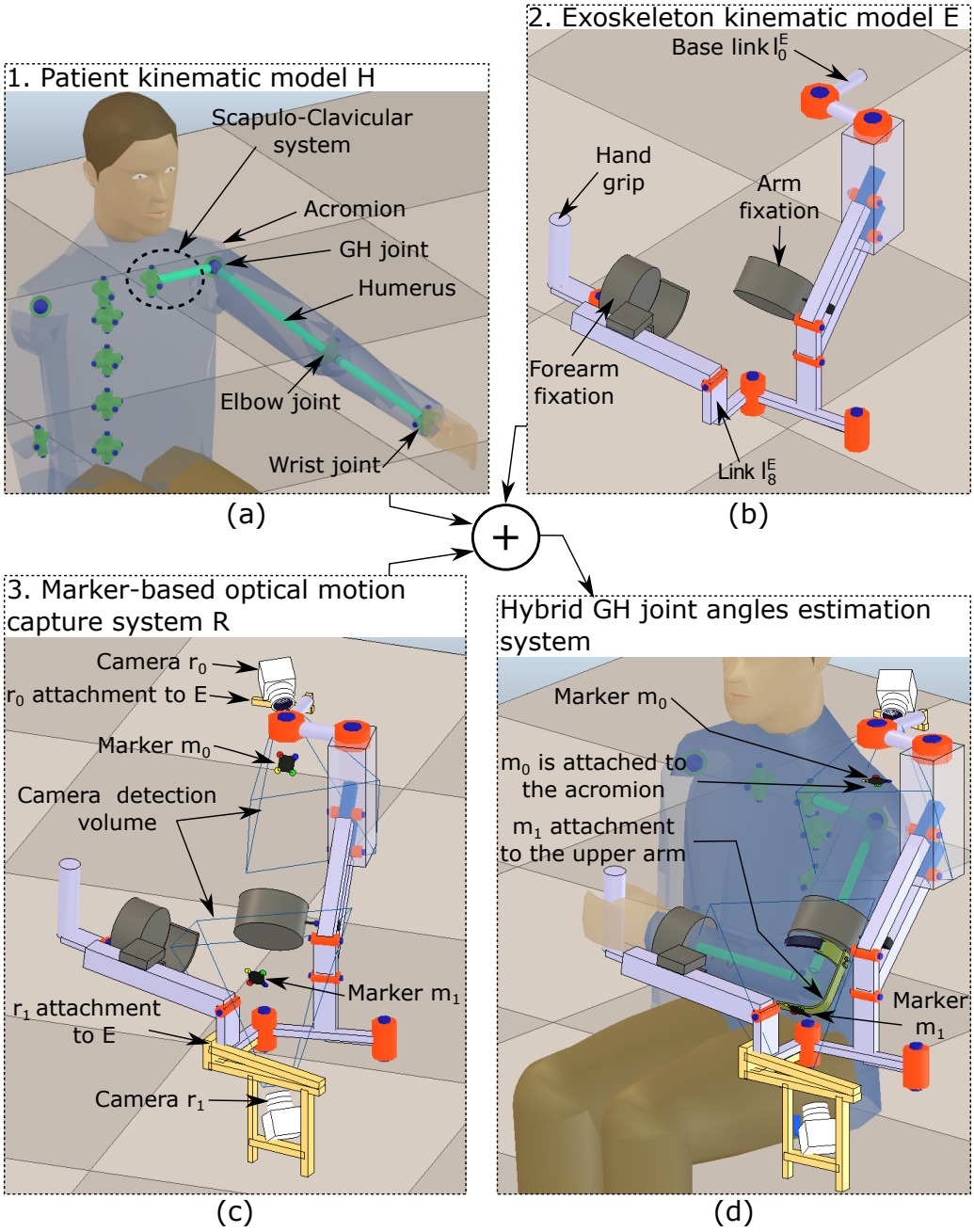

Figure III-E.4.2: Components of the GH joint angles estimation system: (a) Human kinematic model, (b) Exoskeleton kinematic model, (c) Marker-based optical motion capture system, and (d) Hybrid GH joint angles estimation system.

III-E.4.3.2.1 Kinematic Model of the Human Upper Body

The human kinematic model is denoted by $H(L^H, J^H)$, where L^H and J^H are the sets of links and joints, respectively. We use the human upper body model presented in [90] (Fig. III-E.4.2 (a)), which includes joints of the spine, scapulo-clavicular system and arm. The upper limb is modeled with 9-DOF: 2-DOF of the scapulo-clavicular system, 3-DOF of the GH joint (spherical joint), 2-DOF of the elbow and 2-DOF of the wrist (see further details in Appendix III-E.4.A). This model presents the following advantages:

(a) It can be easily implemented in robotic simulators and similar tools.

(b) It is suitable to simulate the human-robot interaction in real-time ([90]).

(c) The spherical model of the GH joint avoids limitations of other representations of such joint, such as the Gimbal lock that occurs when using the three concurrent and orthogonal 1-DOF revolute joints model ([57]).

III-E.4.3.2.2 Kinematic Model of the Exoskeleton

The exoskeleton kinematic model is denoted by $E(L^E, J^E)$, where L^E and J^E are the sets of links and joints, respectively. In this investigation, the rehabilitation exoskeleton that we use is the Armeo Spring (Fig. III-E.4.2(b)), which is a passive system that supports the weight of the arm of the patient ([108]) by using springs. The Armeo kinematic structure includes rotational joints (equipped with encoders [55,109]) and prismatic joints (which allow adjusting the exoskeleton to the size of each patient). We use the Armeo Spring kinematic model presented in [90], which includes both types of joints (see further details in Appendix III-E.4.A).

III-E.4.3.3 GH Joint Angles Estimation Method

The objective of the method is to estimate the angles of the GH joint with respect to (w.r.t.) a coordinate system (CS) attached to the scapulo-clavicular system. Fig. III-E.4.2(d) shows the proposed system for the GH joint angles estimation. Our approach is based on the estimation of the upper arm orientation w.r.t. the acromion (Fig. III-E.4.3(a)). According to such requirements, the rationale to install the markers of the optical MOCAP R is as follows:

(a) Marker m_0 is rigidly installed on the acromion, such that the estimated upper arm orientation can be expressed w.r.t. the m_0 CS (and therefore w.r.t. the scapulo-clavicular system).

(b) Marker m_1 is rigidly installed on the upper arm, such that all the rotations of the upper arm are captured by m_1. The region that was chosen to attach m_1 to the upper arm by using a custom-made fixation (Fig. III-E.4.2 (d)) is the distal part of the humerus (near the elbow). The rotations of the elbow do not affect the orientation of m_1.

Ref. [110] reports a five-marker installation procedure. This reference explicitly mentions five markers as an acceptable number for clinical upper limb tracking. In this manuscript, we report the usage of two markers for upper arm tracking. It is not possible to compare the performance of the marker placement protocol proposed here with the one in [110] because the work in [110] addresses: (a) non-RAR scenarios, (b) the tracking of the whole upper limb and (c) the sensitivity of the protocol w.r.t. its application on the dominant / non-dominant arm and w.r.t. the age of

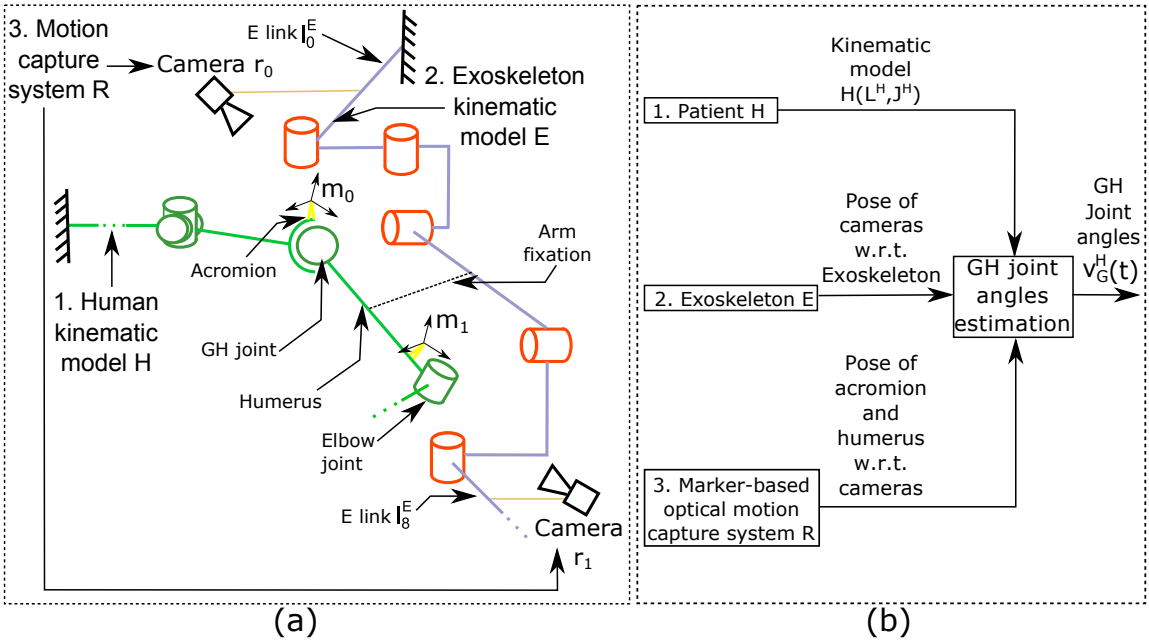

Figure III-E.4.3: (a) Schematic diagram of the hybrid GH joint angles estimation system and (b) high-level operation of the system.

the test subjects. However, the work in [110] helps to establish the number of markers that are compatible with the clinical application of upper limb tracking.

The cameras of the optical motion capture system R are rigidly attached (by using custom-made supports) to the links of the exoskeleton such that camera r_0 is able to detect marker m_0 and camera r_1 is able to detect marker m_1 during the GH joint training. Camera r_0 is mounted on link l_0^E and camera r_1 is mounted on link l_8^E (Fig. III-E.4.3(a)).

The cameras used in our system are low-cost. Commercial cameras that present similar specifications to the ones simulated here (Table III-E.4.1) are: Intel® SR300 (99 USD) [111, 112], DepthSense® 525 (164 USD) [113, 114] and CamBoard pico^S (690 USD) [112, 115].

Fig. III-E.4.3(b) shows an overview of the operation of the estimation method. In order to estimate the pose of the upper arm, the poses of the markers need to be expressed w.r.t. a common CS. A suitable CS to conduct such estimation is the exoskeleton base.

A summary of the steps to estimate the GH joint angles is the following:

1. Estimate the pose of the markers w.r.t. the cameras.
2. Estimate the pose of the cameras w.r.t. the exoskeleton.
3. Estimate the pose of the markers w.r.t. the exoskeleton.
4. Estimate the upper arm pose w.r.t. the exoskeleton.
5. Refer the angles of the GH joint w.r.t. the acromion (marker m_0 CS).

The details of the mentioned steps are presented in the following sections.

III-E.4.3.3.1 Estimation the Pose of the Markers w.r.t. the Cameras

The objective of this step is to estimate the position and orientation of the markers (Fig. III-E.4.4) w.r.t. the CSs of the cameras by using the color and depth images provided by each camera r_i:

(A) The RGB image is I_i^c ($A \times B$ pixels). The pixel coordinates (u, v) take values: $0 \leq u \leq A-1$ and $0 \leq v \leq B-1$. C_i (1×3*A*B) contains the RGB color associated to each pixel $(u, v) \in I_i^c$.

(B) The depth image associated to the scene in I_i^c is I_i^d ($L \times N$ pixels). $L \leq A$ and $N \leq B$. The pixel coordinates (u, v) in I_i^d take values: $0 \leq u \leq L-1$ and $0 \leq v \leq N-1$. The CS of images I_i^c and I_i^d is coincident. D_i ($1 \times L$*N*3) contains the (X, Y, Z) coordinates of the object in each pixel $(u, v) \in I_i^d$ w.r.t. the r_i CS.

The pose estimation of the markers w.r.t. the cameras is based on the reconstruction of the 3-D position of the colored disks on the markers. The following steps are taken to conduct the marker pose estimation:

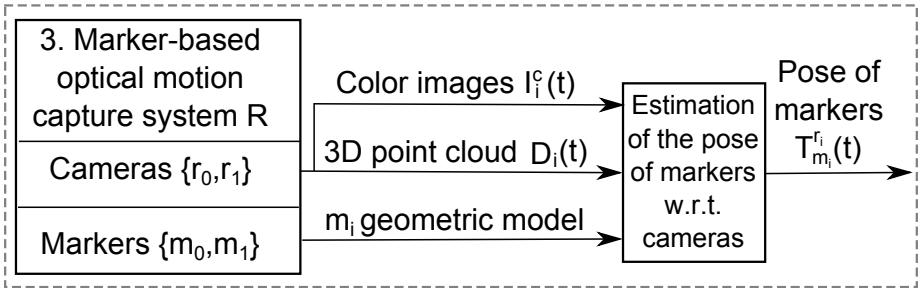

Figure III-E.4.4: Schematic diagram of the iterative estimation of the pose of the markers.

(1) Estimation of disk coordinates in color image (Fig. III-E.4.5): The goal of this step is to find the approximated (u, v) coordinates of the centers of the marker disks in image I_i^c. The following steps are conducted:

   (a) Color segmentation on image I_i^c: Image regions containing the colors of the marker disks are preserved and the remaining regions are assigned with a different color. The resulting image is defined as I_i^{sc}.

   (b) Blob extraction on image I_i^{sc}: Blob extraction consists in finding the connected regions in the image I_i^{sc} that share the same color and to label them according to their color.

   (c) Disk center coordinates estimation: For each j ($j = 0, \ldots, n$) blob extracted from I_i^c, the position $\tilde{p}_j^{I_i^c} \in \mathbb{Z}^2$ of the center of a bounding box for the blob is obtained. This point approximates the actual center of disk $p_j^{I_i^c}$ (Fig. III-E.4.5). The resulting set of the approximate coordinates of the disks centers in I_i^c is $\tilde{P}^{I_i^c} = \left\{\tilde{p}_0^{I_i^c}, \ldots, \tilde{p}_j^{I_i^c}, \ldots, \tilde{p}_n^{I_i^c}\right\}$. The $\mathbb{Z}^2$ center coordinates are referenced w.r.t. the internal image CS. Blobs are extracted with standard connected-component labeling algorithms.

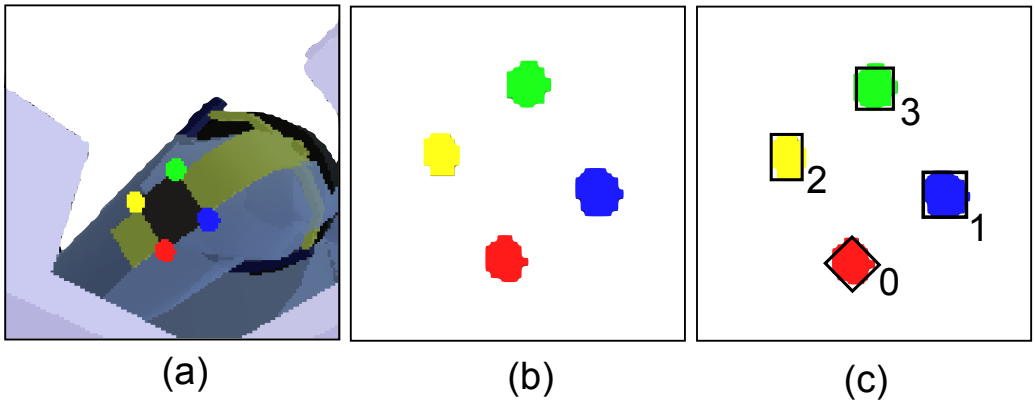

Figure III-E.4.5: Estimation of disk coordinates in color image. (a) Simulated RBG image, (b) result of the color segmentation (zoomed image) and (c) result of the blob extraction (zoomed image).

(2) Estimation of disk coordinates in the camera r_i CS: This step converts disk coordinates in the internal image CS to the $\mathbb{R}^3$ ones w.r.t. the r_i sensor CS, as follows:

(a) Convert to the image I_i^d CS the positions (u, v) of the disk centers in set $\tilde{P}^{I_i^c}$. The CSs of images I_i^c and I_i^d match. Hence:

$$\tilde{p}_j^{I_i^d} = \begin{pmatrix} \frac{L-1}{A-1} & 0 \\ 0 & \frac{N-1}{B-1} \end{pmatrix} \tilde{p}_j^{I_i^c}. \tag{III-E.4.1}$$

(b) Compute the indices $a_j^{I_i^d}$ of the (X, Y, Z) coordinates of point $\tilde{p}_j^{I_i^d}$ in array D_i, as follows:

$$\begin{aligned} a_j^{I_i^d}(x) &= 3 * (\tilde{p}_j^{I_i^d}(u)) + L * (\tilde{p}_j^{I_i^d}(v)) \\ a_j^{I_i^d}(y) &= 3 * (\tilde{p}_j^{I_i^d}(u)) + L * (\tilde{p}_j^{I_i^d}(v)) + 1 \\ a_j^{I_i^d}(z) &= 3 * (\tilde{p}_j^{I_i^d}(u)) + L * (\tilde{p}_j^{I_i^d}(v)) + 2. \end{aligned} \tag{III-E.4.2}$$

The point $\tilde{p}_j^{r_i}$ contains the (X, Y, Z) coordinates of point $\tilde{p}_j^{I_i^d}$ w.r.t. the r_i CS. The coordinates of point $\tilde{p}_j^{r_i}$ are obtained as follows:

$$\begin{aligned} \tilde{p}_j^{r_i}(x) &= D_i[a_j^{I_i^d}(x)] \\ \tilde{p}_j^{r_i}(y) &= D_i[a_j^{I_i^d}(y)] \\ \tilde{p}_j^{r_i}(z) &= D_i[a_j^{I_i^d}(z)]. \end{aligned} \tag{III-E.4.3}$$

The approximated marker disk centers detected by camera r_i form the set $\tilde{P}^{r_i} = \{\tilde{p}_0^{r_i}, \ldots, \tilde{p}_j^{r_i}, \ldots, \tilde{p}_n^{r_i}\}$.

(3) Computation of the marker m_i CS in the r_i camera CS: An $SO(3)$ coordinate frame $T_{m_i}^{r_i} = \left[\hat{V}_x \hat{V}_y \hat{V}_z O_{m_i}\right]$ is attached to each marker.

(a) Make

$$O_{m_i} = (\tfrac{1}{n+1}) \sum_{j=0}^{n} (\tilde{p}_j^{r_i}). \tag{III-E.4.4}$$

(b) Use the four disk centers in the marker (Fig. III-E.4.5) as follows:

$$\begin{aligned} \vec{V_x} &= (\tfrac{1}{2})((\tilde{p}_0^{r_i} - \tilde{p}_1^{r_i}) + (\tilde{p}_2^{r_i} - \tilde{p}_3^{r_i})) \\ \vec{V_y} &= (\tfrac{1}{2})((\tilde{p}_2^{r_i} - \tilde{p}_0^{r_i}) + (\tilde{p}_3^{r_i} - \tilde{p}_1^{r_i})) \\ \hat{V_z} &= \hat{V_x} \times \hat{V_y}. \end{aligned} \tag{III-E.4.5}$$

The sub-matrix $\left[\hat{V_x}\hat{V_y}\hat{V_z}\right]$ is normalized to guarantee its $SO(3)$ nature. The frame $\tilde{T}_{m_i}^{r_i}$ describes the estimated pose of marker m_i w.r.t. the CS of the camera r_i.

III-E.4.3.3.2 Estimation of the Pose of the Cameras w.r.t. the Exoskeleton

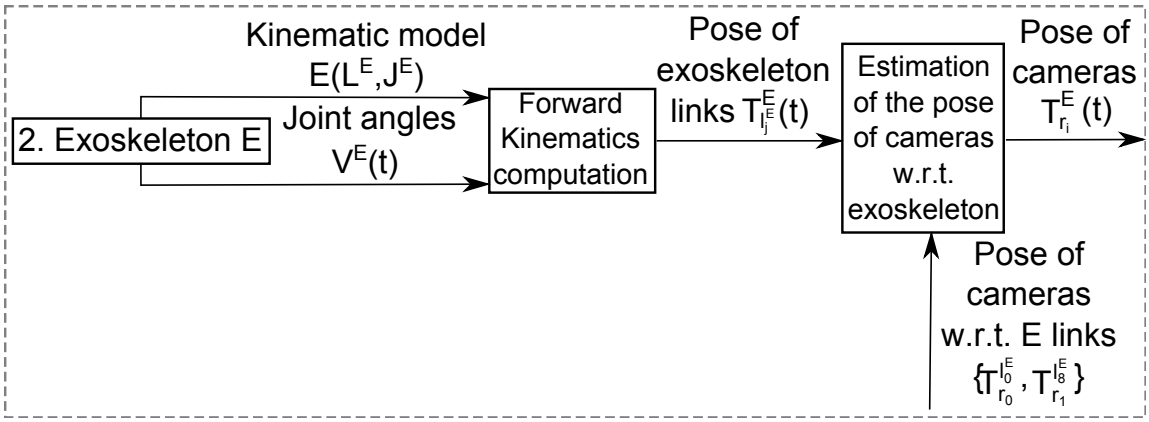

Figure III-E.4.6: Schematic diagram of the iterative estimation of the pose of the cameras.

The goal of this step is to find the transformation $T_{r_i}^E$, which expresses the pose of the camera r_i w.r.t. the base of the exoskeleton (Fig. III-E.4.6).

The rigid transformation matrices $T_{r_0}^{l_0^E}$ and $T_{r_1}^{l_8^E} \in \mathbb{R}^{4\times4}$, which describe the pose of the cameras r_i w.r.t. the CS of the link where they are installed on, are estimated during the calibration of the system (the calibration matrix can be obtained by detecting with the camera a 2-D / 3-D calibration object mounted on a known location of the exoskeleton). The poses $T_{l_0^E}^E$ and $T_{l_8^E}^E$ of the exoskeleton links l_0^E and l_8^E w.r.t. to the exoskeleton base CS are computed by using the Forward Kinematics of exoskeleton E. Then, $T_{r_0}^E$ and $T_{r_1}^E$ are estimated as:

$$\begin{aligned} \tilde{T}_{r_0}^E &= \tilde{T}_{l_0^E}^E * \tilde{T}_{r_0}^{l_0^E} \\ \tilde{T}_{r_1}^E &= \tilde{T}_{l_8^E}^E * \tilde{T}_{r_1}^{l_8^E}. \end{aligned} \tag{III-E.4.6}$$

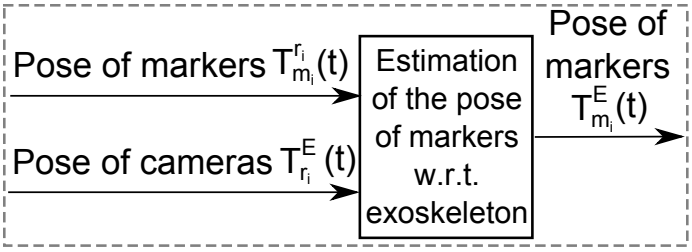

Figure III-E.4.7: Schematic diagram of the iterative estimation of the pose of the markers w.r.t. the Exoskeleton CS.

III-E.4.3.3.3 Estimation of the Pose of the Markers w.r.t. the Exoskeleton

The objective of this step is to estimate the transformation ($T^E_{m_i}$) that describes the pose of marker m_i w.r.t. the exoskeleton base CS (Fig. III-E.4.7). Transformations $T^E_{m_i}$ are estimated as follows:

$$\begin{aligned} \tilde{T}^E_{m_0} &= \tilde{T}^E_{r_0} * \tilde{T}^{r_0}_{m_0} \\ \tilde{T}^E_{m_1} &= \tilde{T}^E_{r_1} * \tilde{T}^{r_1}_{m_1}. \end{aligned} \tag{III-E.4.7}$$

III-E.4.3.3.4 Estimation of the Upper Arm Pose w.r.t. the Exoskeleton

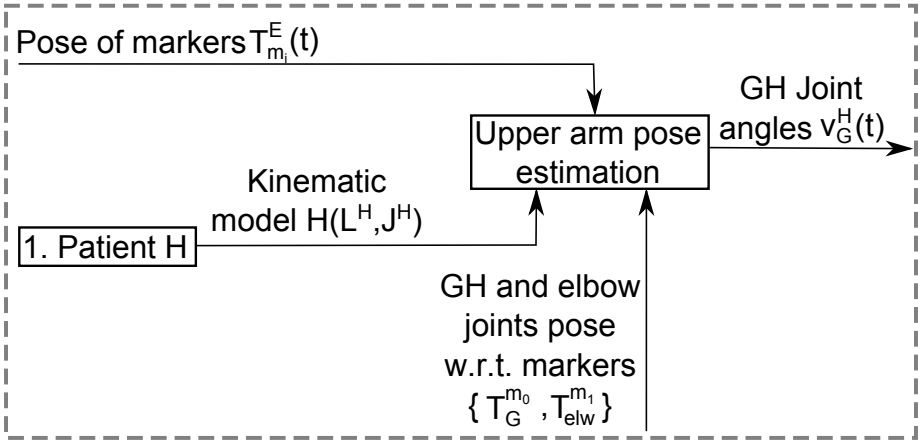

Figure III-E.4.8: Schematic diagram of the iterative estimation of the upper arm pose.

The purpose of this step is to estimate the upper arm pose (T^E_{arm}) w.r.t. the exoskeleton base CS by using the marker poses $T^E_{m_i}$ (Fig. III-E.4.8). The upper arm direction vector is computed from the estimated position of the end-points of the upper arm (GH and elbow joint centers) as follows (CSs in Fig. III-E.4.9):

(1) Estimate the position of the GH joint center: The rigid transformation matrix $T^{m_0}_G$, which expresses the pose of the GH joint CS w.r.t. the m_0 CS, is estimated during the calibration process of the system. Hence, the GH joint center is estimated as follows:

(a) Estimate T_G^E, which is the pose of the GH joint CS w.r.t. the exoskeleton E base CS (Eq. III-E.4.8).

(b) Extract p_G^E from T_G^E. The point p_G^E is the position of the center of the GH joint seen from the E CS.

$$\tilde{T}_G^E = \tilde{T}_{m_0}^E * \tilde{T}_G^{m_0}. \tag{III-E.4.8}$$

(2) Estimate the position of the elbow joint center: The rigid transformation matrix $T_{elw}^{m_1}$ (elbow joint CS w.r.t. the m_1 CS) is estimated during the calibration process of the system. Hence, the elbow joint center is computed as follows:

(a) Estimate T_{elw}^E, which is the pose of the elbow joint CS w.r.t. the exoskeleton E base CS (Eq. III-E.4.9).

(b) Extract p_{elw}^E from T_{elw}^E. The point p_{elw}^E is the position of the center of the elbow joint seen from the E CS.

$$\tilde{T}_{elw}^E = \tilde{T}_{m_1}^E * \tilde{T}_{elw}^{m_1}. \tag{III-E.4.9}$$

(3) Estimate the upper arm position:

(a) Estimate the arm direction vector as: $\hat{V}_{arm} = (\tilde{p}_G^E - \tilde{p}_{elw}^E) / \left\| \tilde{p}_G^E - \tilde{p}_{elw}^E \right\|$.

(b) Estimate the origin of the upper arm CS as: $\tilde{p}_{arm}^E = 1/2 * \left\| \vec{V}_{arm} \right\| * \hat{V}_{arm} + \tilde{p}_{elw}^E$.

(4) Estimate the upper arm orientation: The estimated orientation of the upper arm is computed by using Euler angle YXZ decomposition w.r.t. the base CS of exoskeleton E:

(a) Estimate the rotation of the arm around the Y-axis of the E CS by using the projection of $\hat{V}_{arm}$ on the X-Z plane of the fixed E CS.

(b) Compute the rotation of the arm around the mobile X-axis of E CS from the inner product of $\hat{V}_{arm}$ with the mobile Z-axis of E CS.

(c) Estimate the rotation of the upper arm around its longitudinal axis $\vec{V}_{arm}$ as the rotation of the marker m_1 around vector $\hat{V}_{arm}$. This angle is the one between (i) the mobile X-axis of E CS and (ii) the projection of X-axis of marker m_1 CS onto the X-Y plane of E CS.

(5) Express the pose of the upper arm w.r.t. the E base CS as the 4x4 rigid transformation T_{arm}^E.

III-E.4.3.3.5 Refer the Angles of the GH joint w.r.t. the Acromion

Since m_0 is rigidly attached to the acromion, the upper arm orientation can be expressed w.r.t. the acromion by using the inverse of $T_{m_0}^E$:

$$\tilde{T}_{arm}^{m_0} = \tilde{T}_E^{m_0} * \tilde{T}_{arm}^E. \tag{III-E.4.10}$$

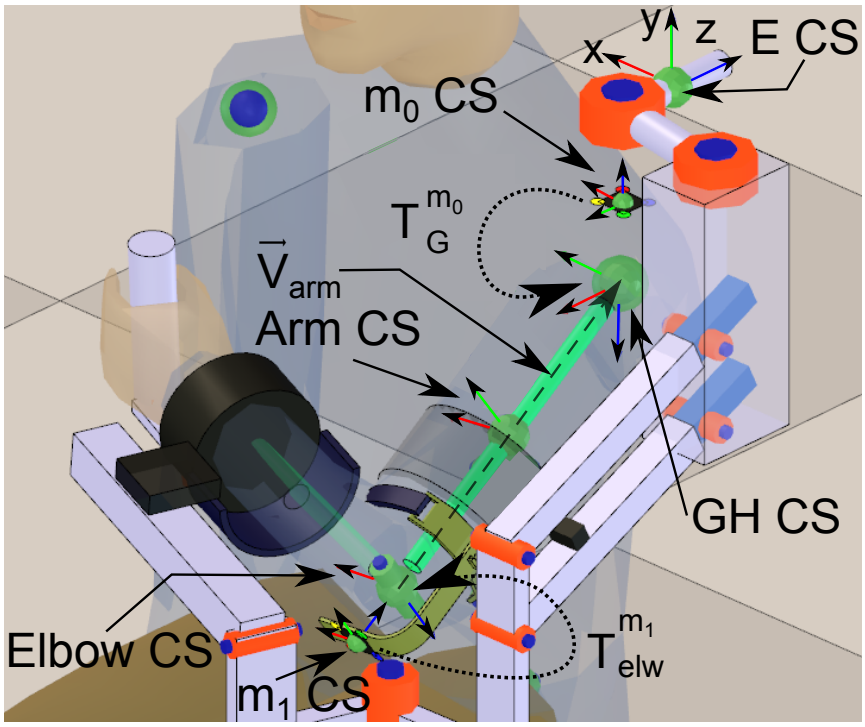

Figure III-E.4.9: Coordinate Systems for the Upper Arm Pose Estimation.

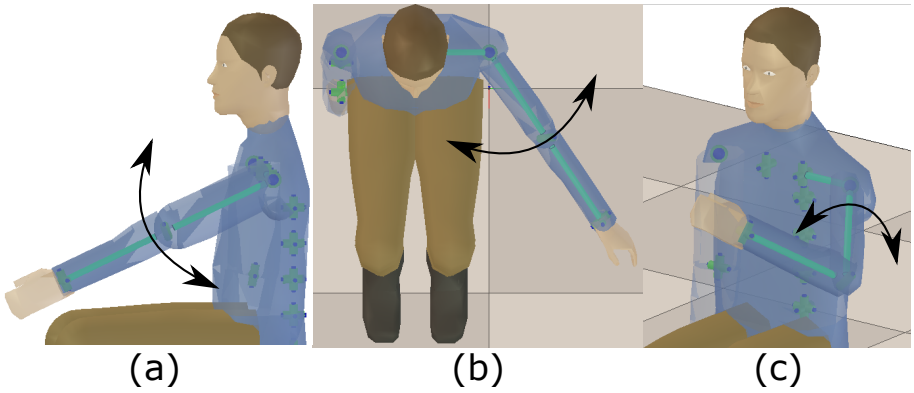

Figure III-E.4.10: GH joint movements: (a) flexion-extension (SFE), (b) horizontal abduction-adduction (SAbAd) and (c) internal rotation (SIR).

III-E.4.3.4 Implementation and Simulation

The arm posture estimation method was implemented by using the V-REP robotics simulator ([63]). In the simulator, the scene in Fig. III-E.4.2(d) is created, which includes the models of: (a) a human patient, (b) an Armeo Spring, (c) the RGB-D vision sensors with the couplings to attach them to the exoskeleton and (d) the planar markers with the couplings to attach them to the human arm. The configuration of the simulated vision sensors is summarized in Table III-E.4.1.

Table III-E.4.1: Vision Sensor Features.

Color camera resolution (px):	128×128
Depth camera resolution (px):	128×128
Field of view (deg.):	Horizontal= 45 ;Vertical= 45
Minimum sensing distance (meters):	0.05
Maximum sensing distance (meters):	0.3

For the estimation of the coordinates of disk centers $P^{I_i^c}$ in the image I_i^c, color segmentation and blob detection algorithms available in the simulator were used. Additional code was written to sort blob centers by color. All additional code was written in LUA (Lightweight embeddable scripting language) scripts.

III-E.4.3.4.1 Generation of the Ground-Truth Poses of the Patient Upper Limb during RAR

The accuracy of the proposed method is determined by comparing its estimations of the upper arm poses with the ones of the simulated human patient (ground-truth values of $T_{arm}^{m_0}$). To generate movements of the simulated patient that resemble the ones of therapy, we performed the next steps:

1. Armeo movement generation: We recorded 4 time sequence datasets of the actual Armeo joint measurements (sampled at 66.6 Hz) while performing the following shoulder movements (Fig. III-E.4.10): (a) horizontal abduction-adduction (SAbAd), (b) flexion-extension (SFE),

(c) internal rotation (SIR) and (d) a combination of all the mentioned movements (COMB). These movement history datasets are used to guide a simulation of the Armeo model.

2. Patient movement generation: The movements of the patient upper limb that correspond to the recorded movements of the Armeo, are computer-generated with the method in [90]. Such method provides an estimation of the patient posture given the joint angles of the exoskeleton by using an inverse kinematics approach.

In this way, four sets (one per movement dataset) of known poses of the upper arm are obtained by simulating the patient movement and compared here with the ones estimated with our method. Our method accuracy is assessed without compensating any time offsets between the reference and estimated angles. In this way, the real-time accuracy of the method is assessed. Table III-E.4.2 presents the approximate amplitudes of the YXZ Euler angle decomposition of the movements of the GH joint of the simulated patient w.r.t. its local CS.

Table III-E.4.2: Movement Dataset Features.

Movement Dataset:	**Amplitude (deg)**	**Samples**
SAbAd	(6°, 31°, 10°)	1000
SFE	(31°, 8°, 1°)	1000
SIR	(3°, 3°, 34°)	1000
COMB	(40°, 90°, 60°)	2000

III-E.4.3.4.2 Measurement of the Estimation Performance

1. Error in the estimation of the markers position: The error in the position estimation of markers m_i is computed as the RMS of expression $e_{pos}^{m_i} = \left\| p_{m_i}^E - \tilde{p}_{m_i}^E \right\|$, where $i \in \{0, 1\}$.

2. Error in the estimation of the arm pose: The error in the arm position estimation for a GH joint movement dataset (e_{pos}^{arm}) is computed as the RMS of $\|p_{arm}^{m_0} - \tilde{p}_{arm}^{m_0}\|$ for all the samples in the movement dataset.

   To quantify the error in the estimation of the arm orientation (e_{ori}^{arm}), the next steps are conducted:

   (a) Compute the matrix of rotation error $Rot_{error} = Rot_{arm}^{m_0} * \left(\tilde{Rot}_{arm}^{m_0}\right)^{-1}$ where $Rot_{arm}^{m_0}$ and $\tilde{Rot}_{arm}^{m_0}$ are the rotation submatrices of transformation matrices $T_{arm}^{m_0}$ and $\tilde{T}_{arm}^{m_0}$, respectively.

   (b) Express Rot_{error} in exponential map notation ([57]) as $e_{ori}^{\vec{arm}} \in \mathbb{R}^3$.

   (c) Compute e_{ori}^{arm} as the RMS of $\left\| e_{ori}^{\vec{arm}} \right\|$ for all the samples in the movement dataset.

III-E.4.3.5 Sensitivity Analysis

A sensitivity analysis is conducted to study the influence of relevant parameters on the method accuracy. Formally, the sensitivity analysis determines the effect of the perturbation of the parameter Q on the objective function $F(Q)$. The relative sensitivity of $F(Q)$ w.r.t. Q, S_Q^F, is given by Eq.

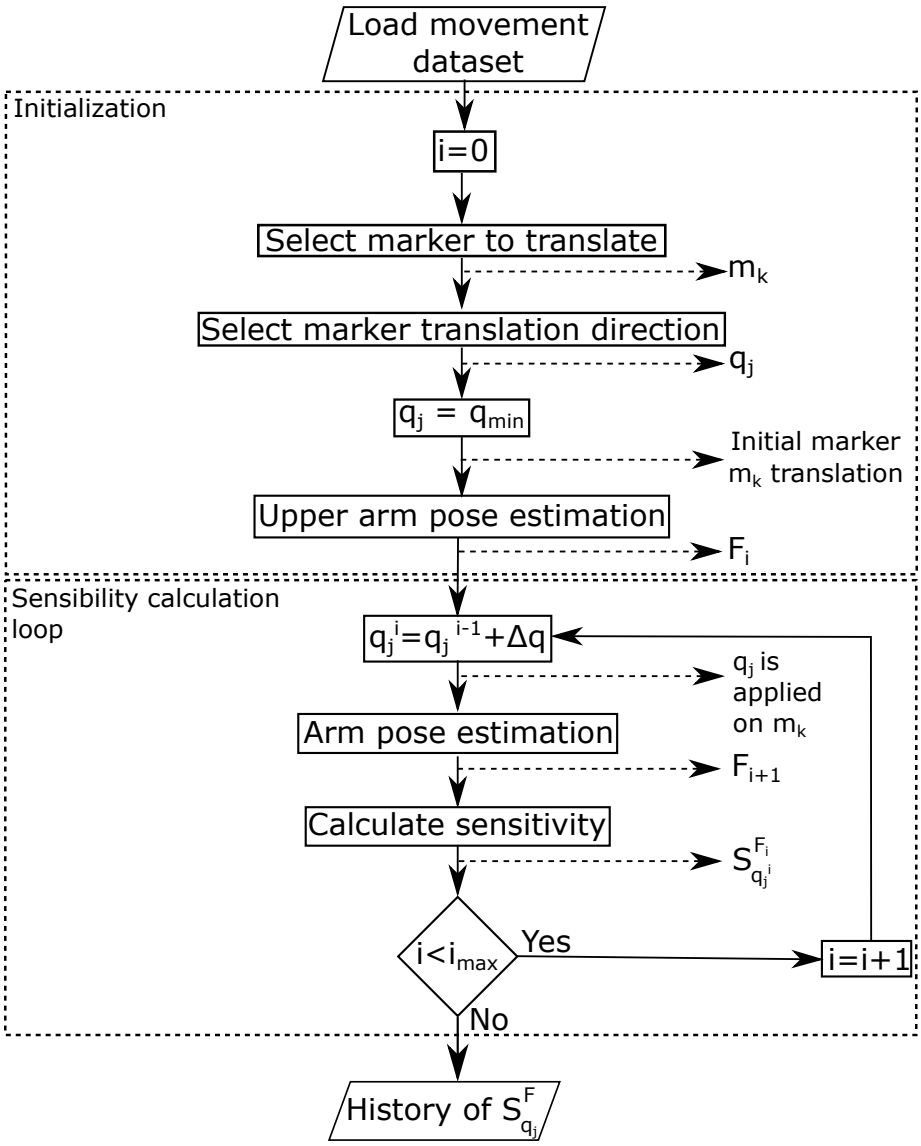

Figure III-E.4.11: Steps of the sensitivity analysis.

III-E.4.11 ([116]). The value of S_Q^F is the ratio (dimensionless) between the percentual changes in F and Q.

$$S_Q^F = \frac{\partial F/F}{\partial Q/Q} = \frac{\partial ln(F)}{\partial ln(Q)}. \tag{III-E.4.11}$$

The upper arm pose accuracy (and therefore, the one of the GH joint angles) relies on the precise estimation of the position of the centers of the elbow and GH joints ($\tilde{p}_{elw}^E$ and $\tilde{p}_G^E$) (section III-E.4.3.3.4), which ultimately depend on following the transformations involving the markers:

(a) $\tilde{T}_{m_0}^E$ and $\tilde{T}_{m_1}^E$ (markers w.r.t. exoskeleton).

(b) $T_G^{m_0}$ and $T_{elw}^{m_1}$ (GH and elbow joints w.r.t. markers).

The conducted sensitivity analysis focuses on errors in $T_G^{m_0}$ and $T_{elw}^{m_1}$, given that errors in the estimation of $\tilde{T}_{m_0}^E$ and $\tilde{T}_{m_1}^E$ (section III-E.4.4.2) are small. Possible causes of errors in $T_G^{m_0}$ and $T_{elw}^{m_1}$ are:

1. Inaccurate computation of $T_G^{m_0}$ and $T_{elw}^{m_1}$ during the system calibration.
2. Relative displacement of the markers w.r.t. the GH and elbow joints due to skin movement.

In the sensitivity analysis, translations errors in matrices $T_G^{m_0}$ and $T_{elw}^{m_1}$ are induced by disturbing the location of the markers m_k ($k = [0, 1]$) w.r.t. the CSs of the GH and elbow joints. Since orientation information in $T_G^{m_0}$ and $T_{elw}^{m_1}$ is not used to estimate the upper arm pose, it is excluded from the sensitivity analysis.

For the sensitivity analysis (Eq. III-E.4.11), the vector-valued function $F(q)$ quantifies the estimation error of the arm position and orientation (Eq. III-E.4.12) and the parameter set q represents the marker translation errors. The parameter set q is defined as $q = \{q_1, q_2, q_3, q_4, q_5, q_6\}$, where each $q_j \in q$ is a scalar representing the magnitude of a translation of a specific marker along a prescribed direction. Table III-E.4.3 describes the meaning of each parameter in set q.

$$F(q) = \big(e_{pos}^{arm}(q), e_{ori}^{arm}(q)\big); F(q) : \mathbb{R}^6 \rightarrow \mathbb{R}^2. \tag{III-E.4.12}$$

Table III-E.4.3: Parameters of function $F(q)$ (error in the position and orientation estimation of the upper arm (Eq.III-E.4.12)) to study in the sensitivity analysis.

Parameter:	**Meaning**	**CS of reference**
q_1	Translation with magnitude $\|q_1\|$ of m_0 along X axis	GH joint
q_2	Translation with magnitude $\|q_2\|$ of m_0 along -Y axis	GH joint
q_3	Translation with magnitude $\|q_3\|$ of m_0 along Z axis	GH joint
q_4	Translation with magnitude $\|q_4\|$ of m_1 along -X axis	Elbow joint
q_5	Translation with magnitude $\|q_5\|$ of m_1 along Y axis	Elbow joint
q_6	Translation with magnitude $\|q_6\|$ of m_1 along -Z axis	Elbow joint

The sensitivity analysis procedure (Fig. III-E.4.11) entails the next steps:

1. Load the movement dataset of the GH joint to test (SFE, SAbAd, SIR, COMB).

2. Select the parameter $q_j \in q$ to perturb (selection of a marker and a direction of translation). Marker m_0 translates along axes of the GH joint CS. Marker m_1 translates along axes of the elbow joint CS (Fig.III-E.4.12).

3. Apply the translation indicated by q_j to the corresponding marker. The marker perturbation q_j is applied for the complete movement dataset.

4. Compute the errors in the estimation of the position and orientation of the upper arm $F_i(q) = (e^{arm}_{pos\ i}(q), e^{arm}_{ori\ i}(q))$ as the simulated patient moves according to the chosen movement dataset of the GH joint. The current iteration of the process is indicated by index i.

5. Compute the position and orientation components of $S^F_{q_j}$ as per Eq. III-E.4.11. The derivative of $F(q)$ w.r.t. q_j is given by Eq. III-E.4.13. The required derivatives are computed numerically ([117, 118]).

$$\partial F(q)/\partial q_j = (\partial e^{arm}_{pos}(q)/\partial q_j, \partial e^{arm}_{ori}(q)/\partial q_j). \quad \text{(III-E.4.13)}$$

6. Increment q_j by Δq and go to step 3. Repeat the process until the desired number of iterations i of the procedure are reached.

The complete sensitivity analysis was performed for each movement dataset (SFE, SAbAd, SIR, COMB). The directions in which marker translations take place (Table III-E.4.3) are chosen such that the makers do not leave the detection volume of the cameras. Table III-E.4.4 summarizes the parameters of the sensitivity analysis. Translation units are meters (mts).

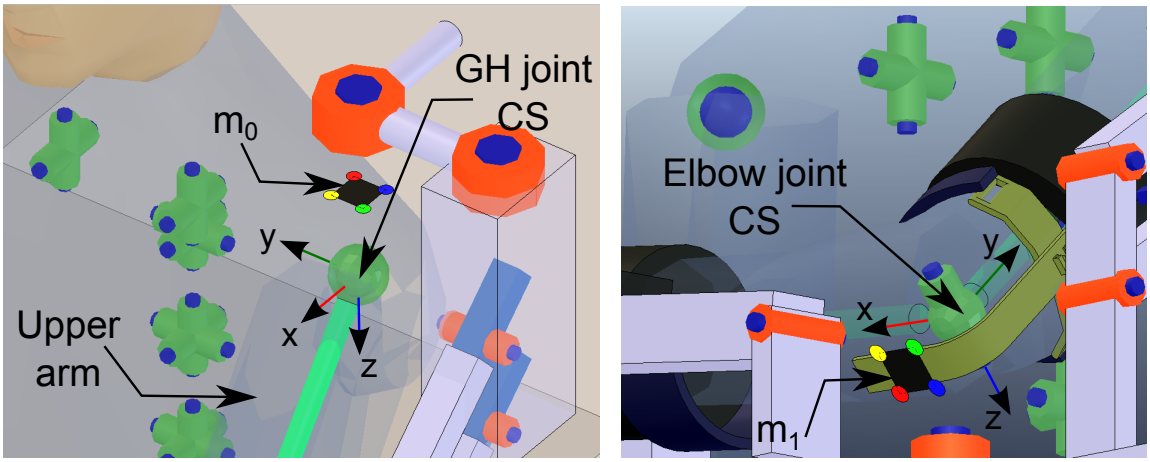

Figure III-E.4.12: Sensitivity Analysis. Coordinate systems of reference for the translations of (a) marker m_0 and (b) marker m_1.

Table III-E.4.4: Parameters of the sensitivity analysis.

Minimum marker translation q_{min} (mts)	0
Maximum iterations of the sensitivity analysis i_{max}	10
Increment of marker translation in each iteration Δq (mts)	0.002
Movement datasets evaluated	4

III-E.4.4 Results and Discussion

This section presents and discusses the results of: (a) accuracy of the estimation of the markers 3D position, (b) accuracy of the estimation of the upper arm pose, and (c) the sensitivity analysis of the accuracy of the pose estimation of the upper arm w.r.t. translation errors in $T_G^{m_0}$ and $T_{elw}^{m_1}$.

III-E.4.4.1 Results of Marker Position Estimation

Table III-E.4.5 presents the RMS of the errors in the estimation of the position of the markers m_i for each movement dataset. The mean RMS errors of the position estimation of m_0 and m_1 for all movement datasets are 0.00083 and 0.00208 mts, respectively.

Fig. III-E.4.13 shows the box plots of the estimation errors in the markers position for all movement datasets. Larger variation in the accuracy of the position estimation of marker m_1, in comparison to the one of m_0, is observed. This is attributed by us to (a) the higher linear and rotational velocities and (b) the larger translations and rotations that m_1 undergoes compared to m_0.

Table III-E.4.5: RMS of errors (and standard deviation in parentheses) in the estimation of the position of markers m_i in the datasets of GH joint movements.

Movement:	m_0 [mts]	m_1 [mts]
SAbAd	0.00089 (0.0001)	0.00175 (0.001)
SFE	0.00060 (0.0002)	0.00197 (0.0008)
SIR	0.00088 (0.0001)	0.00135 (0.0007)
COMB	0.00097 (0.0003)	0.00324 (0.002)

III-E.4.4.2 Results of Upper Arm Pose Estimation

The RMS of errors in the estimation of the upper arm pose are presented in Table III-E.4.6. By averaging the results of all movement datasets, errors of 0.00110 mts. and 0.88921 deg. in the estimation of the upper arm position and orientation are obtained. Fig. III-E.4.13 shows the box plots of the estimation errors in the upper arm position and orientation for all movement datasets.

In motor rehabilitation, angular errors in the range of $3-5$ degrees are considered acceptable for mobility evaluation of patients ([43, 102, 119]). Fig. III-E.4.13 shows that the accuracy in our arm orientation estimation is adequate for exoskeleton-assisted rehabilitation.

Table III-E.4.6: RMS (and standard deviation in parentheses) of errors in the estimation of the position and orientation of the upper arm in the assessed movement datasets.

Movement:	**Position** [mts]	**Orientation** [deg]
SAbAd	0.00109 (0.0005)	0.92039 (0.4842)
SFE	0.00094 (0.0004)	0.83796 (0.3763)
SIR	0.00091 (0.0002)	0.73465 (0.4156)
COMB	0.00145 (0.0008)	1.0638 (0.5238)

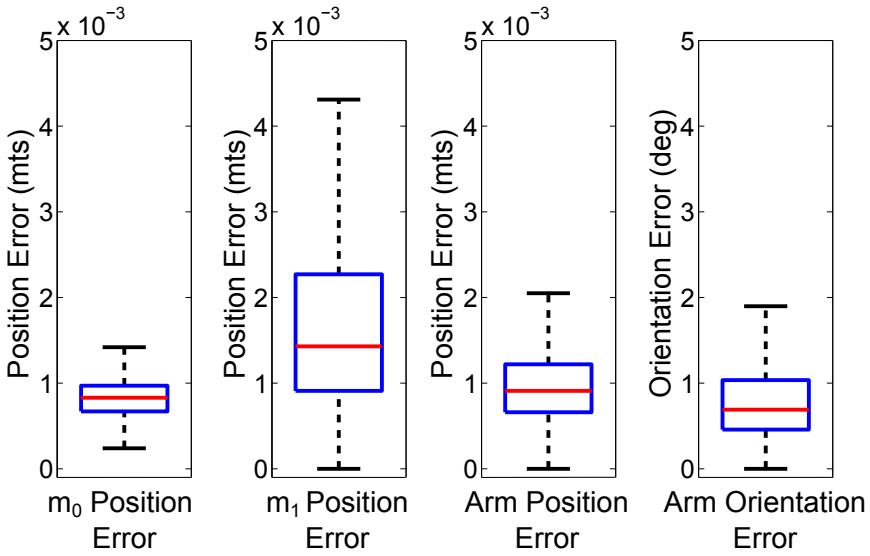

Figure III-E.4.13: Box plots of estimation errors of the markers position, upper arm position and upper arm orientation for all movement datasets.

III-E.4.4.3 Results of the Sensitivity Analysis

The results of the sensitivity analysis for each movement dataset of the shoulder are presented in Figs. III-E.4.14, III-E.4.15, III-E.4.16 and III-E.4.17. In each figure, the following sub-figures are presented:

(a) Error in upper arm position estimation (e_{pos}^{arm}) vs. total marker translation (q_j). This figure shows the evolution of the absolute error in the upper arm position estimation as the error in the translation components of matrices $T_G^{m_0}$ and $T_{elw}^{m_1}$ increases.

(b) Error in upper arm orientation estimation (e_{ori}^{arm}) vs. total marker translation (q_j). This figure shows the evolution of the absolute error in the upper arm orientation estimation as the error in the translation components of matrices $T_G^{m_0}$ and $T_{elw}^{m_1}$ increases.

(c) Position component of $S_{q_j}^F$ vs. total marker translation (q_j). This figure shows the evolution of the relative sensitivity metric corresponding to the error in the upper arm position estimation as the error in the translation components of matrices $T_G^{m_0}$ and $T_{elw}^{m_1}$ increases.

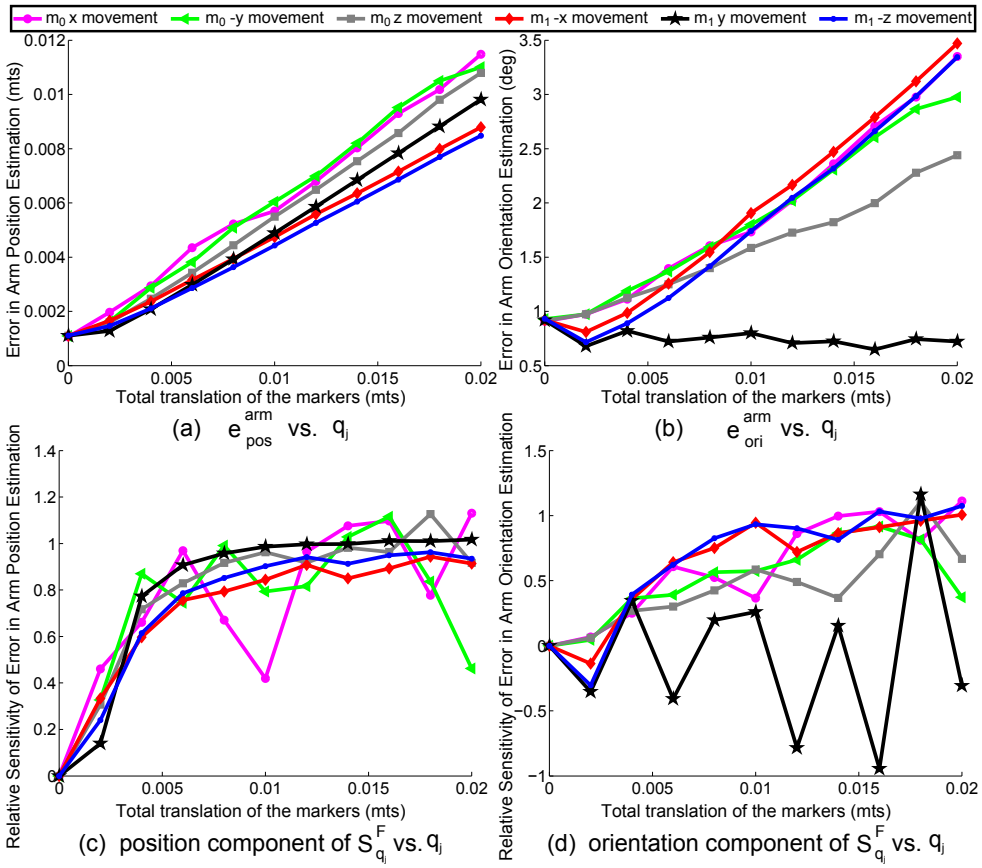

Figure III-E.4.14: Results of the sensitivity analysis with the SAdAd movement dataset (q_j: m_0 X movement / m_0 -Y movement / m_0 Z movement / m_1 -X movement / m_1 Y movement / m_1 -Z movement).

(d) Orientation components of $S^F_{q_j}$ vs. total marker translation (q_j). This figure shows the evolution of the relative sensitivity metric corresponding to the error in the upper arm orientation estimation as the error in the translation components of matrices $T^{m_0}_G$ and $T^{m_1}_{elw}$ increases.

III-E.4.4.3.1 Sensitivity in Arm Position Estimation

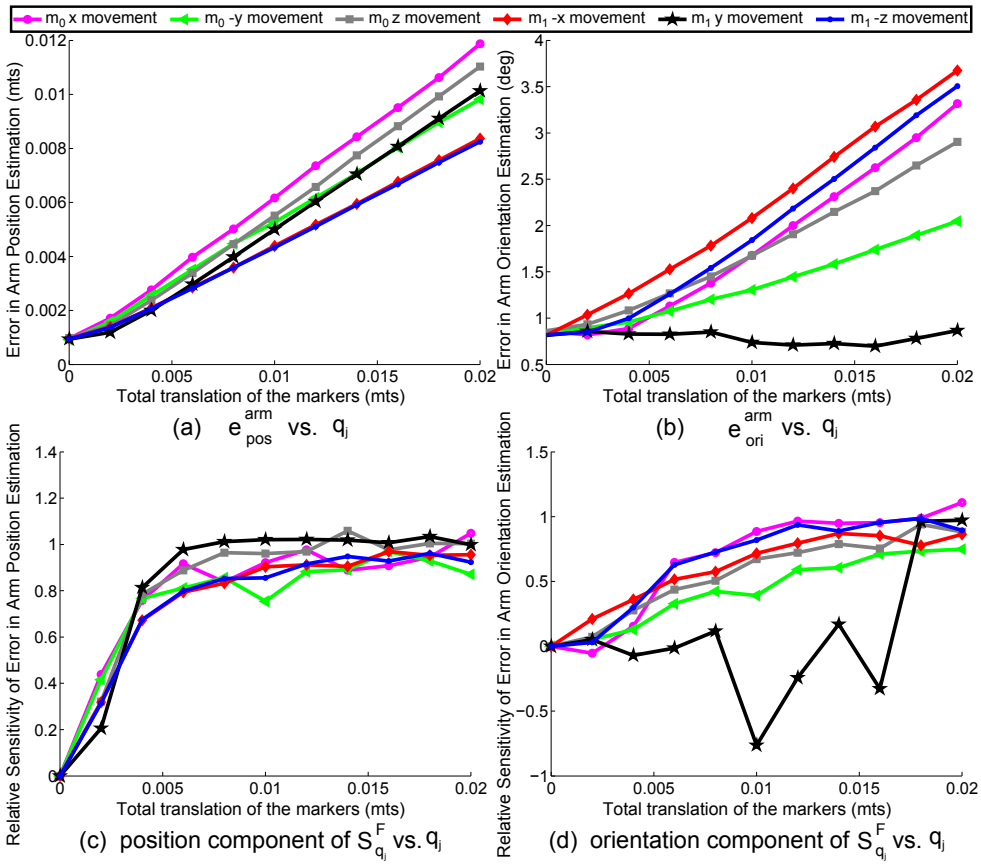

Figure III-E.4.15: Results of the sensitivity analysis with the SFE movement dataset (q_j: m_0 X movement / m_0 -Y movement / m_0 Z movement / m_1 -X movement / m_1 Y movement / m_1 -Z movement).

Regarding the estimation of the arm position, it can be observed that translations of marker m_0 produce larger absolute errors than translations of marker m_1. This difference is due to the fact that the translations of m_0 produce a larger change in $\left\|\vec{V}_{arm}\right\|$ when compared to the one produced by translations of m_1. Note that, since $\tilde{p}^E_{arm}$ is computed by using $\vec{V}_{arm}$, any modification in $\left\|\vec{V}_{arm}\right\|$ directly affects the accuracy of $\tilde{p}^E_{arm}$.

Observing the behavior of the position component of $S^F_{q_j}$, it can be concluded that all the translations of the markers m_0 and m_1 contribute similarly to the error in the estimation of the arm

position. The obtained curves for the position component of $S^F_{q_j}$ resemble a logarithmic function with an asymptote along the value 1 of the ordinate axis. A value of 1 in the magnitude of the position component of $S^F_{q_j}$ means that a percentual change in the magnitude of the marker translation produced the same percentual change (also matching the sign) in the magnitude of the error in the estimation of the arm position.

III-E.4.4.3.2 Sensitivity in Arm Orientation Estimation

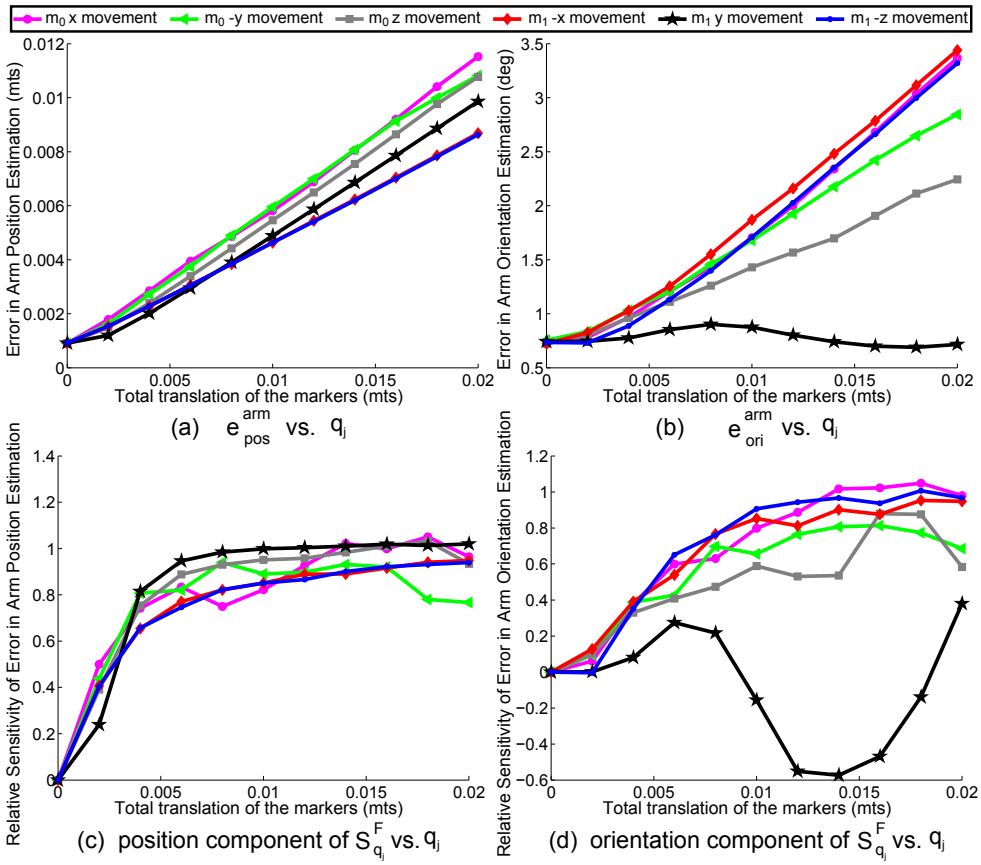

Figure III-E.4.16: Results of the sensitivity analysis with the SIR movement dataset (q_j: m_0 X movement / m_0 -Y movement / m_0 Z movement / m_1 -X movement / m_1 Y movement / m_1 -Z movement).

In Figs. III-E.4.14, III-E.4.15, III-E.4.16 and III-E.4.17, it can be observed that the translations of marker m_1 produce larger absolute errors in the estimation of the upper arm orientation when compared to the ones produced by translations of marker m_0. Notice that the X and Z axes of the elbow joint CS are always perpendicular to the upper arm vector ($\vec{V}_{arm}$) (Fig. III-E.4.12 (b)). When the position of m_1 is perturbed along such axes, the angle between (i) the actual upper arm vector ($\vec{V}_{arm}$) and (ii) the estimated vector of the upper arm ($\tilde{V}_{arm}$) (which is inaccurate because

of the perturbation of the marker position) is maximal.

A side effect of the marker position perturbation is that the marker m_i suffers modifications of scale and level of perspective distortion in the images of the camera r_i, affecting the accuracy of the system. This situation can be observed in Figs. III-E.4.14(b), III-E.4.15(b), III-E.4.16(b) and III-E.4.17(b), where translations of m_1 along the Y axis of the elbow joint CS should not produce variations in the orientation estimation error. However, on the contrary, slight variations in the accuracy of the orientation estimation are indeed present in the mentioned figures.

III-E.4.4.3.3 Robustness of the Upper Arm Pose Estimation Method

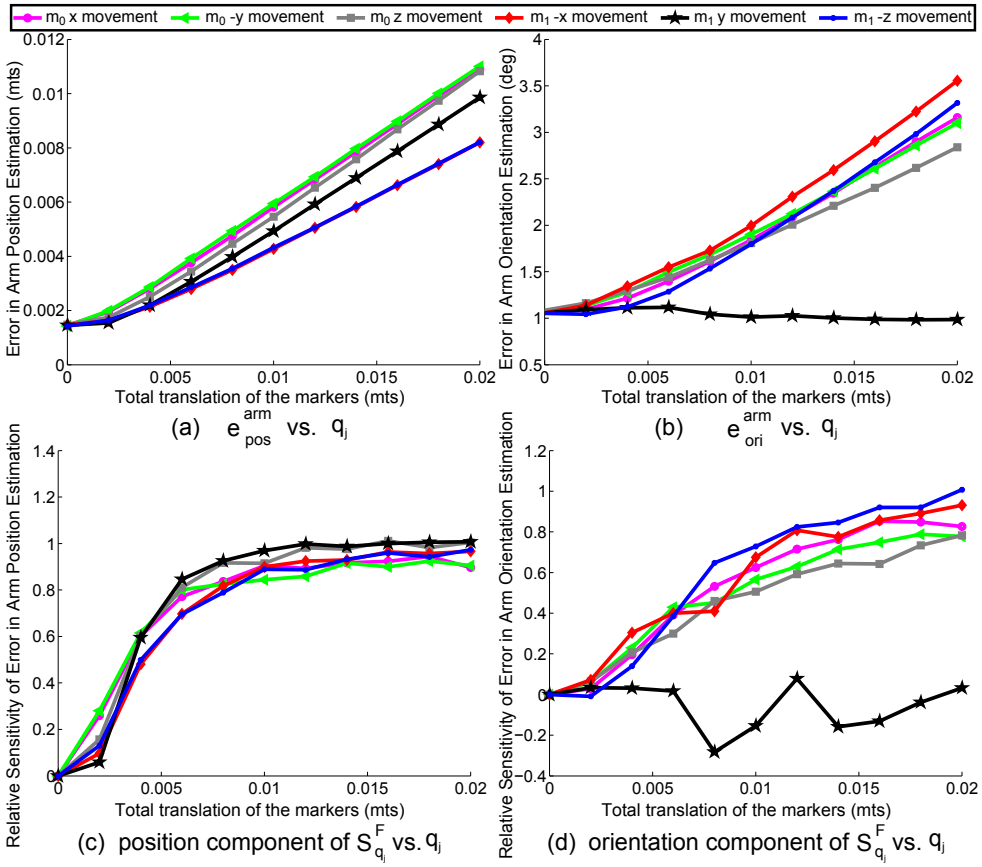

Figure III-E.4.17: Results of the sensitivity analysis with the COMB movement dataset (q_j: m_0 X movement / m_0 -Y movement / m_0 Z movement / m_1 -X movement / m_1 Y movement / m_1 -Z movement).

In Figs. III-E.4.14(c) and (d), III-E.4.15(c) and (d), III-E.4.16(c) and (d) and III-E.4.17(c) and (d) it can be observed that the position component of $S^F_{q_j}$ increases faster than the orientation component of $S^F_{q_j}$. The observed behavior of $S^F_{q_j}$ remains across the datasets used. Hence, the orientation estimation of the upper arm is more robust than the position estimation w.r.t. errors

in the translational components of matrices $T_G^{m_0}$ and $T_{elw}^{m_1}$.

The results of the sensitivity analysis show that the assumption that transformations $T_G^{m_0}$ and $T_{elw}^{m_1}$ are rigid is reasonable. Even with maker drifts of 0.02 mts, the GH joint angles can be estimated with an accuracy (around 3.6 degrees RMS) adequate for the mobility evaluation of patients (in the range of 3 - 5 degrees).

Marker drifts must be mitigated by the attachments of the markers to the human body. Furthermore, marker attachments should be designed to minimize the effect of errors in $T_G^{m_0}$ and $T_{elw}^{m_1}$ on the accuracy of the method. For example, notice how the attachment of marker m_1 (Fig. III-E.4.12(b)) locates marker m_1 with an offset w.r.t. the elbow joint center along the direction that least affects the orientation estimation of the upper arm.

The presented results suggest that our implemented method is a feasible alternative to estimate the GH joint angles in a RAR scenario.

III-E.4.4.4 Comparison with Related Works

The conducted literature review provided no other references than [29,34,88,90,107] for upper limb posture estimation (including the GH joint) in exoskeleton-based rehabilitation by using computational methods. Among the mentioned works, only Ref. [107] reports the errors (mean RMSE 4.8 deg.) in the GH joint angles estimation. Ref. [107] reports RMSE values of the GH joint angles only for the best-case scenario (swivel angle mean RMSE 5 deg.). For all the movement tasks tested, the method in [107] presents a mean RMSE of 10 deg. for the swivel angle estimations. Given that the global errors of the swivel angle double the ones of the best-case scenario, a report of the global errors of the GH joint angle estimations of the method in [107] is required to conclude about its suitability to be used in clinical applications.

Table III-E.4.7 summarizes the comparison of our contributions w.r.t. comparable works (i.e. Ref. [107]).

III-E.4.5 Conclusions and Future Work

In the context of RAR, this article presents the formulation, implementation, and assessment, in silico, of a novel and accurate method to estimate the patient GH joint angles during therapy. Our implemented method does not require redundant markers or cameras and relies on simple geometric relationships and tools of standard robotics and computer vision libraries. These characteristics make it economical and readily applicable in RAR.

The accuracy and the robustness of our method are evaluated using computer-generated human movement data corresponding to actual movement datasets of the Armeo Spring. We present a formal sensitivity analysis of the pose estimation accuracy w.r.t. marker position estimation errors produced by (a) system calibration errors and (b) marker drifts (due to skin artifacts). This analysis indicates that even in presence of large marker position errors our method presents an accuracy that is acceptable for the mobility appraisal of patients.

Future work includes: (a) implementation of the method using commercially available RGB-D vision sensors, (b) evaluation of the method accuracy with actual human movement data, (c) adaptation of the method to use only RGB cameras, and (d) extension of our method to address other limbs.

Table III-E.4.7: Contributions of this article w.r.t. comparable works.

Work	**Method**	**Method Evaluation**	**Accuracy of GH joint angles**
[107]	IK-based swivel angle estimation.	(1) Studied angles: Swivel angle plus the shoulder, elbow and wrist joint angles. (2) Reference angles: Obtained from custom-made inertial MOCAP. Homologation - Calibration of the readings is not reported. (3) Movements: Compound movements. (4) Sensitivity Analysis: No.	mean RMSE: 4.8 deg (best-case scenario).
This article	Hybrid exoskeleton-optical MOCAP	(1) Studied angles: Shoulder angles. (2) Reference angles: Simulated. (3) Movements: 1-DOF and multi-DOF shoulder movements. (4) Sensitivity Analysis: Method accuracy w.r.t. marker position errors produced by marker drift or calibration errors.	(a) mean RMSE: 0.9 deg. (assuming no marker drift or calibration errors). (b) mean RMSE: 3.6 deg. (with marker drift or calibration errors up to 20 mm).

Appendix

III-E.4.A Problem Statement

Given:

1. A human patient upper body with a kinematic model $H(L^H, J^H)$ (Fig. III-E.4.2(a)). Remarks:

   (a) The model is a simplified version of the spine, arm and scapulo-clavicular systems. However, given that we focus on the study of the upper limb, we describe in detail only the kinematic model of such limb.

   (b) The set of Links is $L^H = \left\{l_0^H, \ldots, l_{g+1}^H\right\}$, which contains the sternum, clavicle, upper arm, forearm and hand ($g = 4$).

   (c) The set of Joints is $J^H = \left\{j_0^H, \ldots, j_g^H\right\}$, which contains the sternoclavicular joint, GH joint, elbow joint, and wrist joint.

      i. X_i denotes the number of DOF of j_i^H. $X_i = 1, 2$ or 3 ($i = 0, 1, \ldots, g$).

      ii. $v_i^H = (\theta_1, \ldots, \theta_{X_i})$ is an X_i-tuple whose k-th component is the angle of the k-th DOF of joint i-th, j_i^H ($i = 0, 1, \ldots, g$).

      iii. G is the index of the GH joint ($0 \leq G \leq g$). $X_G = 3$ since the GH joint has 3 DOF. v_G^H is the 3-tuple containing the values of the DOF of the G (GH) joint.

      iv. $v_G^H(t)$ registers the status, at time t, of the DOF of the GH joint.

   (d) H is an open Kinematic Chain, and therefore, l_i^H and l_{i+1}^H are connected by joint j_i^H ($i = 0, 1, \ldots, g$).

2. An exoskeleton with a kinematic model $E(L^E, J^E)$, which is attached to the patient limb H and assists the patient when performing the rehabilitation exercises (Fig. III-E.4.2(b)). Remarks:

   (a) The sets of Links is $L^E = \left\{l_0^E, \ldots, l_{f+1}^E\right\}$.

   (b) The sets of Joints is $J^E = \left\{j_0^E, \ldots, j_f^E\right\}$.

      i. Y_i denotes the number of DOF of j_i^E.

      ii. $v_i^E = (\theta_1, \ldots, \theta_{Y_i})$ is a Y_i-tuple whose k-th component is the angle of the k-th DOF of joint i-th, j_i^E ($i = 0, 1, \ldots, f$).

(c) E is modeled as an open Kinematic Chain, and therefore, l_i^E and l_{i+1}^E are connected by joint j_i^E $(i = 0, 1, \ldots, f)$.

(d) The v^E b-tuple ($b = \sum_{i=0}^{f} Y_i$) contains the set of independent coordinates which uniquely defines a configuration of E.

i. $v^E = \left(v_0^E, \ldots, v_i^E, \ldots, v_f^E\right)$.

ii. $v^E(t)$ registers the state, at time t, of the DOF of E, which is known $\forall t$.

(e) The exoskeleton may be configured to impose specific motion constraints on the patient by blocking specific joints of the J^E set.

3. A marker-based optical tracking system R composed by two RGB-D cameras and two planar markers (Fig. III-E.4.2(c)). Remarks:

(a) A set $M = \{m_0, m_1\}$ of planar markers that are detected by the cameras of R and are installed on the patient upper limb.

i. All m_i present the same 2D square geometry, with a disk on each corner. The position of each disk w.r.t. the marker CS is known. The set of disks is $K = \{k_0, \ldots, k_j, \ldots, k_n\}$.

A. k_j presents a color $s_j \in S$ that can be detected by R (Fig.III-E.4.2(c)).

B. The set of colors of the disks mounted on in each m_i is $S = \{s_0, \ldots, s_j, \ldots, s_n\}$. Each $s_j \in \mathbb{R}^3$ is represented with a RGB color code.

C. $s_j \neq s_i \forall i, j \in [0, n] \wedge i \neq j$.

ii. m_0 is mounted on the acromion with a 0-DOF coupling (Fig. III-E.4.2(d)). A rigid transformation matrix $T_G^{m_0}$ defines the relative position and orientation of the GH joint CS w.r.t. the CS of m_0.

iii. m_1 is mounted on the upper arm with a 0-DOF coupling (Fig. III-E.4.2(d)). A rigid transformation matrix $T_{elw}^{m_1}$ defines the relative position and orientation of the elbow joint CS w.r.t. the CS of m_1. Note that to compute the GH joint angles, the calculation of the elbow joint angles is not necessary with this setup.

iv. The rigid transformation matrices $T_G^{m_0}$ and $T_{elw}^{m_1} \in \mathbb{R}^{4\times4}$ are estimated during the calibration of the system.

(b) A set $R = \{r_0, r_1\}$ of low-cost cameras is installed on the exoskeleton.

i. r_0 is mounted on exoskeleton link l_0^E with a 0-DOF coupling, such that the disks on m_0 are inside its detection volume during the rehabilitation exercises. The rigid transformation matrix $T_{r_0}^{l_0^E}$ defines the relative position and orientation of the CS of r_0 w.r.t. the l_0^E CS.

ii. r_1 is mounted on the exoskeleton link l_8^E with a 0-DOF coupling, such that it can detect the disks on m_1 (see Fig.III-E.4.2(c)). The rigid transformation matrix $T_{r_1}^{l_8^E}$ defines the relative position and orientation of the CS of r_1 w.r.t. the l_8^E CS.

iii. The rigid transformation matrices $T_{r_0}^{l_0^E}$ and $T_{r_1}^{l_8^E} \in \mathbb{R}^{4\times4}$ are estimated during the calibration of the system.

iv. Remarks on each camera r_i:

A. r_i renders a RGB image I_i^c of $A \times B$ pixels. The pixel coordinates (u, v) take values: $0 \leq u \leq A-1$ and $0 \leq v \leq B-1$.

B. r_i renders a depth image associated to the scene in I_i^c, defined as I_i^d, of $L \times N$ pixels. $L \leq A$ and $N \leq B$. The pixel coordinates (u, v) in I_i^d take values: $0 \leq u \leq L-1$ and $0 \leq v \leq N-1$. The CS of images I_i^c and I_i^d is coincident.

C. r_i presents a truncated square pyramid detection volume parametrized by: the minimum and maximum detection distances, and the horizontal and vertical field of view of r_i. Table III-E.4.1 presents the model features of the vision sensors that have been used for the simulations.

v. The system of cameras R produces the following array sequence of each r_i:

A. C_i (1 × 3*A*B) contains the RGB color associated to each pixel $(u, v) \in I_i^c$.

B. D_i (1 × L*N*3) contains the (X,Y,Z) coordinates of the object in each pixel $(u, v) \in I_i^d$ w.r.t. the r_i CS.

Goal:

1. Find the values of $\tilde{v}_G^H(t) \in \mathbb{R}^3$, which approximates $v_G^H(t)$ such that $e = \left\| v_G^H(t) - \tilde{v}_G^H(t) \right\|^2$ be minimum $\forall t$.

   (a) $\|x\|$ is the Euclidean norm of vector x.

Part IV
General Conclusions

This doctoral thesis presents several contributions to the fields of Medical Imaging, Image-Guided Surgery and Motor Neurorehabilitation by developing and applying techniques from the area of Computational Geometry.

Medical Imaging:
We contribute with methods for (a) parametric curve reconstruction and (b) geometry simplification of porous materials. Our curve reconstruction method effectively deals with self-intersecting and non-Nyquist 2D noisy points samples. The formal study on the influence of several parameters on the curve reconstruction method allowed us to devise a strategy to tune such parameters hierarchically. We have also explored the use of spectral analysis to detect faulty curve reconstructions. The automatization of such diagnostic tool is an open opportunity of research.

Our geometry simplification method approximates models of open-cell porous materials with high fidelity to their geometry and topology. Mechanical simulations show that the simplified model reasonably approximates the elastic behavior of a reference finite element model, with the advantage of demanding significantly less computational resources than the reference one. A possible extension of this work is the adaptation of the simplified model for computational fluid dynamics experiments.

Image-Guided Surgery:
Our contributions to the patient registration problem range from the controlled acquisition of medical images to a registration algorithm itself, which are key components for the development of a platform for fully automatic patient registration.

For the controlled acquisition of medical images, we implemented a robotic platform that precisely handles medical image acquisition devices in teleoperation and path following modes. By using such robotic platform, we generated an ultrasound image dataset (publicly available) with ground-truth to test 2D-3D or 3D-3D registration algorithms. The controlled acquisition of the image dataset enables the formal analysis of the design parameters of registration algorithms. Finally, we developed a 3D-3D US-CT registration method that handles any degree of initial misalignment between the US and CT datasets, as long as both datasets have an appropriate degree of geometrical similarity.

Motor Neurorehabilitation:
We contribute with two methods for the patient posture estimation in exoskeleton-based therapy. The first method, EIKPE, estimates the upper limb joint angles solving the limb inverse kinematics. The assessment of EIKPE with simple and compound movements shows that its accuracy is adequate for the mobility appraisal of patients and that it enhances the exoskeleton-based posture estimates significantly. A natural follow-up of this investigation is the assessment of EIKPE with other upper limb movements and several patient groups.

The second method addresses the shoulder angles estimation by using a system composed by a low-cost marker-based vision system and the rehabilitation exoskeleton. The accuracy quantification and sensitivity analysis of the method performance with simulated movement data show its potential for: (a) patient mobility assessment and (b) acquisition of movement data for the evaluation of other posture estimation methods. As extensions of this investigation, we envision the implementation of the method with commercial RGB-D cameras and its assessment with human motion data.

Bibliography

[1] Ethan S Brown, Tony F Chan, and Xavier Bresson. Completely convex formulation of the chan-vese image segmentation model. *International journal of computer vision*, 98(1):103–121, 2012.

[2] Martin Aigner and Bert Jüttler. Robust fitting of parametric curves. *PAMM*, 7(1):1022201–1022202, 2007.

[3] Atul Thakur, Ashis Gopal Banerjee, and Satyandra K Gupta. A survey of cad model simplification techniques for physics-based simulation applications. *Computer-Aided Design*, 41(2):65–80, 2009.

[4] Ali Jahan and Marjan Bahraminasab. Multicriteria decision analysis in improving quality of design in femoral component of knee prostheses: Influence of interface geometry and material. *Advances in Materials Science and Engineering*, 2015.

[5] Fabrizio Matassi, Alessandra Botti, Luigi Sirleo, Christian Carulli, and Massimo Innocenti. Porous metal for orthopedics implants. *Clinical Cases in Mineral and Bone Metabolism*, 10(2):111, 2013.

[6] Zena J Wally, William van Grunsven, Frederik Claeyssens, Russell Goodall, and Gwendolen C Reilly. Porous titanium for dental implant applications. *Metals*, 5(4):1902–1920, 2015.

[7] Julian R Jones, Peter D Lee, and Larry L Hench. Hierarchical porous materials for tissue engineering. *Philosophical Transactions of the Royal Society of London A: Mathematical, Physical and Engineering Sciences*, 364(1838):263–281, 2006.

[8] Steven Milanese, Susan Gordon, Petra Buettner, Carol Flavell, Sally Ruston, Damien Coe, William O'Sullivan, and Steven McCormack. Reliability and concurrent validity of knee angle measurement: Smart phone app versus universal goniometer used by experienced and novice clinicians. *Manual therapy*, 19(6):569–574, 2014.

[9] John W Krakauer. Motor learning: its relevance to stroke recovery and neurorehabilitation. *Current opinion in neurology*, 19(1):84–90, 2006.

[10] Sergei V Adamovich, Alma S Merians, Rares Boian, Jeffrey A Lewis, Marilyn Tremaine, Grigore S Burdea, Michael Recce, and Howard Poizner. A virtual realitybased exercise system for hand rehabilitation post-stroke. *Presence: Teleoperators and Virtual Environments*, 14(2):161–174, 2005.

[11] Robert Riener, Tobias Nef, and Gery Colombo. Robot-aided neurorehabilitation of the upper extremities. *Medical and Biological Engineering and Computing*, 43(1):2–10, 2005.

[12] Alessandro De Mauro, Eduardo Carrasco, David Oyarzun, Aitor Ardanza, Anselmo Frizera-Neto, Diego Torricelli, JosLuis Pons, AngelGil Agudo, and Julian Florez. Advanced hybrid technology for neurorehabilitation: The hyper project. In Tauseef Gulrez and AboulElla Hassanien, editors, *Advances in Robotics and Virtual Reality*, volume 26 of *Intelligent Systems Reference Library*, pages 89–108. Springer Berlin Heidelberg, 2012.

[13] Nathanaël Jarrassé and Guillaume Morel. On the kinematic design of exoskeletons and their fixations with a human member. In *Robotics: Science and Systems*. Citeseer, 2010.

[14] Hyunchul Kim, Levi Makaio Miller, Zhi Li, Jay Ryan Roldan, and Jacob Rosen. Admittance control of an upper limb exoskeleton-reduction of energy exchange. In *Engineering in Medicine and Biology Society (EMBC), 2012 Annual International Conference of the IEEE*, pages 6467–6470. IEEE, 2012.

[15] Marco Guidali, Alexander Duschau-Wicke, Simon Broggi, Verena Klamroth-Marganska, Tobias Nef, and Robert Riener. A robotic system to train activities of daily living in a virtual environment. *Medical & biological engineering & computing*, 49(10):1213–1223, 2011.

[16] Antonio Frisoli, Caterina Procopio, Carmelo Chisari, Ilaria Creatini, Luca Bonfiglio, Massimo Bergamasco, Bruno Rossi, Maria Chiara Carboncini, et al. Positive effects of robotic exoskeleton training of upper limb reaching movements after stroke. *Journal of neuroengineering and rehabilitation*, 9(June), 2012.

[17] Maxime Gilliaux, Thierry Lejeune, Christine Detrembleur, Julien Sapin, Bruno Dehez, and Gaetan Stoquart. A robotic device as a sensitive quantitative tool to assess upper limb impairments in stroke patients: A preliminary prospective cohort study. *Journal of Rehabilitation Medicine*, 44(3):210–217, 2012.

[18] Susan E Fasoli, Hermano I Krebs, Joel Stein, Walter R Frontera, and Neville Hogan. Effects of robotic therapy on motor impairment and recovery in chronic stroke. *Archives of physical medicine and rehabilitation*, 84(4):477–482, 2003.

[19] Bambi R Brewer, Sharon K McDowell, and Lise C Worthen-Chaudhari. Poststroke upper extremity rehabilitation: a review of robotic systems and clinical results. *Topics in stroke rehabilitation*, 14(6):22–44, 2007.

[20] Robert W Teasell and Lalit Kalra. Whats new in stroke rehabilitation. *Stroke*, 35(2):383–385, 2004.

[21] Gorka Epelde, Xabier Valencia, Aitor Ardanza, Elsa Fanchon, Alessandro De Mauro, Francisco Molina Rueda, Eduardo Carrasco, and Shabs Rajasekharan. Virtual arm representation and multimodal monitoring for the upper limb robot assisted teletherapy. In *Proceedings of NEUROTECHNIX 2013*, pages 69–80. ScitePress, 2013.

[22] Ho Shing Lo and Sheng Quan Xie. Exoskeleton robots for upper-limb rehabilitation: State of the art and future prospects. *Medical engineering & physics*, 34(3):261–268, 2012.

[23] Anne Shumway-Cook and Marjorie H Woollacott. *Motor control: translating research into clinical practice*. Wolters Kluwer Health, 2007.

[24] Richard A Schmidt and Tim Lee. *Motor Control and Learning, 5E*. Human kinetics, 1988.

[25] Jurgen Broeren, Katharina S Sunnerhagen, and Martin Rydmark. A kinematic analysis of a haptic handheld stylus in a virtual environment: a study in healthy subjects. *Journal of NeuroEngineering and Rehabilitation*, 4(1):13, 2007.

[26] Don B Chaffin. Human motion simulation for vehicle and workplace design. *Human Factors and Ergonomics in Manufacturing & Service Industries*, 17(5):475–484, 2007.

[27] Julian Faraway and Matthew P Reed. Statistics for digital human motion modeling in ergonomics. *Technometrics*, 49(3), 2007.

[28] Paolo Baerlocher and Ronan Boulic. An inverse kinematics architecture enforcing an arbitrary number of strict priority levels. *Vis. Comput.*, 20(6):402–417, August 2004.

[29] Hyunchul Kim, Levi Makaio Miller, Nancy Byl, Gary Abrams, and Jacob Rosen. Redundancy resolution of the human arm and an upper limb exoskeleton. *Biomedical Engineering, IEEE Transactions on*, 59(6):1770–1779, 2012.

[30] Eui S Jung and Yongtak Shin. Two-handed human reach prediction models for ergonomic evaluation. *Human Factors and Ergonomics in Manufacturing & Service Industries*, 20(3):192–201, 2010.

[31] Yujiang Xiang, Jasbir S Arora, and Karim Abdel-Malek. 3d human lifting motion prediction with different performance measures. *International Journal of Humanoid Robotics*, 9(02), 2012.

[32] Liang Ma, Wei Zhang, Damien Chablat, Fouad Bennis, and François Guillaume. Multi-objective optimisation method for posture prediction and analysis with consideration of fatigue effect and its application case. *Computers & Industrial Engineering*, 57(4):1235–1246, 2009.

[33] Zan Mi, Jingzhou Yang, and Karim Abdel-Malek. Optimization-based posture prediction for human upper body. *Robotica*, 27(4):607–620, 2009.

[34] Zhi Li, Hyunchul Kim, Dejan Milutinović, and Jacob Rosen. Synthesizing redundancy resolution criteria of the human arm posture in reaching movements. In *Redundancy in Robot Manipulators and Multi-Robot Systems*, pages 201–240. Springer, 2013.

[35] Jingzhou Yang, R Timothy Marler, Steven Beck, Karim Abdel-Malek, and Joo Kim. Real-time optimal reach-posture prediction in a new interactive virtual environment. *Journal of Computer Science and Technology*, 21(2):189–198, 2006.

[36] Jared Gragg and J Yang. Posture reconstruction-some insights. In *First international symposium on digital human modeling-IEA-DHM*, pages 14–16, 2011.

[37] Jingzhou Yang, Salam Rahmatalla, Tim Marler, Karim Abdel-Malek, and Chad Harrison. Validation of predicted posture for the virtual human santos®. In *Proceedings of the 1st international conference on Digital human modeling*, pages 500–510. Springer-Verlag, 2007.

[38] Jingzhou Yang, R Timothy Marler, HyungJoo Kim, Jasbir Arora, and Karim Abdel-Malek. Multi-objective optimization for upper body posture prediction. In *10th AIAA/ISSMO multidisciplinary analysis and optimization conference*, volume 30, 2004.

[39] Ilaria Pasciuto, Sergio Ausejo, Juan Tomás Celigüeta, Ángel Suescun, and Aitor Cazón. A comparison between optimization-based human motion prediction methods: data-based, knowledge-based and hybrid approaches. *Structural and Multidisciplinary Optimization*, pages 1–15, 2013.

[40] Yujiang Xiang, Jasbir S Arora, and Karim Abdel-Malek. Hybrid predictive dynamics: a new approach to simulate human motion. *Multibody System Dynamics*, 28(3):199–224, 2012.

[41] Nathanaël Jarrasse, Vincent Crocher, and Guillaume Morel. A method for measuring the upper limb motion and computing a compatible exoskeleton trajectory. In *Intelligent Robots and Systems (IROS), 2012 IEEE/RSJ International Conference on*, pages 3461–3466. IEEE, 2012.

[42] Joel C Perry, Jacob Rosen, and Stephen Burns. Upper-limb powered exoskeleton design. *Mechatronics, IEEE/ASME Transactions on*, 12(4):408–417, 2007.

[43] Andrea Giovanni Cutti, Andrea Giovanardi, Laura Rocchi, Angelo Davalli, and Rinaldo Sacchetti. Ambulatory measurement of shoulder and elbow kinematics through inertial and magnetic sensors. *Medical & biological engineering & computing*, 46(2):169–178, 2008.

[44] Huiyu Zhou and Huosheng Hu. Reducing drifts in the inertial measurements of wrist and elbow positions. *Instrumentation and Measurement, IEEE Transactions on*, 59(3):575–585, 2010.

[45] J Yang, K Abdel-Malek, and K Nebel. Reach envelope of a 9-degree-of freedom model of the upper extremity. *International Journal of Robotics and Automation*, 20(4):240–259, 2005.

[46] Q Zou, Q Zhang, Jingzhou Yang, A Cloutier, J Gragg, Esteve Pena-Pitarch, et al. Determining weights of joint displacement objective function for standing reach tasks. In *First international symposium on digital human modeling, Lyon, France*, 2011.

[47] Qiuling Zou, Qinghong Zhang, Jingzhou Yang, Robyn Boothby, Jared Gragg, and Aimee Cloutier. An alternative formulation for determining weights of joint displacement objective function in seated posture prediction. In *Proceedings of the Third international conference on Digital human modeling*, pages 231–242. Springer-Verlag, 2011.

[48] Jared Gragg, Jingzhou James Yang, and Brad Howard. Hybrid method for driver accommodation using optimization-based digital human models. *Computer-Aided Design*, 44(1):29–39, 2012.

[49] AM Hill, AMJ Bull, AL Wallace, and GR Johnson. Qualitative and quantitative descriptions of glenohumeral motion. *Gait & posture*, 27(2):177–188, 2008.

[50] Walter Maurel and Daniel Thalmann. Human shoulder modeling including scapulo-thoracic constraint and joint sinus cones. *Computers and Graphics*, 24:203–218, 1998.

[51] Katherine RS Holzbaur, Wendy M Murray, and Scott L Delp. A model of the upper extremity for simulating musculoskeletal surgery and analyzing neuromuscular control. *Annals of biomedical engineering*, 33(6):829–840, 2005.

[52] Jorge Ambrósio, Carlos Quental, Bartlomiej Pilarczyk, João Folgado, and Jacinto Monteiro. Multibody biomechanical models of the upper limb. *Procedia IUTAM*, 2:4–17, 2011.

[53] SeongYong Kim, Dong-Min Kim, and Soo-Won Chae. Musculoskeletal upper limb modeling with muscle activation for flexible body simulation. *International Journal of Precision Engineering and Manufacturing*, 10(4):123–129, 2009.

[54] J Denavit and R. S Hartenberg. A kinematic notation for lower-pair mechanisms based on matrices. *Trans ASME J. Appl. Mech*, 22:215–221, 1955.

[55] HOCOMA AG. Armeo spring - functional arm and hand therapy. http://www.hocoma.com/products/armeo/armeospring/, October 2013.

[56] Aimee Cloutier, Robyn Boothby, and Jingzhou Yang. Motion capture experiments for validating optimization-based human models. In *Proceedings of the Third international conference on Digital human modeling*, pages 59–68. Springer-Verlag, 2011.

[57] F. Sebastian Grassia. Practical parameterization of rotations using the exponential map. *J. Graph. Tools*, 3(3):29–48, March 1998.

[58] Jacob Rosen, Joel C Perry, Nathan Manning, Stephen Burns, and Blake Hannaford. The human arm kinematics and dynamics during daily activities-toward a 7 dof upper limb powered exoskeleton. In *Advanced Robotics, 2005. ICAR'05. Proceedings., 12th International Conference on*, pages 532–539. IEEE, 2005.

[59] Pyung Chang. A closed-form solution for inverse kinematics of robot manipulators with redundancy. *Robotics and Automation, IEEE Journal of*, 3(5):393–403, 1987.

[60] Samuel R Buss. Introduction to inverse kinematics with jacobian transpose, pseudoinverse and damped least squares methods. http://math.ucsd.edu/~sbuss/ResearchWeb/ikmethods/iksurvey.pdf, 2009.

[61] Samuel R Buss and Jin-Su Kim. Selectively damped least squares for inverse kinematics. *journal of graphics, gpu, and game tools*, 10(3):37–49, 2005.

[62] DE Schinstock, TN Faddis, and RB Greenway. Robust inverse kinematics using damped least squares with dynamic weighting. In *NASA. Johnson Space Center, Conference on Intelligent Robotics in Field, Factory, Service and Space(CIRFFSS 1994),*, volume 2, 1994.

[63] Coppelia Robotics. V-rep. http://www.coppeliarobotics.com/, October 2013.

[64] Anne Shumway-Cook and Marjorie H Woollacott. *Motor control. Translating research into clinical practice*. Lippincott Williams & Wilkins, 4 edition, 2012.

[65] Beatrix Vereijken, Richard EA van Emmerik, HTA Whiting, and Karl M Newell. Free (z) ing degrees of freedom in skill acquisition. *Journal of motor behavior*, 24(1):133–142, 1992.

[66] R Cano-de-la Cuerda, A Molero-Sánchez, M Carratalá-Tejada, IM Alguacil-Diego, F Molina-Rueda, JC Miangolarra-Page, and D Torricelli. Teorías y modelos de control y aprendizaje motor. aplicaciones clínicas en neurorrehabilitación. *Neurología*, 2012.

[67] OpenSceneGraph. Openscenegraph. http://trac.openscenegraph.org/projects/osg/, April 2014.

[68] NDI. Polaris family of optical tracking systems. http://www.ndigital.com/medical/polarisfamily.php, January 2014.

[69] WHK De Vries, HEJ Veeger, AG Cutti, C Baten, and FCT Van der Helm. Functionally interpretable local coordinate systems for the upper extremity using inertial & magnetic measurement systems. *Journal of biomechanics*, 43(10):1983–1988, 2010.

[70] HEJ Veeger and Bing Yu. Orientation of axes in the elbow and forearm for biomechanical modelling. In *Biomedical Engineering Conference, 1996., Proceedings of the 1996 Fifteenth Southern*, pages 377–380. IEEE, 1996.

[71] Rosana Martins Ferreira de Carvalho, Nilton Mazzer, and Claudio Henrique Barbieri. Analysis of the reliability and reproducibility of goniometry compared to hand photogrammetry. *Acta ortopedica brasileira*, 20(3):139, 2012.

[72] Morey J Kolber, Cydne Fuller, Jessica Marshall, Amanda Wright, and William J Hanney. The reliability and concurrent validity of scapular plane shoulder elevation measurements using a digital inclinometer and goniometer. *Physiotherapy Theory and Practice*, 28(2):161–168, 2012.

[73] Gazihan Alankus, Amanda Lazar, Matt May, and Caitlin Kelleher. Towards customizable games for stroke rehabilitation. In *Proceedings of the SIGCHI Conference on Human Factors in Computing Systems*, pages 2113–2122. ACM, 2010.

[74] N Alberto Borghese, David Murray, Anisoara Paraschiv-Ionescu, Eling D de Bruin, Maria Bulgheroni, Alexander Steblin, Andreas Luft, and Carlos Parra. Rehabilitation at home: A comprehensive technological approach. In *Virtual, Augmented Reality and Serious Games for Healthcare 1*, pages 289–319. Springer, 2014.

[75] Nurdiana Nordin, Sheng Quan Xie, and Burkhard Wünsche. Assessment of movement quality in robot-assisted upper limb rehabilitation after stroke: a review. *Journal of neuroengineering and rehabilitation*, 11(1):137, 2014.

[76] Ana de los Reyes-Guzmán, Iris Dimbwadyo-Terrer, Fernando Trincado-Alonso, Félix Monasterio-Huelin, Diego Torricelli, and Angel Gil-Agudo. Quantitative assessment based on kinematic measures of functional impairments during upper extremity movements: A review. *Clinical Biomechanics*, 29(7):719–727, 2014.

[77] José Zariffa, Naaz Kapadia, John LK Kramer, Philippa Taylor, Milad Alizadeh-Meghrazi, Vera Zivanovic, Urs Albisser, Rhonda Willms, Andrea Townson, Armin Curt, et al. Relationship between clinical assessments of function and measurements from an upper-limb robotic rehabilitation device in cervical spinal cord injury. *Neural Systems and Rehabilitation Engineering, IEEE Transactions on*, 20(3):341–350, 2012.

[78] Enio Walker Azevedo Cacho, Roberta de Oliveira, Rodrigo L Ortolan, Renato Varoto, and Alberto Cliquet. Upper limb assessment in tetraplegia: clinical, functional and kinematic correlations. *International Journal of Rehabilitation Research*, 34(1):65–72, 2011.

[79] Florence I Mahoney. Functional evaluation: the barthel index. *Maryland state medical journal*, 14:61–65, 1965.

[80] Robert Allen Keith. The functional independence measure: a new tool for rehabilitation. *Advances in clinical rehabilitation*, 2:6–18, 1987.

[81] Huiyu Zhou and Huosheng Hu. Human motion tracking for rehabilitation − a survey. *Biomedical Signal Processing and Control*, 3(1):1–18, 2008.

[82] P Daponte, L De Vito, M Riccio, and C Sementa. Experimental comparison of orientation estimation algorithms in motion tracking for rehabilitation. In *Medical Measurements and Applications (MeMeA), 2014 IEEE International Symposium on*, pages 1–6. IEEE, 2014.

[83] Mahmoud El-Gohary and James McNames. Shoulder and elbow joint angle tracking with inertial sensors. *Biomedical Engineering, IEEE Transactions on*, 59(9):2635–2641, 2012.

[84] Chris T Freeman, Eric Rogers, Ann-Marie Hughes, Jane H Burridge, and Katie L Meadmore. Iterative learning control in health care: electrical stimulation and robotic-assisted upper-limb stroke rehabilitation. *Control Systems, IEEE*, 32(1):18–43, 2012.

[85] Robert Riener and Matthias Harders. Virtual reality for rehabilitation. In *Virtual Reality in Medicine*, pages 161–180. Springer, 2012.

[86] Hang Zhang, Sivakumar Balasubramanian, Ruihua Wei, Hiroko Austin, Sharon Buchanan, Richard Herman, and Jiping He. Rupert closed loop control design. In *Engineering in Medicine and Biology Society (EMBC), 2010 Annual International Conference of the IEEE*, pages 3686–3689. IEEE, 2010.

[87] S Kousidou, NG Tsagarakis, C Smith, and DG Caldwell. Task-orientated biofeedback system for the rehabilitation of the upper limb. In *Rehabilitation Robotics, 2007. ICORR 2007. IEEE 10th International Conference on*, pages 376–384. IEEE, 2007.

[88] Hyunchul Kim and Jacob Rosen. Predicting redundancy of a 7 dof upper limb exoskeleton toward improved transparency between human and robot. *Journal of Intelligent & Robotic Systems*, pages 1–21, 2015.

[89] Y Wang and P Artemiadis. Closed-form inverse kinematic solution for anthropomorphic motion in redundant robot arms. *Adv. Robot. Autom*, 2(3):100–110, 2013.

[90] Camilo Cortés, Aitor Ardanza, F Molina-Rueda, A Cuesta-Gómez, Luis Unzueta, Gorka Epelde, Oscar E. Ruiz, Alessandro De Mauro, and Julian Florez. Upper limb posture estimation in robotic and virtual reality-based rehabilitation. *BioMed research international*, 2014, 2014.

[91] Jacques Denavit. A kinematic notation for lower-pair mechanisms based on matrices. *Trans. of the ASME. Journal of Applied Mechanics*, 22:215–221, 1955.

[92] Ana de los Reyes-Guzmán, Angel Gil-Agudo, Benito Peñasco-Martín, Marta Solís-Mozos, Antonio del Ama-Espinosa, and Enrique Pérez-Rizo. Kinematic analysis of the daily activity of drinking from a glass in a population with cervical spinal cord injury. *Journal of neuroengineering and rehabilitation*, 7(1):41, 2010.

[93] Inc C-Motion. Visual 3d. http://www.c-motion.com/products/visual3d/, January 2016.

[94] Charnwood Dynamics Ltd. System hardware. http://www.codamotion.com/index.php/applications/hardware, January 2016.

[95] Che Fai Yeong, Alejandro Melendez-Calderon, and Etienne Burdet. Analysis of pick-and-place, eating and drinking movements for the workspace definition of simple robotic devices. In *Rehabilitation Robotics, 2009. ICORR 2009. IEEE International Conference on*, pages 46–52. IEEE, 2009.

[96] RF Woolson. Wilcoxon signed-rank test. *Wiley Encyclopedia of Clinical Trials*, 2008.

[97] IBM Corp. Spss software. http://www-01.ibm.com/software/analytics/spss/, January 2016.

[98] Maria Laitenberger, Maxime Raison, Delphine Périé, and Mickael Begon. Refinement of the upper limb joint kinematics and dynamics using a subject-specific closed-loop forearm model. *Multibody System Dynamics*, 33(4):413–438, 2014.

[99] G Paraskevas, A Papadopoulos, B Papaziogas, S Spanidou, H Argiriadou, and J Gigis. Study of the carrying angle of the human elbow joint in full extension: a morphometric analysis. *Surgical and Radiologic Anatomy*, 26(1):19–23, 2004.

[100] P Van Roy, JP Baeyens, D Fauvart, R Lanssiers, and JP Clarijs. Arthro-kinematics of the elbow: study of the carrying angle. *Ergonomics*, 48(11-14):1645–1656, 2005.

[101] James Patton, Greg Dawe, Chris Scharver, Ferdinando Mussa-Ivaldi, and Robert Kenyon. Robotics and virtual reality: a perfect marriage for motor control research and rehabilitation. *Assistive Technology*, 18(2):181–195, 2006.

[102] Karina Lebel, Patrick Boissy, Mathieu Hamel, and Christian Duval. Inertial measures of motion for clinical biomechanics: comparative assessment of accuracy under controlled conditions-effect of velocity. *PloS one*, 8(11):e79945, 2013.

[103] Jeffrey D. Kertis. Biomechanical evaluation of an optical system for quantitative human motion analysis. Master's thesis, Marquette University, 2012.

[104] Rong Zhu and Zhaoying Zhou. A real-time articulated human motion tracking using tri-axis inertial/magnetic sensors package. *Neural Systems and Rehabilitation Engineering, IEEE Transactions on*, 12(2):295–302, 2004.

[105] Yaqin Tao, Huosheng Hu, and Huiyu Zhou. Integration of vision and inertial sensors for 3d arm motion tracking in home-based rehabilitation. *The International Journal of Robotics Research*, 26(6):607–624, 2007.

[106] Justin Fong, Vincent Crocher, Denny Oetomo, Ying Tan, and Iven Mareels. Effects of robotic exoskeleton dynamics on joint recruitment in a neurorehabilitation context. In *Rehabilitation Robotics (ICORR), 2015 IEEE International Conference on*, pages 834–839. IEEE, 2015.

[107] Qing-Cong Wu, Xing-Song Wang, and Feng-Po Du. Analytical inverse kinematic resolution of a redundant exoskeleton for upper-limb rehabilitation. *International Journal of Humanoid Robotics*, page 1550042, 2015.

[108] Domien Gijbels, Ilse Lamers, Lore Kerkhofs, Geert Alders, Els Knippenberg, Peter Feys, et al. The armeo spring as training tool to improve upper limb functionality in multiple sclerosis: a pilot study. *Journal of neuroengineering and rehabilitation*, 8(5):5, 2011.

[109] Claudia Rudhe, Urs Albisser, Michelle L Starkey, Armin Curt, and Marc Bolliger. Reliability of movement workspace measurements in a passive arm orthosis used in spinal cord injury rehabilitation. *Journal of neuroengineering and rehabilitation*, 9(37), 2012.

[110] Marco Caimmi, Eleonora Guanziroli, Matteo Malosio, Nicola Pedrocchi, Federico Vicentini, Lorenzo Molinari Tosatti, and Franco Molteni. Normative data for an instrumental assessment of the upper-limb functionality. *BioMed Research International*, 2015:14, 2015.

[111] Intel. Intel realsense developer kit featuring sr300. http://click.intel.com/intelrrealsensetm-developer-kit-featuring-sr300.html, March 2016.

[112] pmdtechnologies gmbh. Purchase order form. http://pmdtec.com/html/pdf/order_CamBoard_pico_s.pdf, March 2016.

[113] Softkinetic. Softkinetic store. http://www.softkinetic.com/Store/ProductID/36, March 2016.

[114] Softkinetic. Depthsense cameras. http://www.softkinetic.com/Products/DepthSenseCameras, March 2016.

[115] pmdtechnologies gmbh. Reference design brief camboard pico^s 71.19k. http://pmdtec.com/html/pdf/PMD_RD_Brief_CB_pico_71.19k_V0103.pdf, March 2016.

[116] T.F. Edgar, D.M. Himmelblau, and L.S. Lasdon. *Optimization of chemical processes*. McGraw-Hill, 2001.

[117] Jorge Nocedal and Stephen Wright. *Numerical optimization*. Springer Science & Business Media, 2006.

[118] Anthony V Fiacco. *Introduction to sensitivity and stability analysis in nonlinear programming*. Elsevier, 1983.

[119] Karina Lebel, Patrick Boissy, Mathieu Hamel, and Christian Duval. Inertial measures of motion for clinical biomechanics: Comparative assessment of accuracy under controlled conditions–changes in accuracy over time. *PloS one*, 10(3):e0118361, 2015.